# A NEW APPROACH IN EMPIRICAL MODELLING OF $CO_2$ CORROSION WITH THE PRESENCE OF HAc AND $H_2S$

YULI PANCA ASMARA

DOCTOR OF PHILOSOPHY

MECHANICAL ENGINEERING

UNIVERSITI TEKNOLOGI PETRONAS

NOVEMBER 2010

**Abstract**

$CO_2$ corrosion is the main threat in upstream oil and gas operations. The requirement to predict the corrosion in design and operational stage is critical. However, the presence of other corrosion species and operational parameters complicate the mechanism of the corrosion. The interaction between those factors affect the accuracy of the corrosion prediction. Although many publications on $CO_2$ corrosion prediction had been published, most of the prediction models rely on specific algorithms to combine individual effect of the interacting species to represent the total corrosion rate. This effort is inefficient and needs a large number of experiments to process all possible corrosion data simultaneously. In order to study $CO_2$ corrosion of carbon steel involving interactive effects of several key parameters, a proven systematic statistical method that can represent the multitude interactive effects is needed. In this research, a combination of response surface methodology (RSM) and mechanistic corrosion theories were used to construct an empirical model that relates the effects of acetic acid (HAc), temperature, and rotation speed on $CO_2$ and $CO_2/H_2S$ corrosion rate simultaneously. The corrosion experiments are based on both linear polarization resistance (LPR) and electrochemical impedance spectroscopy (EIS) methods. Flow condition is simulated using rotating cylinder electrode (RCE). The RSM regression models for the carbon steel corrosion in $CO_2$ environments involving HAc, temperature and rotation speed as parameters have been successful developed and validated with experimental data and commercial predictive models. In the form of mathematical equations, the effects of independent variables will be easily identified and developed. The combination RSM and mechanistic theory applied in this research is efficient to determine the empirical relationship of the variables tested simultaneously. Furthermore, RSM models can be used to determine scaling temperature, limiting current density and flow dependency characters.

*Key words: $CO_2$ corrosion, response surface methodology, corrosion model.*

## Abstrak

Kakisan karbon dioxide ($CO_2$) adalah merupakan masalah utama kepada operasi huluan bagi industri minyak dan gas bumi. Keperluan untuk meramal tahapan kakisan di dalam peringkat reka bentuk dan operasi adalah kritikal. Kehadiran spesies-spesies kakisan yang lain dan juga parameter operasi menjadikan mekanisme kakisan bertambah kompleks antara fakor-faktor berkenaan mempengaruhi ramalan berkaitan kakisan. Walaupun terdapat banyak penerbitan tentang ramalan kakisan $CO_2$ diterbitkan namun kebanyakan model hanya tertumpu kepada algoritme yang khusus untuk menggambarkan kesan masing-masing spesies yang berinteraksi bagi mewakili keseluruhan kadar kakisan. Usaha ini tidaklah berapa berkesan dan ia memerlukan bilangan uji kaji yang besar untuk memproses secara serentak semua data kakisan yang mungkin. Bagi kajian kakisan $CO_2$ terhadap keluli yang melibatkan kesan interaksi maka kaedah statistik yang sistimatis yang dapat mewakili pelbagai kesan interaksi adalah diperlukan. Pengkaedahan permukaan gerak balas digabungkan dengan dengan teori mekanisme kakisan digunakan untuk membina model empirik yang berkaitan dengan kesan daripada kepekatan asid asetat, suhu, dan laju putaran pada kadar kakisan $CO_2$ dan kakisan $CO_2/H_2S$ serentak. Uji kakisan adalah berdasarkan pada rintangan pengutuban linear dan spektroskopi impedans elektrokimia. Keadaan aliran disimulasikan dengan menggunakan elektrod silinder berputar. Model regresi menggunakan pengkaedahan permukaan gerak balas untuk kesan kakisan pada karbon keluli yang melibatkan asid asetat, $CO_2$, suhu dan laju putaran telah berjaya dibangunkan dan diaktifkan dengan data eksperimen dan model ramalan komersil. Dalam bentuk persamaan matematik, kesan daripada pembolehubah bebas akan mudah dikenalpasti dan dibina. Kombinasi pengkaedahan permukaan gerak balas adalah cekap dalam menentukan hubungan empirik antara kebarangkalian yang diuji secara bersamaan. Seterusnya, model Pengkaedahan permukaan gerak balas boleh digunakan untuk menentukan suhu pembekalan, ketumpatan arus batas, dan kebersamaan aliran.



*Kata Kunci: Kakisan $CO_2$, pengkaedahan permukaan gerak balas, model kakisan.*

TABLE OF CONTENTS

## LIST OF TABLES

## LIST OF FIGURES

# CHAPTER 1

# INTRODUCTION

## 1.1 Background

Carbon dioxide ($CO_2$) corrosion has always been an important corrosion management issue in oil and gas industry. Although, the understanding of pure $CO_2$ corrosion is well accepted, the corrosion mechanism with the presence of other species such as acetic acid (HAc) and hydrogen sulfide ($H_2S$) is unclear [1-5]. The $CO_2$ corrosion problem is further complicated as the corrosion can be influenced not only by various reservoir species but also operational parameters such as temperature, pH, and flow condition. The possible interactions between various species and operating condition pose a challenge in the $CO_2$ corrosion prediction. The accuracy of a corrosion prediction hinges on realistic treatment of the possible interactive effects between these chemical species and operational variables.

In fact, corrosion modeling in a $CO_2$ containing environment has been studied extensively for the last decades. Many published papers on $CO_2$ corrosion prediction studied the effects of species like $H_2S$ and HAc in conjunction with other operating parameters including temperature, pH, and flow condition. Most of the prediction models rely on specific algorithms to combine individual effect of the interacting species to represent a cumulative total corrosion rate. The individual effect was determined from the experimental routine of holding constant certain variables and changing the values of another variable. This experimental method is inefficient and needs a large number of experiments to process all possible corrosion data.

Hence, this complex nature of $CO_2$ corrosion poses a challenge to construct $CO_2$ corrosion model efficiently. Existing empirical models have shown acceptable results

in predicting the individual effects but apparently not qualified to predict corrosovity of the system arises from simultaneous interactions of different variables. The need to represent the interactive effect of several key parameters in $CO_2$ corrosion is undoubtedly important in the corrosion study.

The simultaneous effects of many variables in the $CO_2$ corrosion could be optimized by using a statistical methodology such as design of experiment methodology. A systematic statistical method can represent the multitude of the interactive effects of variables considered.

## 1.2 Problem Statement

A multitude of factors can affect $CO_2$ corrosion, particularly when HAc and $H_2S$ species are present. The presence of HAc and $H_2S$ bring complexity into the experimental methodology to predict corrosion rate based on an empirical method. Using a normal empirical method, an attempt to model possible interactive effects between the species and the operational conditions, not only requires a large number of experiments but most important the resultant modeling could not be statistically validated. Thus the empirical relationship obtained through best fit regression, for example of many empirical $CO_2$ corrosion models, tends to misinterpret the real corrosion kinetics. Furthermore, the resultant models were not usually based on theoretical basis to guide data fitting to formulate the regression model. Moreover, there are limited expressions in the literature to quantify the mixed variables simultaneously and no expressions were previously developed to express the corrosion model in $CO_2/H_2S$/HAc environment. Considering these limitations, it is important to develop a $CO_2$ corrosion model founded on fundamental theory and systematic statistics approaches that expresses relationship between the reservoir species (HAc, $H_2S$) and operational conditions (temperature, pH, flow condition).

## 1.3 Research Objectives

The main objective of this research is to predict corrosion rate of carbon steel due to the combined effect of $H_2S$/HAc species at various operating conditions in $CO_2$ environment, using the response surface methodology (RSM). The work has been carried out to meet the following specific objectives:

- Develop empirical models of carbon steel corrosion rate in aqueous $CO_2$ solutions and $CO_2/H_2S$ environments at various HAc, pH, temperature and flow condition.
- Investigate the effects of HAc in combination with pH, temperature, and flow condition simultaneously on carbon steel corrosion in $CO_2$ environment.
- Investigate the effects of HAc acid in combination with pH, temperature, and flow condition simultaneously on carbon steel corrosion in $CO_2$ and $H_2S$ environment.

## 1.4 Scope of Study

The research is on prediction of the corrosion behavior of carbon steel in $CO_2$ environment with the presence $H_2S$, and HAc at different pHs, temperatures and flow conditions. The analyses of the model was based on mechanistic theory, published experimental data, and commercial corrosion predictive software. The Linear Polarization Resistance (LPR) technique was used to measure the polarization resistance (Rp) and calculate corrosion rate. The corrosion rate and mechanism was determined using Electrochemical Impedance Spectroscopy (EIS) technique. The parameters used are HAc concentration, $H_2S$ concentration at various temperature, pH and flow conditions. Rotating cylinder electrode (RCE) equipment was used to simulate flow condition in pipeline.

The empirical modeling is based on the RSM technique that relates effects of HAc, temperature, and flow condition on $CO_2$ and $CO_2/H_2S$ corrosion rate simultaneously

## 1.5 Organization of the Theses

This dissertation consists of six chapters. Chapter 1 describes the research background related to $CO_2/H_2S$/HAc corrosion of carbon steel. It gives an overview of oil field environments, corrosion predictions models, problem statement, research objectives, and scope of study.

Chapter 2 contains extensive literature review on $CO_2$ corrosion. It also describes literature review about $H_2S$, HAc and parameters influencing corrosion mechanism. The literature review on design of experiment is also presented in this chapter. In addition Chapter 2 also discusses predictive models developed by researchers and their comparison with published papers for justification.

In Chapter 3, detail of material specification, material preparation, corrosion testing methodology, and experimental design methodologies were explained.

Analyses of the results are presented in Chapter 4 and Chapter 5. Chapter 4 presents results and discussion relating effects of HAc in $CO_2$ gas condition, while Chapter 5 discusses effects of HAc in $CO_2/H_2S$ condition. In this study, published papers, corrosion experimental data from researchers and from experiments were compared and discussed to verify the models.

Finally, Chapter 6 contains conclusion. The conclusion summarizes the results and compares the models to determine the most appropriate model for the $CO_2/H_2S$/HAc corrosion pattern.

# CHAPTER 2

# LITERATURE REVIEW

## 2.1 $CO_2$ Corrosion

Corrosion mechanism of mild steel in the presence of $CO_2$ has been widely reviewed , particularly in relation to the oil and gas application [6, 7]. The mechanism influencing $CO_2$ corrosion, the effects of main parameters such as HAc concentration, temperature and flow conditions have been identified. In $CO_2$ corrosion prediction, theoretical analysis involving chemistry, electrochemistry, mass transport processes and various possible reactions should be considered. Researchers have investigated various variables that affect the corrosion rate in order to develop a prediction model. However, the accuracy of existing $CO_2$ corrosion model is still debatable and at worst contradictory. Thus, further researches on the effects of parameters such as temperature, HAc and flow conditions in $CO_2$ corrosion are still open to explore.

Several $CO_2$ corrosion models were based on experimental and field studies. The study in $CO_2$ corrosion conducted by C. deWaard and Milliams [8] has become a foundation for further studies on the $CO_2$ corrosion phenomenon. The latest publications of $CO_2$ corrosion mechanism was proposed by Nesic et al. [9]. Based on their model, $CO_2$ corrosion covers anodic dissolution of iron and cathodic evolution of hydrogen which involve the electrochemical reactions at the steel surface, transport of reactive species between the metal surface and the bulk, and the chemistry in the bulk solution. The following is a summary of the mechanism processes in $CO_2$ corrosion as proposed by Nesic and Miran [10]. At the cathodic site, $CO_2$ dissolves into the water phase and becomes hydrated to form carbonic acid as represented by Equations 2.1 and 2.2.

$$CO_{2\,(g)} \leftrightarrow CO_{2(aq)} \tag{2.1}$$

$$CO_{2\,(aq)} + H_2O \leftrightarrow H_2CO_3 \quad (2.2)$$

Then, carbonic acid dissociates by further reactions depending on the pH of the solution. At pH 4 or lower, carbonic acid dissociates into bicarbonate ions and carbonate ions in two steps (Equations 2.3 and 2.4).

$$H_2CO_3 \leftrightarrow HCO_3^- + H^+ \quad (2.3)$$

$$HCO_3^- \leftrightarrow CO_3^{2-} + H^+ \quad (2.4)$$

At pH values between 4 and 6, carbonic acid dissociates to produce bicarbonate ions. The direct reduction of carbonic acid to produces hydrogen gas as described in Equations 2.5.

$$2H_2CO_3 + 2e^- \rightarrow H_2 + 2HCO_3^- \quad (2.5)$$

At higher pH around 5, it was proposed that the bicarbonate ion reduces into carbonate ion and releases hydrogen gas as expressed in Equation 2.6:

$$2HCO_3^- + 2e^- \rightarrow H_2 + 2CO_3^{2-} \quad (2.6)$$

At higher pH and pressure, the evolved hydrogen can adsorb to the diffusion layer according to Equation 2.7.

$$H^+ + e^- + H_{(ads)} \rightarrow H_{2(ads)} \quad (2.7)$$

At pH more than 6, the cathodic rate is also controlled by the production of carbonic acid (Equations 2.8).

$$HCO_3^- + H_2O \rightarrow H_2CO_3 + OH^- \quad (2.8)$$

It was suggested that $H^+$ ions are the dominant species promoting corrosion. $H^+$ ions are able to diffuse to the metal surface through boundary layer. On the metal

surface, the $H^+$ ions participate in hydrogen evolution reaction. These additional charge transfer reactions are suggested as the factors governing the corrosion rate (Equations 2.9 and 2.10).

$$H^+ + e^- \rightarrow H_{(ads)} \quad (2.9)$$

$$H_{(ads)} + H_{(ads)} \rightarrow H_{2(ads)} \quad (2.10)$$

At the anodic site, oxidation reaction occur to form ferrous ions ($Fe^{2+}$). The general reaction is shown in Equations 2.11.

$$Fe \rightarrow Fe^{2+} + 2e^- \quad (2.11)$$

Bockris [11] proposed anodic dissolution of Fe ions ($Fe^{2+}$) according to the following mechanism (Equations 2.12 and 2.14) :

$$Fe + OH^- \rightarrow FeOH + e^- \quad (2.12)$$

$$FeOH \rightarrow FeOH^+ + e^- \quad (2.13)$$

$$FeOH^+ \rightarrow Fe^{2+} + OH^- \quad (2.14)$$

This steady state anodic reaction that brings the variation to Tafel slopes was also discussed by Videm [12]. However, according to Nesic et al. [13], the presence of $CO_2$ does not have any effects on the anodic dissolution of iron and Tafel slopes due to effects of catalyzes of chemical ligand in the metal surface.

### 2.1.1 Carbonate Film Formation

$CO_2$ corrosion reaction leads to the formation of iron carbonate ($FeCO_3$) film. This corrosion film may be protective or non-protective depending on the conditions of the environment, such as pH, $CO_2$ pressure, temperature and flow conditions, and ferrous ions concentration. The corrosion product of the bicarbonate ion can increase pH of the solution to reach its solubility limit [14]. At temperature less than $60^oC$, protective film does not form due to the solubility of $FeCO_3$ is high and the precipitation rate is

slow [15]. However, at temperatures more than 60°C, the high precipitate rate, the film is protective that can reduce corrosion rate substantially [15].

The formation $FeCO_3$ occurs through two processes as shown in Equations 2.15 – 2.17. When ferrous ions react with bicarbonate ions, iron bicarbonate forms, which subsequently dissociates into iron carbonate [16].

$$Fe^{2+} + CO_3^{2-} \rightarrow FeCO_3 \quad (2.15)$$

$$Fe^{2+} + 2HCO_3^{-} \rightarrow Fe(HCO_3)_2 \quad (2.16)$$

$$Fe(HCO_3)_2 \rightarrow FeCO_3 + CO_2 + H_2O \quad (2.17)$$

The $FeCO_3$ formation will precipitate when the local concentration of $Fe^{2+}$ and $CO_3^{2-}$ species exceeds the solubility limit $K_{sp}$ [17].

The solubility limit $K_{sp}$ is defined as:

$$K_{sp} = -\frac{10.13 + 0.0182T}{0.0115I^{-0.6063}} \quad (2.18)$$

*T* is temperature in ºC and *I is* ionic strength in mol/L. The ionic strength is defined as:

$$I = \sum_i \frac{1}{2} c_i z_i^2 \quad (2.19)$$

Where *c* is species concentration and *z* is the species charge.

Typically, in order to obtain significant rates of film formation, high temperature (>60°C) and considerable supersaturation *($S_S$)* is required. Conditions favoring the formation of the protective iron carbonate scale are in high temperature and high pH. Dependency on temperature and ion activities of the bulk saturation value for iron carbonate, $S_S$ ($FeCO_3$), is calculated using the equation 2.24 for solubility product [18]. Johnson and Tomson [19] developed a model for the precipitation kinetics of $FeCO_3$ in which the precipitation rate (in kmol/Jm$^3$s) as follows:

$$R_{FeCO_3} = \partial \frac{\left[Fe^{2+}\right]}{\partial t} \tag{2.20}$$

$$= K_r \frac{A}{V} K_{sp} \left(SS^{0,5} - 1\right)^2 \tag{2.21}$$

Where, $K_r$ is the temperature-dependent rate constant, $A/V$ is the surface/volume ratio, $K_{sp}$, the solubility product of $FeCO_3$ and $S_S$ is supersaturation level defined as [18]:

$$S_S = \frac{\left[Fe^{2+}\right]\left[CO_3^{2-}\right]}{K_{sp}} \tag{2.22}$$

Equation 2.22 is based on the assumption that the precipitation rate of $FeCO_3$ in corrosion systems is controlled by kinetics and not by nucleation. Another formula to calculate $FeCO_3$ precipitation has been proposed by Johnson and Tomson [19], and Hunnik et al [16]. with different expressions for the precipitation (crystal growth) rate. According to Johnson and Tomson [19]:

$$R_{FeCO_3} = Ae^{54.8 - \frac{123.0}{RT}} K_{sp} (S_S{}^{0.5} - 1)^2 \tag{2.23}$$

According to Hunnik, et al.[16]:

$$R_{FeCO_3} = Ae^{52.4 - \frac{119.8}{RT}} K_{sp} (S_S - 1)(1 - S_S{}^{-1}) \tag{2.24}$$

Where $R_{FeCO3}$ is precipitation growth, $A$ is the surface area available for precipitation per unit volume, $K_{sp}$ is the precipitation rate constant, $R$ is universal gas constant, $T$ is temperature, and $S_S$ is super saturation. From the two different rate of precipitation equations, it can be distinguished that the Johnson and Tomson equation (2.23) is suitable for very low levels of supersaturation that represents a nucleation growth. While Hunnik equation is used for large supersaturations of a film precipitation [17, 18].

### 2.1.2 Transport processes

It has been known that during electrochemical processes, there is a transport of certain species in the solution. At metal surface, ferrous ions ($Fe^{2+}$) will increase while other species will be depleted [7, 20]. The concentration of the species will be higher near the metal surface than in the bulk solution. This concentration differences will lead to molecular diffusion of the species toward and away from the surface. In cases when the diffusion processes are much faster than the electrochemical processes, the concentration change at the metal surface will be small [21].

Many of the dissolved species in $CO_2$ solutions are controlled by electrically charged ions and have different diffusion coefficients. This means that they diffuse through the solution with different speeds depending on the potential difference. Consequently, any diffusion occurring as a result of the existence of concentration gradients will tend to change the charges ions [21]. In general, transport processes that occur in solution containing $CO_2$ involves convective diffusion, molecular diffusion and diffusion via corrosion film. The film acting as a barrier on the metal surface depends on time, hydrodynamic stresses, chemical reaction, precipitation rate, change of mass scale removal of the outer scale and material microstructure [22 - 26].

### 2.1.3 Factors affecting $CO_2$ corrosion

There are many factors that can influence both thermodynamics and kinetics of $CO_2$ corrosion. Main factors as experienced by field operations, such as operating conditions and solution chemistry, have shown a significant impact on corrosion mechanistic model and caused different types of corrosion morphology. In the following sections, several main factors that govern the corrosion rate are discussed.

#### 2.1.3.1 pH

pH is an important parameter for any corrosion process. The pH is determinated by $H^+$ ions concentration which is influenced by temperature, pressure, and ionic strength. Dissolved iron bicarbonate will also contribute to an increase in pH of the solution

[27]. Normally, an increase in pH will cause the film to become thicker, denser and protective that relates to the passivity [29].

### 2.1.3.2 Temperature

Temperature has been identified to affect corrosion rate. The role of temperature in influencing corrosion rate is related to corrosion kinetic; diffusion coefficient and activation energy of species. At the higher temperature, diffusion coefficient of species is higher that can accelerate the species to corrode the metal surface. Temperature facilitates conditions for formation of the protective carbonate layers and affects lower corrosion rate. This temperature is called scaling temperature that is affected by flow rate and pH, where higher flow rate and lower pH will produce higher scaling temperature. The correlation between scaling temperature and those variables have been studied by researchers [30, 31].

### 2.1.3.3 Effects of $CO_2$ partial pressure

Corrosion rate will increase when the partial pressure of $CO_2$ increases. At higher partial pressure of $CO_2$, $CO_3^{2-}$ ions concentration will have higher super saturation (at the high pH) which leads to increase corrosion rate. An increase in the total pressure of the gas will lead to an increase in corrosion rate too, especially for the non-ideal gas at high pressure [28].

### 2.1.3.4 Effect of $Fe^{2+}$ concentration

The effects of $Fe^{2+}$ ions on corrosion rate are influenced by its ability to form iron carbonate. It has been commonly known that solid iron carbonate scale precipitates on steel surface when the concentrations of $Fe^{2+}$ and $CO_3^{2-}$ ions in the $CO_2$ water solution exceed the solubility limit. The increase of $Fe^{2+}$ results in higher supersaturation, which consequently accelerates the precipitation rate and leads to higher surface scaling tendency to form a corrosion product films [21]. Protective films will not form when the scaling tendency is very low although $Fe^{2+}$ has achieved

a saturation value. In this condition, the iron carbonate film that forms is very porous and is not protective, which will not be effective in reducing corrosion rate [16].

#### 2.1.3.5 The effect of flow conditions

The effect of fluid velocity on corrosion rate is associated with higher turbulence and mixing in the solution. This mixing affects the corrosion rate and the iron carbonate film formation. High velocity leads to an increase in corrosion rate as the transport of cathodic species toward the steel surface is enhanced by turbulent flow. At the same time the transport of $Fe^{2+}$ ions away from the steel surface is also increased, leading to a lower concentration of $Fe^{2+}$ ions at the steel surface. This results in a lower surface supersaturation and slower precipitation rate. Both contribute to less protective films formed at high velocities. More details about the effects of velocity on corrosion rate are described in the subsequent discussion as reported by Silverman et al. [32-38].

The degree of corrosiveness caused by velocity is also related to crude oil type, multiphase condition and water cut. Those parameters determine how well the water can wet the steel surface and lead to govern corrosion rate [39 - 43].

## 2.2 $H_2S$ Corrosion

Incorporating the effects of $H_2S$ gas in corrosion calculations is important for the prediction of $CO_2$ corrosion since many of the oil fields around the world contain this acid gas [1, 3, 4]. The $CO_2$ corrosion mechanism will change if $H_2S$ gas exists in the system. Intensive studies have been conducted to study the effect of $H_2S$ gas in $CO_2$ system. As discussed in many published papers, the complex chemistry and mechanism of corrosion process make it difficult to predict $CO_2$ and $H_2S$ corrosion processes. The corrosion process may involve a combination of reactions between corrosion rate and film formation rate. Thus, further research is needed to investigate how $H_2S$ gas affects corrosion rate in $CO_2$ system.

### 2.2.1 $H_2S$ in aqueous solution

The dissociation of hydrogen sulfide in water involves a series of chemical reactions as described from Equations 2.25 to 2.29. The proposed chemical reactions steps are [44]:

i. $H_2S$ dissolution

$$H_2S_{(g)} \leftrightarrow H_2S_{(aq)} \tag{2.25}$$

ii. $H_2S$ dissociation

$$H_2S_{(aq)} \leftrightarrow HS^-_{(aq)} + H^+_{(aq)} \tag{2.26}$$

iii. $HS^-$ dissociation

$$HS^-_{(aq)} \leftrightarrow H^+_{(aq)} + S^{2-}_{(aq)} \tag{2.27}$$

iv. $H_2S$ Reduction

$$2H_2S_{(aq)} + 2e^- \rightarrow H_{2(g)} + 2HS^-_{(aq)} \tag{2.28}$$

v. FeS formation by precipitation

$$Fe^{2+}_{(aq)} + S^{2-}_{(aq)} \leftrightarrow FeS_{(s)} \tag{2.29}$$

At pressures less than 200 kPa, the solubility of molecular $H_2S$ in water is given by Henry's law as:

$$M_{H2S}\, H = Y_{H2S}\, P \tag{2.30}$$

Where $Y_{H2S}$ is the mole fraction of hydrogen sulfide in vapor, $P$ is the total pressure, $M_{H2S}$ is the molality of the molecular form of hydrogen sulfide in water (moles per kilogram of water), and $H$ is Henry's constant.

The reactions of $H_2S$ in aqueous vary with pH. At acidic solutions, the dominant sulfide species is molecular $H_2S$. At pH of about 6, the solutions will contain bisulfide ions. The higher pH will result in the formation of bisulfide will increase. At pH of around 7, the amount of $H_2S$ molecular and bisulfide forms is similar [45].

### 2.2.2 Iron sulfides formation

In $H_2S$ corrosion system, there are different possibilities of iron sulfide formation in aqueous solution [46]. The formation of solid film on the surface is due to anodic dissolution of iron. Ferrous ions dissolve into solution and react with sulfide ions (FeS) in the solution, hence no film of corrosion product on the surface. The formation of sulfide can also by mixing reaction between ferrous ions that react on the surface and in solution. Those film formations bring different film porosities of FeS. The porous surface facilitates the cathodic reaction and creates anodic dissolution of iron that affects to the corrosion rate [46]. The types of FeS are influenced by temperature and $H_2S$ activity [45]. Based on kinetics theories, several types of FeS are commonly found in oil field corrosion are pyrite ($FeS_2$), pyrrhotite, and mackinawite.

When $H_2S$ gas presents with $CO_2$ gas, there will be a growth competition between $FeCO_3$ and FeS films which affects to the corrosion rate. Nesic et al. [47] constructed a model to simulate film formation growth of $CO_2/H_2S$ competition reactions. From the simulated model, they identified that the growth of film formation containing $H_2S/CO_2$ gas, initially, is started by FeS film formation. Then, the $FeCO_3$ film becomes thicker and denser at the metal/film interface due to an increase in pH and $Fe^{2+}$ concentration.

### 2.2.3 Experiments related to the role of $H_2S$ on mild steel corrosion in $CO_2$ environments

The role of $H_2S$ in $CO_2$ corrosion was studied by Brown [44]. In his experiment, he found that the corrosion rate in $CO_2$ saturated water will increase in the presence of small $H_2S$ concentration of less than 30 ppm. However, he also observed a reduced corrosion rate in 100 ppm $H_2S$ concentration, and pH solution < 5. In single phase and multi phase flow experiment, the scale produced was adherent and protective enough to retard corrosion attack. The scale was more protective when temperature was increased to $80^oC$.

The findings by Brown was supported by Lee [18]. Lee set the experimental variable as; temperature 20°C, pH 5, partial pressure 1 bar, flow rate 1000 rpm, concentration of $H_2S$ in $CO_2$ in the range of 0 - 340 ppm. All of the experiments indicated that very small of amount of $H_2S$ (10 ppm) in phase gas lead to rapid reduction of the corrosion rate. Based n the SEM observation, they found that the scale formed on the surface that inhibited corrosion rate have a mackinawite structure. They stated that the mechanism of scale growth was not of mass-transport control, but rather a charge transfer controlled. Brown and Lee revealed that at 20°C – 60°C, a competition to form the protective film takes place between $H_2S$ and $CO_2$ corrosion mechanism.

In experimental research work done by Agrawal et al. [48], observed that the phenomena of accelerated corrosion in a $CO_2$ and $H_2S$ environment occurs at low $H_2S$ concentration. They also found that there was a strong correlation between the corrosion rates and the temperature. In the range of $H_2S$ concentration studied, the corrosion rate showed a polynomial curve with increasing the temperature.

Andrzej et al. [49] proposed a model involving thermophysical properties, electrochemical properties, and scale effects to predict corrosion rate. They reported significant drop in corrosion rate for partial pressures of $H_2S$ ranging from $2.10^{-6}$ to $10^{-4}$ bar and the rate reached a plateau in a relatively wide range of $H_2S$ partial pressures above $10^{-4}$ bar. Reduction in corrosion rates has been reported when the $H_2S$ partial pressure exceeds $10^{-3}$ bar in some systems. At substantial $H_2S$ partial pressures (above $10^{-2}$ bar), the aqueous $H_2S$, and $HS^-$ species become sufficient to increase the corrosion rate. That observation is supported by Chengqiang [3] who found that corrosion rate in $CO_2$ system will decrease quickly as compared to sweet corrosion in low concentration of $H_2S$.

Kvarekval et al. [50] worked with 150 – 450 ppm of $H_2S$. Experiments with up to 2 bar $CO_2$ and temperatures up to 80°C resulted in slightly higher corrosion rates than in corresponding experiments without $H_2S$. The corrosion rates were in the range of 0.1-2 mm/y. In an experiment with 0.5 mbar of $H_2S$ at a $CO_2/H_2S$ partial pressure ratio of 4500, both iron sulfides (FeS) and iron carbonates ($FeCO_3$) were detected on the steel surface. The mixed sulfide/carbonate films were 30-80 µm thick.

Experiments with $CO_2/H_2S$ ratios of 1200-1500 resulted in formation of thin iron sulfide films (1- 10 μm ) on the corroding surfaces. No iron carbonates were found in corrosion product films formed at $CO_2/H_2S$ ratios below 1500.

Singer et al. [51] found that trace amounts of $H_2S$ greatly retards the $CO_2$ corrosion with general corrosion rates usually 10 to 100 times lower than their pure $CO_2$ equivalent. The most protective conditions were observed at the lowest partial pressure of $H_2S$. However, corrosion rate increased when more $H_2S$ was added. The presence of trace amounts of $H_2S$ (0.004 bar) in the $CO_2$ environment sharply decreases the corrosion rate by two orders of magnitude. As the partial pressure of $H_2S$ is increased to 0.13 bar, the tendency is reversed and the general corrosion rate increased by an order of magnitude.

Carew et al. [43] observed a rapid and significant reduction in the $CO_2$ corrosion rate both in single and multiphase flow in the presence of 10 ppm $H_2S$. At higher $H_2S$ concentrations (up to 250 ppm) the trend was reversed and a mild increase of the corrosion rate was observed. An acceleration of $CO_2$ corrosion rate was observed at 60°C, 0.79 MPa $CO_2$ at multiphase flow with only 3 ppm $H_2S$. Similar result was reported by Zhang [52] who discussed effects of high $H_2S$ partial pressure on corrosion of API-X52 and X60 pipeline steels. The results showed that the corrosion rate of the two steels increased with the $H_2S$ partial pressure at the temperature of $60^oC$. General corrosion was at the $H_2S$ partial pressure of 0.15MPa, 0.33MPa and 1.5MPa, and at the $H_2S$ partial pressure of 2.0MPa, localized corrosion was observed.

Schmitt et al. [53] stated that a change in pH from 4 to 6 had only little effect on the corrosion rate, and at pH 6, 60 °C and 25 ppm $H_2S$, protective corrosion films were formed and no localized corrosion were observed [54]. The effect seems to vanish at higher pH values (5.5-7) and higher temperatures (>80°C), when a protective film is formed. They concluded that an increase of the $CO_2$ partial pressure in the same flow system from 3.8 to 10.6 bar reduces the maximum corrosion rates from about 15 to 0.2 mm/y (Fig. 6) [55] under conditions when semi-protective films are formed, e.g. in the pH range below 5.2.

Kermani [56] expressed a reduction of corrosion rate due to formation of FeS film by a formula below.

$$F_{H2S} = 1 / (1 + 1800 (pH_2S/pCO_2)) \quad (2.31)$$

Where $F_{H2S}$ is scaling factor for corrosion reduction due to FeS precipitation. Further, in combining with the presence of $CO_2$ and $H_2S$, there is a competitive interaction between $FeCO_3$ and FeS corrosion products that may lead to localized corrosion. Subject to the type and nature of the corrosion product, $H_2S$ may lead to an increase in $CO_2$ corrosion until certain concentration threshold after which can reduce corrosion rate.

On further research, Papavinasam et al. [57], concluded that corrosion rate increased both with $H_2S$ partial pressure and with rotation speed up to approximately 500 rpm. Beyond 500 rpm, the synergism was lost and the corrosion rate decreased (at 20 psi $CO_2$). At 100-2000 rpm, corrosion rate increased due to $H_2S$ pressure until 75 psi, then decreased after that (at 20 psi $CO_2$). At 25 – 100 psi $H_2S$ pressure, corrosion rate decreased with the rotation speed until 500 rpm, and increased beyond this value (at 20 psi $CO_2$).

In combination with $CO_2$, corrosion rate of $H_2S$ showed different phenomena compared to without $CO_2$ as reported by Makarenko et al. [58]. With $CO_2$, the corrosion process is accelerated by cathodic reaction of hydrogen ion reduction. It has been proven that $CO_2$ corrosion of carbon steel increases by 1.5–2 times with increase of $H_2S$ content in the mixture (p $H_2S$<0.5 MPa) in the temperature range 20–80°C. Further increasing in $H_2S$ content (p $H_2S$≥0.5–1.5 MPa), the corrosion rate will decrease, especially in the temperature range 100–250°C, because of the influence of FeS and $FeCO_3$ on corrosion. It may relate to formation of protective film [58].

From the literature review, it is found that the mechanistic equations by Nesic et al. [54] is the feasible theories for describing effect of $H_2S$ on $CO_2$ corrosion. It should be noted here that, based on the theories, the corrosion rate can be calculated by considering overall individual anodic/cathodic reactions involving in the systems. In general, the results are considerable. However, the reasons behind effects of $H_2S$ on $CO_2$ corrosion are not fully understood, especially for the complex parameters. Current laboratory research is conducted based on individual anodic/cathodic

experiments using specific parameters which are not an accurate enough to represent multi interaction effects. Almost all researchers, in their design experiments, did not consider effect of $H_2S/CO_2$ with varying temperature and flow on corrosion rate simultaneously. In fact that the effects of $H_2S$, in $CO_2$ corrosion, are controlled by film formation or activation process depends on the $H_2S$ concentration, temperature, HAc (as a representative of main component in reservoir) and flow condition. Mostly, the researchers agreed that at the higher $H_2S$ concentration (>250 ppm), the corrosion rate will increase. But, they did not account how the corrosion behavior will change when the various values of temperature, HAc concentration and rotation speed were involved simultaneously. Studying simultaneous effects of variables will be useful to describe not only individual effects but also synergistic interaction of variables tested. The synergistic interactions of the corrosion reactions among the variables are important in $CO_2/H_2S$ corrosion prediction, but not yet fully understand.

Since no $CO_2/H_2S$ corrosion experiments consider parameters effects simultaneously in the modeling, and there are possibilities interaction effects that bring the complexities, a new experimental design technique should be conducted to investigate the following phenomena:

- How does the corrosion rate change when the corrosion parameters was involved in the experiments simultaneously?
- How does the model of corrosion rate behaves when multi interaction conditions occurs?
- Will each anodic/cathodic reaction have linear correlation with corrosion rate when experiments are conducted simultaneously?

## 2.3 Effects of HAc

### 2.3.1 Introduction

HAc is a possible catalyst in the $CO_2$ corrosion. The failures were reported in many cases and the effects of HAc on corrosion rate have been studied by many researches [59-62]. The effect of HAc on $CO_2$ corrosion is to either increase or decrease

corrosion strongly depending on pH and temperature. However, research on the combined effect of $H_2S$ and HAc in $CO_2$ system is still limited. In the literature, the effects of those factors are debatable and sometime contradictory. Therefore, it is very important to improve the understanding of carbon steel corrosion related to $CO_2/H_2S$ and HAc.

### 2.3.2 Chemistry of HAc

The structural formula of HAc is $CH_3COOH$. It is a weak acid that does not completely dissociate in aqueous solutions. It has been reported that free HAc can cause an increase of corrosion rate [60]. The mechanism of dissolved HAc in $CO_2$ corrosion can be correlated to the concentration of undissociated HAc present in the brine [62 - 63]. Laboratory tests conducted by George et al. [62] have validated that dissociated acid can alter the corrosion rate in $CO_2$ environment. The dissociation of HAc in water occurs according to the Equations 2.32 below [17]:

$$HAc_{(aq)} + H_2O \leftrightarrow H_3O^+_{(aq)} + Ac^-_{(aq)} \quad (2.32)$$

The aqueous HAc, then partly dissociation into hydrogen and acetate ions (Equations 2.33 and 2.34).

$$HAc_{(aq)} \leftrightarrow H^+_{(aq)} + Ac^-_{(aq)} \quad (2.33)$$

$$H^+_{(aq)} + e^- \rightarrow \tfrac{1}{2} H_{2(g)} \quad (2.34)$$

The equilibrium constant for HAc dissociation, $K_{HAc}$ is:

$$K_{HAc} = \frac{[H^+][Ac^-]}{[HAc]} \quad (2.35)$$

In a $CO_2$ environment with the presence of HAc, the overall corrosion reaction for carbon steel is shown in Equations 2.36 and 2.37:

$$Fe + H_2CO_3 \rightarrow FeCO_3 + H_2 \quad (2.36)$$

$$Fe + 2HAc \rightarrow Fe(Ac)_2 + H_2 \quad (2.37)$$

The dependency of HAc equilibrium constant on temperature is expressed in the following formula [17]:

$$K_{HAc} = 10^{-(6.66104 - 0.013491 T_K + 23.7856 x 10^{-6} T_K^2} \quad (2.38)$$

Where $T_K$ is temperature in Kelvin. The rate of reaction involving $CO_2$ and HAc acid is believed to be limited by the preceding slow hydration of $CO_2$ (Equations 2.39) [17]:

$$CO_2 + H_2O \rightarrow H_2CO_{3(aq)} \quad (2.39)$$

The reaction mechanism and kinetics of the overall reactions are influenced by HAc concentration, $CO_2$ partial pressure, pH, and water contaminants.

### 2.3.3 Corrosion mechanism of HAc

The effect of HAc on the corrosion of mild steel has been studied by a number of researchers. Crolet and Bonis [64] made the point that $CO_2$ induced acidification also can cause partial re-association of anions. Such weak acids then will increase the oxidizing of $H^+$ by raising the limiting diffusion current for cathodic reduction. The presence of this acid also will tend to solubilise the dissolving iron ions.

The electrochemical behavior of carbon steel on the additions of HAc has shown that the presence of HAc in the solution decreases pH, increases the cathodic limiting current, and decreases $E_{corr}$. In this condition, the cathodic reaction will become the rate determining step. The limitation is due to diffusion of proton to the steel surface rather than electron transfer. In general, it has been agreed that HAc can increase the cathodic reaction rate (hydrogen evolution reaction) if the concentration is significant.

Garsany et al. [65] published work using voltametry to study the effect of acetate ions on the rates and mechanisms of corrosion using a rotating disc electrode (RDE)

on film-free surfaces. They found a figure that can be attributed to hydrogen ion and HAc reduction on steel surface. They argued that since HAc dissociation can occur very quickly, it is not possible to distinguish the reduction of hydrogen ions from direct HAc reduction at the electrode surface. They argued that the increase of corrosion rate of HAc in $CO_2$ environment must be proportional to the concentration of undissociated HAc in the brine. They emphasized that the electrochemistry of HAc at steel cannot be distinguishable from free proton because of its rapid dissociation. This conclusion was recorded after they used a cyclic voltammetry to study the effect of $Ac^-$ ions on the rate of corrosion using rotating disk electrode.

Crolet et al. [64] suggested that the presence of HAc inhibited the anodic (iron dissolution) reaction at low concentrations of HAc (6-60 ppm). They found that the increase of corrosion rate in the presence of HAc was due to an inversion in the bicarbonate/acetate ratio. At this inversion point, HAc is the predominant acid compared to carbonic acid and is therefore the main source of acidity.

Although the data of HAc on corrosion rate has been provided by many published work in the literature and field experience as presented above, the data did not predict the interactions effects of the HAc with various conditions clearly. In fact, the prediction becomes complicated when temperature and flow condition was considered as HAc that could interfere in the $FeCO_3$ film formation. This complexity becomes another unknown problem to solve since there is no published work carried out to study the interaction effects.

### 2.3.4 Effects of HAc on carbonate film formation

An investigation of HAc role in corrosion rate on film formation was done by George [62]. The experiment succeeded in creating a film on the steel surface after exposing the specimen for three days at a temperature of $80^oC$ and high pH using LPR and EIS corrosion measurement methods to identify the effect of HAc on the cathodic and anodic reactions of $CO_2$ corrosion. He concluded that HAc does not affect the charge transfer mechanism of cathodic reaction but affects the limiting current. At room temperature ($22^oC$) the HAc acts as a source of hydrogen ions.

Vennesa et al. [66] observed that the role of HAc can retard the time to reach scaling temperature due to an increase in the area of corrosion. This argument was supported by experimental observations which showed a reduction in corrosion rate in experiments without acetate ion. There was an evidence that acetate ion can attack existing iron carbonate films and make them thinner. If the attack was localized, it would result in local film thinning, thus causing pitting corrosion. Hedges [22] published results on the role of acetate role in $CO_2$ corrosion. Experiments using both HAc and sodium acetate (NaAc) as a source of acetate ions in various media (3% NaCl and two synthetic oilfield brines) were performed using rotating cylinder electrodes. Both sources of acetate ions were shown to increase the corrosion rate, while HAc decreased the pH and NaAc increased the pH. The increased corrosion rates were attributed to the formation of thinner iron carbonate films since acetate ions have the ability to form iron acetate and transport iron away from the steel surface.

## 2.4 Prediction of $CO_2$ corrosion

Since $CO_2$ corrosion involves multi species corrosion mechanisms, numerous corrosion predictions models with different parameters and using different approaches have been developed [10, 67, 68]. Each model predicts corrosion rate in different ways. Researchers used parameters and formula from literatures, experimental data and their own experiences to construct corrosion model. The results predicted by the corrosion models may differ and sometimes contradicting. Since different results may be obtained for the same case, therefore the understanding of the basis of model development is required in order to interpret the corrosion data meaningfully. Nesic et al. [10] have classified the model into three categories: mechanistic, semi-empirical, and empirical model.

### 2.4.1 Mechanistic models

Mechanistic models use theoretical background to describe the mechanisms of reactions. It has a strong theoretical background and physical results. The main concepts of mechanistic models are the interrelation between chemical reactions and

physical changes. The mechanistic corrosion model is developed using information of standard state properties of all species, Gibbs energy and thermodynamics theory, which are applied to predict the concentration and activities of the species. It covers electrochemical reactions and diffusion process. In the case of corrosion occurring at the metal surface, it can be identified as convective diffusion, molecular diffusion, or diffusion via solid film.

Mechanistic model can also be formulated from electrochemical reactions where electrons are transferred between molecules which are called oxidation/reduction reactions. The Tafel diagram can be applied to investigate corrosion mechanisms that occur by electrochemical processes at the metal surface and transport processes for the chemical species involved. The model focuses on cathodic and anodic reactions which occur in the system involving several species. The mechanism of anodic dissolution depends on the dissolution rate and on the activity of hydroxide ions. While cathodic processes are related to the reduction of the species involved. Examples of mechanistic corrosion models are de Waard and Milliams models [8], Lee [18] and Nesic et al. [10].

Because of the large number of variables involved and their complex interactions may occur, the mechanistic model is not simple and over simplified. Parameters assumed and variables considered were not accurately modeled. Therefore, the mechanistic corrosion need to be further evaluated in laboratory for reliable performance.

### 2.4.2 Empirical models

Empirical corrosion prediction models are developed based on best-fit parameter in experimental regression. Empirical models are usually developed by involving several fixed variables. However, in subsequent considerations, other factors are added to give a better correction factors. There have been a number of empirical models developed based on field experience and laboratory data. French et al. [69] have investigated corrosion film characteristics of gas wells containing $CO_2$ in the range temperature from 20 to 149$^{o}$C. Smith [70] developed a model for a slightly sour system. The model shows various corrosion products of steel formed in the presence

of $CO_2$ as a function of temperature and partial pressure of $H_2S$. Nyborg [71] has recently reviewed an empirical model to estimate the corrosion rate using two variables; temperature and partial pressure of $CO_2$. Norsok M-506 [72] is an empirical model based on experiments conducted in a single phase water flow loop. The experiment data cover effects of pH, $CO_2$ fugacities, wall shear stresses,the temperature range from 5$^o$C to 150$^o$C. The newest empirical model of $CO_2$ corrosion was reported by Martin [60] and Ismail [61]. However, the use of use pure empirical model is not efficient. Empirical model needs a large and reliable experimental database that takes long duration time and costly.

### 2.4.3 Semi-empirical models

Semi empirical models are developed using parameters and formula from literatures and based on the researchers' own experiences. There are many equations that predicts the corrosion rate in $CO_2$ environments. These include the de Waard [72] and its many subsequent derivatives, Yuhua [74], Vera [39] and George et al. [62]. All of these were developed based on different systems and assumptions. Some corrosion predictions softwares that have been developed based on semi-empirical approach are discussed herewith.

- *ECE (Electronic Corrosion Engineer)*

ECE [75] program software calculates corrosion rate based on the modified de Waard and Milliams method [8]. ECE model includes oil wetting correlation based on field correlation. For low horizontal flow velocities < 1 m/s, the $F_{oil}$ =1. ECE proposes a corrosion prediction expression as follows:

$$V_{cor} = \frac{1}{\frac{1}{V_r} + \frac{1}{V_m}} \tag{2.40}$$

Where, $V_r$ is corrosion reaction and $V_m$ is mass transfer effect.

The corrosion reaction can be calculated using the following equation:

$$\log V_r = 4.84 - \frac{119}{T+273} + 0.581\log(f_{CO_2}) - 0.34(pH_{act} - pH_{CO_2}) \quad (2.41)$$

And the mass transfer variable is defined as:

$$V_m = 2.8\frac{U^{0.8}}{d^{0.2}} f_{CO_2} \quad (2.42)$$

Where; $T$ is temperature ($^oC$), $f_{CO2}$ is fugacity $CO_2$ (bar), $pH_{act}$ *is pH* actual, $pH_{CO2}$ is the pH of pure water saturated with $CO_2$ at prevailing temperature and pressure.

The fugacity of $CO_2$ is similar to its partial pressure, but corrected for non-ideality of $CO_2$ at high pressure and temperature. The mass transfer represents the main part of the dependence on flow velocity U and pipe diameter d.

- *Cassandra (DWM 93)*

Cassandra [76] is developed based on the experiences of de Waard and Milliams [8]. The input includes pH, $CO_2$ concentration, temperature, and water contaminant. This model does not consider scaling temperature. The user must set an assumption of the scaling temperature. The basic formula to calculate corrosion rate is expressed as in Equation 2.51 below:

$$\log(V_r) = 5.8 - 1710/T + 0.67\log(P_{CO_2}) \quad (2.43)$$

This model can be used to calculate effects of corrosion inhibitor availability and corrosion risk categories on corrosion rate. The model also accounts for the presence of acetate in water as HAc.

The major input to the model are: $CO_2$ mole %, temperature, total pressure, liquid velocity and water chemistry. Besides that, the model has secondary input, such as hydraulic diameter and glycol concentration, oil type (crude or condensate) and water type (condensed water or formation water). The effect of oil wetting in this model is

not included. Semi empirical model is developed both based on best fit parameters and theoretical background to understand physical parameters. Same with description presented above, semi empirical model needs large experiments database used to either model regression and to find fundamentals variables involved.

From the brief model description presented above, it is clear that for an improved empirical, semi empirical and mechanistic model, a better understanding of both design of experiment (DOE) and mechanistic of $CO_2$ corrosion theory is crucially needed. Using DOE, an optimum model improvement can be achieved efficiently. The present research work will develop a $CO_2$ corrosion model founded on fundamental theory and systematic statistics approaches that expresses relationship between the reservoir species (HAc, $H_2S$) and operational conditions (temperature, pH, flow condition).

## 2.5 Simulation of Flow Analyses

Flow-induced corrosion is a type of corrosion caused by a combination of mechanical and electrochemical effects. Mechanical effects due to water motion causes impingement that leads to metal removal and material abrasion. Water that flows to the surface can wear the corrosion product film or create shear stress to the surface. Corrosion rate also can increase due to effects of differences in velocity turbulence across the surface. Parallel flow can also reduce thickness of the boundary layer, thus allowing active species to reach the metal surface quickly. Parameters that influence flow induced corrosion are hydrodynamic boundary layer and rate of momentum transfer from the bulk to the wall. In this condition, corrosion may be controlled by the rate of mass transfer of a reactant or the rate of corrosion products [36].

### 2.5.1 The uses of rotating cylinder electrode to simulate flow induced corrosion

Rotating Cylinder Electrode (RCE) has been widely used to simulate flow in the pipeline. RCE is an alternative corrosion test that can be used to simplify flow induced corrosion phenomena from flow loop system [35]. Laboratory flow loop

system requires complex arrangements and is expensive to maintain. RCE is a simple equipment that can be used to study corrosion process under velocity and turbulent conditions. By using RCE, fluid flow effects on corrosion can be simulated in the laboratory and it is possible to control the hydrodynamic conditions that occurs on the surface of the metal sample.

### 2.5.2 Turbulent and mass transport in RCE experiments

At high rotation flow, the solution flow will have complex mechanism creating several model flows [32]. The shear stress on the sample surface becomes significant to form turbulent flow. The transition from laminar flow to turbulent flow can be related to Reynold's number as in the following equation [38]:

$$\mathrm{Re} = ul/\nu \tag{2.44}$$

$$\nu = \mu/\rho \tag{2.45}$$

Where $\rho$ is the solution density (g $cm^{-3}$), and $\mu$ is the absolute viscosity of the solution (g $cm^{-1}s^{-1}$).

The linear velocity, $U_{cyl}$ ($cms^{-1}$), at the outer surface of the cylinder is given by $U_{cyl} = \omega\, r_{cyl} = \pi\, d_{cyl}\, f\, /2$

Where the rate can be expressed either as angular rotation rate, $\omega$ *(rad* $s^{-1}$*)*, or as $f$ (rpm). In general, turbulent flow will be achieved by rotating cylinder when the Reynold's number is greater than 200 or 20 rpm.

This turbulent flow creates a concentrated solution near the metal surface from the bulk solution, thus a concentration gradient is formed. This condition can be a factor that governs corrosion behavior as an effect of oxygen transport. Corrosion reaction occurs at the solution through diffusion mechanism. Thus the current can be limited by rate of diffusion reactions. The diffusion limited current density is given by:

$$i = -FD\left(\frac{dc}{dx}\right) \tag{2.46}$$

Where $\frac{dc}{dx}$ is concentration gradient.

For the maximum of concentration gradient, the diffusion limited current density can be written as:

$$i_{\lim} = -FD\left(\frac{c_{bulk} - c_{x=0}}{\delta}\right) \tag{2.47}$$

Where: $i_L$ is limiting current for anodic reaction, $C_{bulk}$ is bulk concentration of cathodic current, $\delta$ is diffusion layer thickness, $D$ is coefficient of diffusion and $F$ is Faraday's constant.

As reported by Eisenberg [77] the most commonly accepted description for RCE mass transport, particularly, the mass transfer coefficient, $Km$ ($cms^{-1}$) to a rotating cylinder is given by the following relationship:

$$\begin{aligned} K_m &= (D / d_{\text{cyl}})\, S_h \\ &= (D / d_{\text{cyl}})\, (0.0791\, R_e^{0.7}\, S_c^{0.356}) \end{aligned} \tag{2.48}$$

Where the diffusivity, $D$ ($cm^2s^{-1}$), is usually taken as the diffusion coefficient for the molecule or ion undergoing mass transport, and $S_h$ and $R_e$ are the dimensionless Sherwood's and Reynold's numbers, respectively. The Schmidt number, $S_c = \mu / (\rho D)$, is also a dimensionless number. The overall mass transfer coefficient to an RCE can be expressed in one of three forms [37]:

$$K_m = 0.0791\, d_{\text{cyl}}^{\ -0.3}\, (\mu / \rho)^{-0.344}\, D^{+0.644}\, U_{\text{cyl}}^{\ +0.7} \tag{2.49}$$

In general, the mass transport limited current density, $j_{lim}$ (A cm$^{-2}$), observed in an electrochemical experiment is related to the mass transfer coefficient by the following relationship,

$$J_{\text{lim}} = i_{\text{lim}} / A = z\,F\,C\,Km \tag{2.50}$$

Combining Equation 2.49 and Equation 2.50, the mass transport limited current density can be expressed as follows:

$$\begin{aligned} j_{\text{lim}} &= 0.0791\, z\,F\,C\,d_{\text{cyl}}{}^{-0.3}\,(\mu/\rho)^{-0.344}\,D^{0.644}\,U_{\text{cyl}}{}^{0.7} \\ &= 0.0487\, z\,F\,C\,d_{\text{cyl}}{}^{+0.4}\,(\mu/\rho)^{-0.344}\,D^{0.644}\,\omega^{0.7} \end{aligned} \tag{2.51}$$

Where $F$ is Faraday's Constant (96484.6 C / mol), $i_{lim}$ (Ampere) is the limiting current, and $A$ (cm$^2$) is the area of the electrode. To make full quantitative use of this relationship, both the number of electrons exchanged, $z$, and the bulk concentration, $C$ of the ion or molecule involved in the electrochemical process must be known.

### 2.5.3 Wall shear stress for RCE

Shear stress is a stress, which is either parallel or tangential to the surface of a material. The physical quantity of shear stress is measured in force divided by area. In fluid flow, fluid moving along a surface will cause a shear stress on that surface. In a no-slip condition, the fluid will have zero velocity relative to the boundary. The fluid velocity at all liquid–solid boundaries is equal to that of the solid boundary. The speed of the fluid at the boundary (relative to the boundary) is 0, but at some height from the boundary the flow speed must equal that of the fluid. The region between these two points is named the boundary layer. The shear stress can be expressed as [36]:

$$\tau_w = \mu \left.\frac{\partial U}{\partial Y}\right|_{y=0} \tag{2.52}$$

Where $\mu$ is the dynamic viscosity of the fluid, $U$ is the velocity of the fluid along the boundary and $Y$ is the height of the boundary. The turbulent flow at the RCE

induces a wall shear stress on the surface of the cylinder. Again, Eisenberg reported a well-accepted equation for the wall stress, $\boldsymbol{\tau}_{cyl}$ (g $cm^{-1}$ $s^{-2}$):

$$\boldsymbol{\tau}_{cyl} = 0.0791\ \rho\ R_e^{-0.3}\ U_{cyl}^{2} \tag{2.53}$$

Where $\boldsymbol{\tau}_{cyl}$ is wall stress, $\rho$ is density, *Re* is Reynold's number and $U_{cyl}$ is velocity. There are relationships between rotation speed and wall shear stress for RCE are calculated and tabulated in Table 2.1.

Table 2.1 Hydrodynamic Computations for a Typical Rotating Cylinder Electrode in Water [78]

| N (rpm) | ω (rad / sec) | $U_{cyl}$ (cm / sec) | $\tau_{cyl}$ (g $cm^{-1}$ $s^{-2}$) | $R_e$ (unitless) |
|---|---|---|---|---|
| 5 | 0.524 | 0.31 | 0.0025 | 42 |
| 10 | 1.047 | 0.62 | 0.0082 | 84 |
| 20 | 2.094 | 1.26 | 0.0267 | 169 |
| 50 | 5.236 | 3.14 | 0.1270 | 422 |
| 100 | 10.47 | 6.28 | 0.4125 | 844 |
| 200 | 20.94 | 12.6 | 1.3402 | 1688 |
| 500 | 52.36 | 31.4 | 6.3631 | 4219 |
| 1000 | 104.7 | 62.8 | 20.674 | 8438 |
| 2000 | 209.4 | 125.7 | 67.169 | 16876 |
| These quantities assume a typical RCE tip with outer diameter 1.2 cm rotating in water at 25ºC. For pure water at 25ºC, the density is 0.997 g cm–3 and the absolute viscosity is 0.00891 g $cm^{-1}$ $s^{-1}$. | | | | |

## 2.6 Design of Experiment (DOE) and Statistical Modeling

Empirical models have been used to predict corrosion process involving several independent variables. However, most of the empirical models do not predict the corrosion rate in the presence of several variables simultaneously [61]. Generally, corrosion experimental data are limited by determination of dependent factors. Most researchers use selected dependent variables based on specific interval variables which have not been well verified (planned interval test). This is a simple method and believed to represent overall unselected variables, but, this method lacks statistical analysis that supports the conclusion.

In fact, there have been many theoretical papers on statistical analyses with response surface methodology technique published the last decade [79-82]. Although those papers have discussed response surface design in the research, there are not many applications of response surface methodology in corrosion processes were published, especially corrosion in $CO_2$ system and $CO_2/H_2S$/HAc system. There was one paper registered for NACE conference in 2009 [68] discussed corrosion mechanism of mild steel in the presence of $CO_2$, $O_2$ and inhibitor. However, the paper did not consider for other various conditions, especially corrosion that occurs in the presence of HAc and $H_2S$. In order to identify the key mechanism influencing $CO_2$ corrosion simultaneously, the effects of main parameters such as HAc, temperature, pH, and flow are still under investigation and need more widely reviewed by researchers.

### 2.6.1 Design of experiments (DOE) and response surface methodology (RSM)

The application of response surface methodology (RSM) allows a visualization of the experimental results in a 3-D display [83]. RSM is used to determine optimal levels for variables input. RSM is a sequential procedure for constructing empirical relation for the experimental data. Using response information, the optimum data between factors can be developed and model improvements can be achieved. It has been proven that researchers have used response surface method (RSM) to process data systematically that can allow to apply multiple regression simultaneously[68, 84]. Response surface design methodology is also often used to refine models to obtain an optimum design. Using RSM, the following advantages can be obtained [84].

- Displays region of an experimental result in the form of response surface. Response surface obtains the equation models that inform changes in input variables, which influence a response of interest.
- Selects the operating conditions to meet specifications.

### 2.6.2 Types of response surface designs

There are several types of response surface design in literature. Generally, each model is developed based on the number of experiments and the number of design variations that can be constructed. The following are four types of RSM design.

- *CCD*

CCD is appropriate for incorporating the full quadratic models. CCD consists of a factorial design (the corners of a cube) together with *center* and axial points that allow for estimation of second-order effects. For a full quadratic model with $n$ factors, CCD sets ($2^n + 2n + 1$) minimum number of experimental running for estimating and ($n + 2$)($n + 1$)/2 for number of coefficients [81]. The central CCD comprises $2^n$ factorial points taken from a full factorial at levels ± 1, 2n axial points at locations ± α, and $n_C$ the center point of origin. Figure 2.1 illustrates a CCD for three variables. Box and Hunter [83] have discussed and calculated the values for α and central point needed to run the experiments.

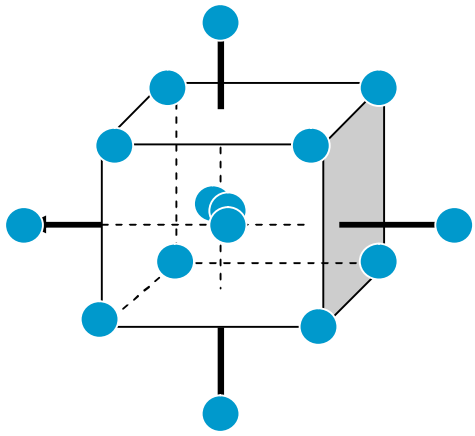

Figure 2.1 Location of experiments running in CCD for 3 variables [83].

- *Box-Behnken design*

Box-Behnken design (BBD) [83] typically has fewer design points, therefore it has less experiments to run. BBD is an appropriate design to estimate the first-order coefficients. In estimating second model regression, Box-Behnken designs are not recommended. Box-Behnken designs are rotatable and suitable for a small number of factors that require fewer runs than CCD. By avoiding the corners of the design space, BBD will reduce experimental cost compared to CCD.

- *Factorial Experiments*

Full factorial designs measure response variables using every treatment (combination of the factor levels). A full factorial design for *n* factors with $N_1$, ..., $N_n$ levels requires $N_1 \times ... \times N_n$ experimental runs for each treatment. Fractional factorial designs use a fraction of the runs required by full factorial designs. Factorial design is selected based on an assumption of which factors and interactions have the most significant effects. The factorial experiment does not have center points and no replicates. Therefore, there are only limited experimental runs [83].

- *Plackett-Burman Designs*

Plackett-Burman designs are used when only the main effects are considered significant. Two-level Plackett-Burman designs require less number of experimental runs.

### 2.6.3 Determination of the stationary conditions

RSM is useful to obtain critical points in the experimental variables. The surfaces generated by linear or polynomial models will be used to indicate the direction in which the original design must be started to attain the optimal conditions. For polynomial models, the critical point can be characterized as maximum, minimum, or saddle. Using RSM, it is possible to calculate the coordinates of the critical point through the first derivative of the mathematical function. First derivative equals to zero indicates that critical points is located.

### 2.6.4 Model estimation

Model estimation is a type of model used to predict trend of data [84]. The model order is an important factor in making model regression that relates independent variables. There are common fitting regression model that can be used to predict trend.

$$\text{Linear} \quad : Y = B_0 + B_1X_1 + B_2X_2 + \ldots .. \; B_kX_k \tag{2.54}$$

$$\text{Power} \quad : Y = B_0(X_1^{B1})(X_2^{B2}) \ldots\ldots\ldots .. \; (X_k^{Bk}) \tag{2.55}$$

Exponential : $Y = B_0(B_1^{X1})(B_2^{X2}) \ldots\ldots\ldots (B_k^{Xk})$ (2.56)

- **Linear model estimation**

The response is modeled as linear combination functions of the predictor, plus a random error $\varepsilon$. The expressions $f_j(\boldsymbol{x})$ ($j$ = 1, ..., $p$) are the *terms* of the model. The $\beta_j$ ($j$ = 1, ..., $p$) are the *coefficients*. The errors, $\varepsilon$ are assumed to be uncorrelated and distributed with mean 0 and constant variance.

The estimated linear model is given by:

$$Y = b_0 + b_1X_1 + b_2X_2 + \ldots b_kX_k. \quad (2.57)$$

Where, $Y$ = response or independent variable, $b$ = coefficient variables and $x$ = dependent variables.

- **Multiple linear regression**

If the predictor $\boldsymbol{x}$ is multi dimensional, the functions $f_j$ that form the terms of the model, consist of several functions. The model might include $f_1(\boldsymbol{x}) = x_1$ (a linear term), $f_2(\boldsymbol{x}) = x_1^2$ (a quadratic term), and $f_3(\boldsymbol{x}) = x_1x_2$ (interaction term). Response variable $y$ is modeled as a combination of constant, linear, interaction, and quadratic terms formed from two predictor variables $x_1$ and $x_2$. Uncontrolled factors and experimental errors are modeled by $\varepsilon$. Given the data for $x_1$, $x_2$, and $y$, *regression* estimates the model parameters $\beta_j$ ($j$ = 1, ., $n$).

There is a curvature of general second order model which is expressed as [83]:

$$Y = \beta_0 + \sum_{i=1}^{k} \beta_i X_i + \sum_{i=1}^{k} \beta_{ii} X_i^2 + \sum_{i<j} \sum \beta_{ij} X_i X_j + \varepsilon \quad (2.58)$$

Where $Y$ = response that can fit the following linear, quadratic, or cubic regression models, $\beta$ = regression constant, $X_i$ *and* $X_j$ = main effect of dependence factors, and $X_iX_j$ = interaction effects between dependence factors.

- **Power and exponential model regression**

To estimate the power model, ln(Y) is regressed on $\ln(X_1)$, $\ln(X_2)$, . . . , $\ln(X_k)$. Coefficients for the original predictor variables are $b_0 = \exp(b0')$ and bi = bi', for i = 1, . . . , k. The estimated power regression model is given by:

$$Y = b_0(X_1^{b1})(X_2^{b2}) \ldots (X_k^{bk}). \quad (2.59)$$

Exponential model regression can be estimated using ln(Y) regressed on $X_1, X_2, \ldots X_k$. Coefficients for the original predictor variables are:

$b_i = \exp(b_i')$ , i = 0, . . . , k. The estimated exponential model is:

$$Y = b_0(b_1^{X1})(b_2^{X2}) \ldots (b_k^{Xk}). \quad (2.60)$$

### 2.6.5 Calculation of regression coefficients

In experiments, there are observed variables called responses, and variables that can be adjusted called predictors. Those two parameters can be entered to the data matrices as [83]:

Predictors : $X_{nx(k+1)}$ = $[\ 1\ X_{n1}\ X_{n2} \ldots X_{nk}\ ]$

$[\ 1\ X_{11}\ X_{12} \ldots X_{1k}\ ]$

$[\ 1\ X_{21}\ X_{22} \ldots X_{2k}\ ]$

Response : $Y_{x1}$ = $[\ Y_1, Y_2, \ldots\ldots, Y_n\ ]$

Unit vector : $U_{x1}$ = $[\ 1, 1, \ldots\ldots\ldots, 1\ ]$

The estimated regression coefficient *(b)* for the model is calculated using the least squares method to fit the regression model, and is given by the equation:

$$b = [X^T.X]^{-1}.X^TY \quad (2.61)$$

Then,

$$\hat{y} = Xb \quad (2.62)$$

$$e = Y - \hat{y} \quad (2.63)$$

### 2.6.6 Model accuracy measurement

#### 2.6.6.1 Model adequacy

To check how accurately the model describes the data and predicts a response, there are common parameters that can be used to observe the data. To check model performance, the following model assumptions should be met [83]:

- Linearity – The true relationship between the mean of the response variable e *(Y)* and the explanatory variables $x_1, \ldots, x_k$ is a straight line.
- The random errors, $\varepsilon_i$, are independent, identically distributed random variables with distributions.

The assumption of the linearity and random error are analyzed using [83]:

- *Normality Assumption*

  The normality plot for assessing data set is approximately normally distributed. Normality plot shows a normal distribution centered at zero for the normality assumption.
- *Residuals vs. Time Sequence*

  The plot of residuals vs. time sequence is used to determine residuals correlation or dependency of residuals in time sequence. A positive correlation is represented by runs of positive and negative residuals which are translated as independent assumptions on the errors.
- *Residuals vs. Fitted Values*

  The better model, plot of residuals versus fitted values should exhibit no particular structure. A plot with no obvious pattern indicates residuals are unrelated to any other variables.
- *Residual plots*

  It is used to examine the goodness of a model fit in regression and ANOVA. Examining residual plots to determine the least squares assumptions are being met.

### 2.6.6.2 Model validation

Model validation of empirical model equation is used to evaluate experimental data which referred to proven data. The accuracy and precision of the model is represented as [83]:

- *Residual*

The residual sum of squares is the variation attributed to the error. The larger this value is, the better the relationship explaining data.

Residual (e) is defined by:

$$e = y - \hat{y} \tag{2.64}$$

- *Coefficient determination*

Coefficient determination $(R^2)$is defined as [83]:

$$R^2 = \frac{ss_{reg}}{ss_{total}} = \frac{\sum\left(\hat{y} - \bar{y}_i\right)}{\sum\left(y_i - \bar{y}_i\right)} \tag{2.65}$$

Where $y_i$ = observed response, $\hat{y}_i$ = predicted response value, $\bar{y}_i$ = mean response and $SS_{reg}$ = sum of square of regression, $SS_{total}$ = sum of square of total.

In matrix form, scalars $SS_{reg}$ and $SS_{total}$ are calculated and used to obtain the coefficient of determination $R^2$ (goodness-of-fit), sum square of error ($SS_e$) and $F_{stat}$ (statistical significance) as follows [83]:

$$SS_{reg} = b^T X^T Y - (1/n)(Y^T U U^T Y) \tag{2.66}$$

$$SS_e = Y^T Y - b^T X^T Y \tag{2.67}$$

$$SS_{total} = Y^T Y^T - (1/n)(Y^T U U^T Y) \tag{2.68}$$

$$R^2 = SS_r/SS_{total} \tag{2.69}$$

$$F_{stat} = (SS_r/k)/(SS_e/(n-k-1)) \tag{2.70}$$

- *P-value*

It determines the appropriateness of rejecting the null hypothesis in a hypothesis test. P-values range from 0 to 1. A commonly used p-value is 0.05. If the p-value of a statistical testis less than the setting *(α)*, the null hypothesis is rejected. A null hypothesis is when there is no effect of the variables to the response [83].

- $F_{stat}$

It is a hypothesis test that examines the ratio of two variances to determine their equality that can evaluate distribution of data. If the observed F-statistic exceeds the critical value, the null hypothesis is rejected. That other equation is more commonly shown in an equivalent form [83]:

$$F_{stat} = \frac{(SS_1 - SS_2)/(DF_1 - DF_2)}{SS_2 / DF_2} \tag{2.71}$$

Where, $SS_i$ = Sum of square of variable $i$ and $DF_i$ = Degree of freedom of variable i.

- *Correlation*

The correlation coefficient allows researchers to determine if there is a possible linear relationship between two variables measured on the same subject [83].

$$S_{xy} = \frac{\sum\left(x-\bar{x}\right)\left(y-\bar{y}\right)}{\sqrt{\sum\left(x-\bar{x}\right)^2 \sum\left(y-\bar{y}\right)^2}} \tag{2.72}$$

Where $S_{xy}$ is correlation, $y$ and $x$ are the response prediction and experimental results respectively. While $\bar{y}$ and $\bar{x}$ are response prediction and average experimental results sample mean respectively.

- *Standard error*

The standard error for the predicted response is calculated by:

$$St.error = \frac{y_i - \hat{y}_i}{y_i} \tag{2.73}$$

The variable *St.error* is a standard error of the response while $y_i$ and $\hat{y}$ are the response variable and response variable predicted respectively.

In order to develop a model that considers effects of species and operation conditions on corrosion rate simultaneously, it is important to select a statistical methodology that can be applied in $CO_2$ corrosion. In this research, a statistical technique of RSM is proposed for the construction of an empirical model that relates effects of HAc, temperature, and rotation speed on $CO_2$ and $H_2S$ environments. The RSM offers the best alternative to study the corrosion rate of carbon steel in $CO_2$ environments. In addition to, RSM can also be combined with mechanistic theories to analyze experimental data efficiently. Once the data were collected, the data were generalized using least sum square method to estimate the parameters in regression model. Then, the model was validated and verified with proven data to quantify the performance of the model.

# CHAPTER 3

# RESEARCH METHODOLOGY

The research methodology can be divided to the three main steps; modeling design of the experiment, experimental work, and model development and evaluation. The first step was conducted by screening suitable design experiment and identifying historical data variables to find the trending of the $CO_2$ corrosion model. Historical data was provided by $CO_2$ corrosion database and calculation from mechanistic theory. Once $CO_2$ corrosion trending was found, the best type of experiment design and the model regression can be selected. The next step involved the experimental work based on design of experiment to develop the model. In order to evaluate the model performance, the model was verified with published experimental data and corrosion software calculation. The model performance was stated by the value of standard error estimation, coefficient determination and correlation that represents the accuracy and precision of the model compared to the data provided. The steps are summarized in Figure 3.1.

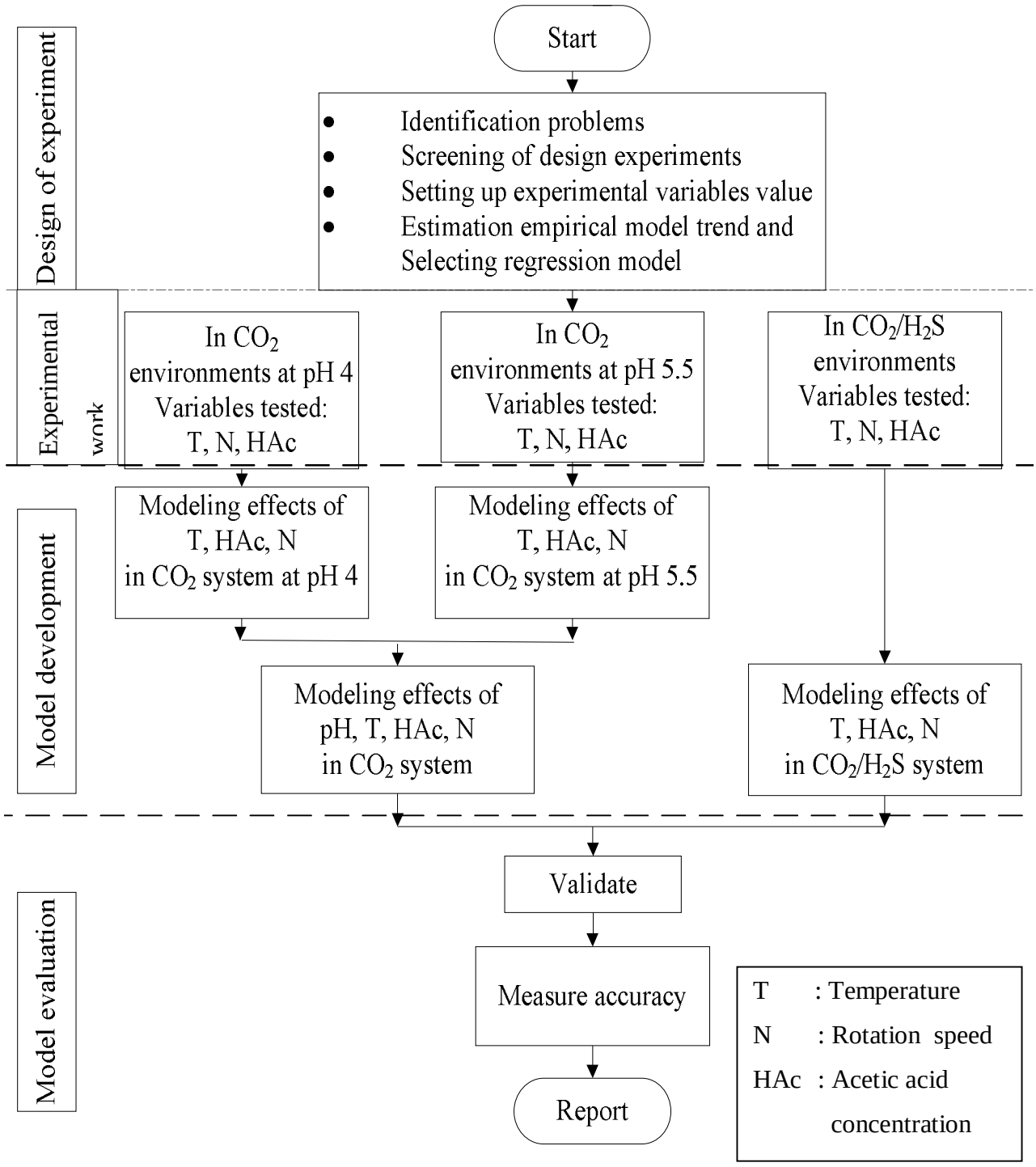


Figure 3.1 Flow chart of the research methodology.

## 3.1 Design of Experiment

Design of experiment (DOE) is used to plan experiment in order to obtain the results that can be analyzed analytically and proven statistically. Thus, the individual and interaction effects from the experiment can be analyzed simultaneously. Using design of experiment allows controlling the independent and dependent variables to meet the statistical criteria. This experiment used central composite design (CCD) to model the $CO_2$ corrosion model. CCD is designed to build a second order (quadratic) model for the response variable without performing full randomized variables in the experiment. In other cases, full factorial design (FFD) was applied in the calculation by combining the experimental data conducted in condition at pH 4 and pH 5.5. A full factorial experiment is an experiment whose design consists of two levels which can be applied to predict effect of pH as independent variables. The pH values used to study corrosion rate are similar to many field operation conditions [1,2].

### 3.1.1 Selection of Experimental Factors

Before designing the experiments that will be used for the corrosion RSM model, the corrosion problem and available design experiment must be identified. This stage is conducted by screening the variables values that will be used in design experiments in order to obtain a RSM model that can represent the behavior of output response. The RSM model output will be analyzed using DOE. In this research, CCD and FFD were selected to study $CO_2$ corrosion. CCD was used to construct a $CO_2$ corrosion model with temperature, HAc and rotation speed as independents variables. While, FFD was to construct model which involving pH as an additional independents variables including temperature, HAc and rotation speed.

The first step to construct the RSM model is to determine a possible model trend. Initially, corrosion model trends were identified in correlation with the selected factors mechanistically. This was performed by studying the history of the corrosion data and examining their behavior from corrosion mechanistic theories. The corrosion model can be developed when the factors affecting $CO_2$ corrosion are known. The factors tested are presented in Table 3.1.

Table 3.1 Experimental Parameters

| | |
|---|---|
| Purged gas | $CO_2$, $N_2$, $CO_2/H_2S$ (300 ppm $H_2S$) |
| Total pressure | Atmospheric |
| HAc concentration | 0 to 340 ppm |
| Temperature | 22 to 80°C |
| Rotation rate (N) | 0 rpm to 6000 rpm |
| pH | 4.0 and 5.5 |
| Measurement techniques | Potentiodynamic sweeps (PS),<br>Linear polarization resistance (LPR),<br>Electrochemical impedance spectroscopy (EIS) |

The experimental variables values selected in the experiments were based on considerations that those values are similar to which found in many field production conditions. It was recorded that the natural gas produced in many other locations around the world have $H_2S$ content in the range of 0 -1000 ppm and HAc concentration that reaches 800 ppm [1-5]. While operating conditions such as temperature is from 22 to 120$^oC$ [4]. Many researchers have studied effects of those species variables on corrosion rate, so data provided by previous researchers can be used for additional corrosion information and for model evaluating to show the methodology performances which used in this experiments.

### 3.1.2 Variable coding and experimental design

A CCD, with three variables, was used to study the response pattern and to determine the combined effect of variables. The effect of the independent variables of HAc concentration, temperature and rotation speed in $CO_2$ environments are shown in Table 3.2. Table 3.3 was used to study effects of HAc, Temperature and rotation speed in $CO_2/H_2S$ environments. In order to make variables in the experiments vary in the same range, the value of variables should be in coding value. This code value is also important in controlling the result to meet a normal distribution pattern [85]. The variables were coded according to the following equation [85].

$$x_{code} = \frac{2(X - X_{high})}{(X_{high} - X_{low})} + 1 \qquad (3.1)$$

Where

$x_i$ = dimensionless value of an independent variable

$X_i$ = real value of an independent variable

Table 3. 2 Natural and coded independent variables used in RSM to study corrosion rate in $CO_2$ system.

| Level | Code | HAc (ppm) | T ($^oC$) | N (rpm) | pH |
|---|---|---|---|---|---|
| Axial point | √3 | 340 | 80 | 6000 | - |
| High | 1 | 270 | 70 | 4000 | 5.5 |
| Centre | 0 | 170 | 50 | 2000 | 5 |
| Low | -1 | 70 | 35 | 1000 | 4 |
| Axial point | -√3 | 0 | 22 | 500 | - |

Table 3.3 Natural and coded independent variables used in RSM to study for $CO_2/H_2S$ system.

| Level | Code | T ($^oC$) | HAc (ppm) | N (rpm) |
|---|---|---|---|---|
| Axial point | √3 | 80 | 136 | 6000 |
| High | 1 | 70 | 108 | 4000 |
| Centre | 0 | 50 | 68 | 2000 |
| Low | -1 | 35 | 28 | 1000 |
| Axial point | -√3 | 22 | 0 | 500 |

### 3.1.3 Setting up experimental design

The technique used to calculate independent variables simultaneously and to estimate model regression of $CO_2$ corrosion was response surface methodology. In this method, the independent variables are calculated based on matrices operations to find

regression equations. The following Table 3.4 was an experimental matrix designed using RSM method to obtain $CO_2$ corrosion equations at pH 4 and pH 5.5.

Table 3.4 CCD experimental design matrix with three variables (coded and natural) used to study the response pattern and to determine the effects of combined variables

| Experimental points | No. of run | Coded variables | | | Natural variables | | |
|---|---|---|---|---|---|---|---|
| | | HAc | T | N | HAc (ppm) | T ($^oC$) | N (rpm) |
| Factorial points | 1 | 1 | 1 | 1 | 270 | 70 | 4000 |
| | 2 | -1 | 1 | 1 | 70 | 70 | 4000 |
| | 3 | 1 | -1 | 1 | 270 | 35 | 4000 |
| | 4 | -1 | -1 | 1 | 70 | 35 | 4000 |
| | 5 | 1 | 1 | -1 | 270 | 70 | 1000 |
| | 6 | -1 | 1 | -1 | 70 | 70 | 1000 |
| | 7 | 1 | -1 | -1 | 270 | 35 | 1000 |
| | 8 | -1 | -1 | -1 | 70 | 35 | 1000 |
| Axial points | 9 | √3 | 0 | 0 | 340 | 50 | 2000 |
| | 10 | -√3 | 0 | 0 | 0 | 50 | 2000 |
| | 11 | 0 | √3 | 0 | 170 | 80 | 2000 |
| | 12 | 0 | -√3 | 0 | 170 | 22 | 2000 |
| | 13 | 0 | 0 | √3 | 170 | 50 | 6000 |
| | 14 | 0 | 0 | -√3 | 170 | 50 | 500 |
| Centre points | 15 | 0 | 0 | 0 | 170 | 50 | 2000 |
| | 16 | 0 | 0 | 0 | 170 | 50 | 2000 |
| | 17 | 0 | 0 | 0 | 170 | 50 | 2000 |
| | 18 | 0 | 0 | 0 | 170 | 50 | 2000 |

Table 3.5 shows a FFD design where the experimental matrix arrangement where data were taken from the factorial design within CCD matrix at pH 4 and pH 5.5. As can be seen from the Table 3.4 and Table 3.6, that, in CCD, the experiments consist of 8

runs as a factorial, 6 runs as a axial points that used to extend the model regression, and 4 runs as a repetition to evaluate repetitions of the experiment.

Table 3.5 Factorial experimental design matrix with four variables (coded and natural) used to study the effect of pH on $CO_2$ corrosion.

| No. of run | Coded variables | | | | Natural variables | | | |
|---|---|---|---|---|---|---|---|---|
| | pH | T | HAc | N | pH | T ($^oC$) | HAc (ppm) | N (rpm) |
| 1 | -1 | -1 | -1 | -1 | 4 | 22 | 0 | 1000 |
| 2 | 1 | -1 | -1 | -1 | 5.5 | 22 | 0 | 1000 |
| 3 | -1 | 1 | -1 | -1 | 4 | 60 | 0 | 1000 |
| 4 | 1 | 1 | -1 | -1 | 5.5 | 60 | 0 | 1000 |
| 5 | -1 | -1 | 1 | -1 | 4 | 22 | 60 | 1000 |
| 6 | 1 | -1 | 1 | -1 | 5.5 | 22 | 60 | 1000 |
| 7 | -1 | 1 | 1 | -1 | 4 | 60 | 60 | 1000 |
| 8 | 1 | 1 | 1 | -1 | 5.5 | 60 | 60 | 1000 |
| 9 | -1 | -1 | -1 | 1 | 4 | 22 | 0 | 6000 |
| 10 | 1 | -1 | -1 | 1 | 5.5 | 22 | 0 | 6000 |
| 11 | -1 | 1 | -1 | 1 | 4 | 60 | 0 | 6000 |
| 12 | 1 | 1 | -1 | 1 | 5.5 | 60 | 0 | 6000 |
| 13 | -1 | -1 | 1 | 1 | 4 | 22 | 60 | 6000 |
| 14 | 1 | -1 | 1 | 1 | 5.5 | 22 | 60 | 6000 |
| 15 | -1 | 1 | 1 | 1 | 4 | 60 | 60 | 6000 |
| 16 | 1 | 1 | 1 | 1 | 5.5 | 60 | 60 | 6000 |
| 17 | -1 | 0 | 0 | 0 | 4 | 35 | 40 | 3000 |
| 18 | 1 | 0 | 0 | 0 | 5.5 | 35 | 40 | 3000 |
| 19 | 0 | -1 | 0 | 0 | 5 | 22 | 40 | 3000 |
| 20 | 0 | 1 | 0 | 0 | 5 | 60 | 40 | 3000 |
| 21 | 0 | 0 | -1 | 0 | 5 | 35 | 0 | 3000 |
| 22 | 0 | 0 | 1 | 0 | 5 | 35 | 60 | 3000 |
| 23 | 0 | 0 | 0 | -1 | 5 | 35 | 40 | 1000 |
| 24 | 0 | 0 | 0 | 1 | 5 | 35 | 40 | 6000 |

Table 3.6 CCD experimental design matrix with three variables (coded and natural) used to study corrosion in $CO_2/H_2S$ system.

| Experimental points | No of run | Coded variables | | | Natural variables | | |
|---|---|---|---|---|---|---|---|
| | | HAc | T | N | HAc (ppm) | T ($^oC$) | N (rpm) |
| Factorial points | 1 | 1 | 1 | 1 | 108 | 70 | 4000 |
| | 2 | -1 | 1 | 1 | 28 | 70 | 4000 |
| | 3 | 1 | -1 | 1 | 108 | 35 | 4000 |
| | 4 | -1 | -1 | 1 | 28 | 35 | 4000 |
| | 5 | 1 | 1 | -1 | 108 | 70 | 1000 |
| | 6 | -1 | 1 | -1 | 28 | 70 | 1000 |
| | 7 | 1 | -1 | -1 | 108 | 35 | 1000 |
| | 8 | -1 | -1 | -1 | 28 | 35 | 1000 |
| Axial points | 9 | 1.7 | 0 | 0 | 136 | 50 | 2000 |
| | 10 | -1.7 | 0 | 0 | 0 | 50 | 2000 |
| | 11 | 0 | 1.7 | 0 | 68 | 80 | 2000 |
| | 12 | 0 | -1.7 | 0 | 68 | 22 | 2000 |
| | 13 | 0 | 0 | 1.7 | 68 | 50 | 6000 |
| | 14 | 0 | 0 | -1.7 | 68 | 50 | 500 |
| Centre points | 15 | 0 | 0 | 0 | 68 | 50 | 2000 |
| | 16 | 0 | 0 | 0 | 68 | 50 | 2000 |

### 3.1.4 Parameters estimation

The constants of parameters estimations were used to determine empirical relationship in regressions equations. Data from the CCD matrices (Table 3.4 – 3.6) were analyzed using the least sum squares method to fit the second–order polynomial. The second order model selected was based on $CO_2$ corrosion mechanistic theories developed by George et.al [86]. Constants parameters model was calculated using Equation 2.68 (second order model) to obtain the regression model that represents an empirical relationship between the tested variables.

### 3.1.5 Model accuracy measurement

Model accuracy is a technique that can be used to check the appropriateness of the regression model. It can be divided into model adequacy and model validation [83].

- Model Adequacy is used to evaluate how accurate the model describes the data and meet the statistical criteria.
- Model Validation is an indicator how well the regression model fit the observed data.

## 3.2 Corrosion Experiments

The experiments were performed both in stagnant (static test) and flow simulation condition (dynamic test) with using rotating cylinder electrode (RCE) as simulation of flow in pipeline. The electrochemical technique measurements used in this experiment were linear polarization resistance (LPR) and electro chemical impedance spectroscopy (EIS) were used to measure the corrosion rate. The procedure is similar to ASTM Experimental test G 5-94 [87].

### 3.2.1 Specimen preparation

The working electrodes were carbon steel with chemical composition shown in Table 3.7. The cylindrical specimens have a diameter of 12 mm and length of 10 mm. Before immersion, the specimen surfaces were polished successively with 150, 240, 400 and 600 grit SiC paper, rinsed with methanol and degreased using acetone as referred from reference [61]. The experiments were repeated at least twice in order to ensure reasonable reproducibility.

Table 3.7 Composition of 080A15 (BS 970) carbon steel used in the experiments.

| Steel | C (%) | Si (%) | Mn (%) | P (%) | S (%) | Cr (%) | Ni (%) | Fe (%) |
|---|---|---|---|---|---|---|---|---|
| 080A15 | 0.15 | 0.18 | 0.799 | 0.01 | 0.03 | 0.06 | 0.065 | Balance |

### 3.2.2 Static test

In static test, corrosion behavior was studied in stagnant condition where there was no flow rate occurring in the solution. A typical experimental arrangement for the static test is illustrated in Figure 3.2. The test assembly consists of one liter glass cell bubbled with $CO_2$. The required test temperature was set at the hot plate. The electrochemical measurements were based on a three-electrode system, using a commercially available potentiostat with a computer control system. The reference electrode used was Ag/AgCl and the auxiliary electrode was a platinum electrode.

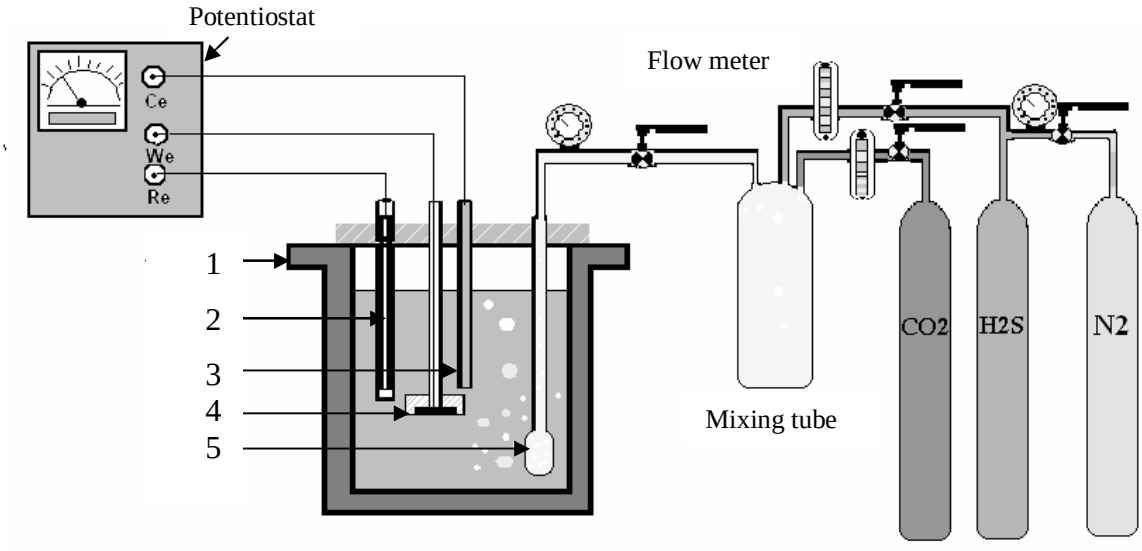


Legend: 1-Glass cell, 2-Reference electrode, 3-Counter electrode, 4-Working electrode, 5-$CO_2$ gas bubbler.

Figure 3.2 Experimental set-up for static test.

### 3.2.3 Dynamic experiments

Dynamic experiments were conducted in a one liter glass cell with polypropylene cell lids. A three-electrode arrangement was used. The RCE, used to simulate flow condition used in this research was made by PINE Research Instruments (Model AFMSRCE) with rotation speeds from 0 to 10,000 rpm. The set-up is shown as in Figure 3.3 below. A cylindrical working electrode was screwed to an electrode holder at the center of the cell for rotation in the RCE. The Linear Polarization Resistance (LPR) technique was used to measure the corrosion rate. The procedure is similar to ASTM G 5-94 [87].

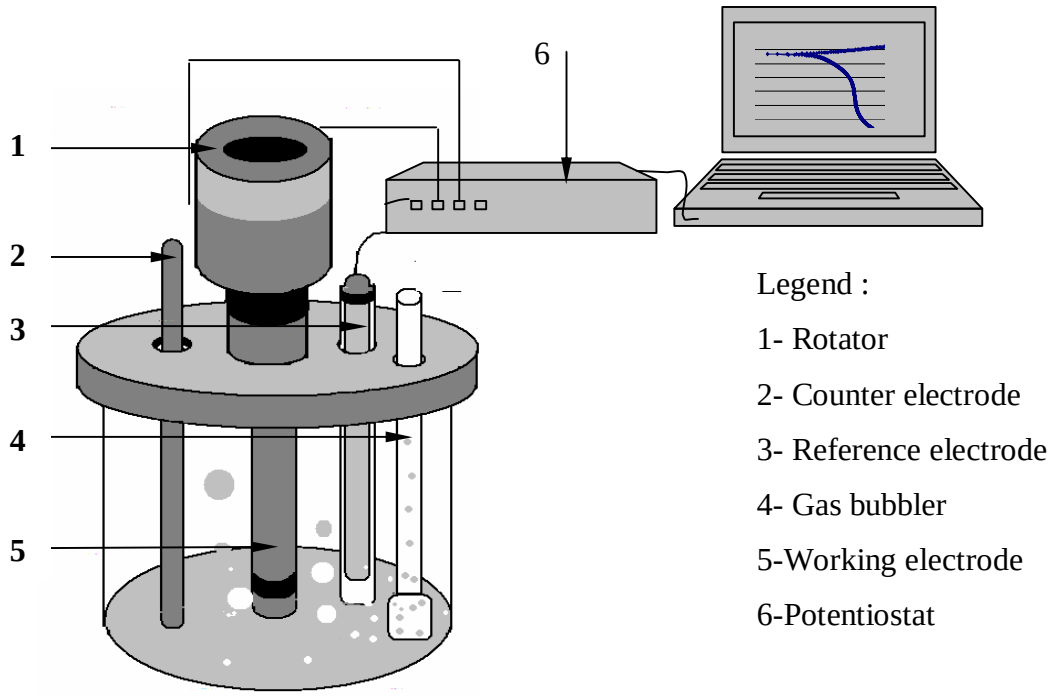


Figure 3.3 Experimental set-up for RCE test.

The shaft and the specimen holder of the RCE were made of stainless steel. The cylindrical sample was held in position with the use of PTFE holder and an end cap screwed at the end of the specimen holder. The cylindrical samples used in the RCE apparatus were machined from commercial carbon steel grade. The sample surface was polished to 600-grade finishing using silicon carbide papers. The specimen was degreased and rinsed with methanol and deionised water prior to immersion. A schematic diagram of the specimen assembly, with dimensions of the samples, is shown in Figure 3.4.

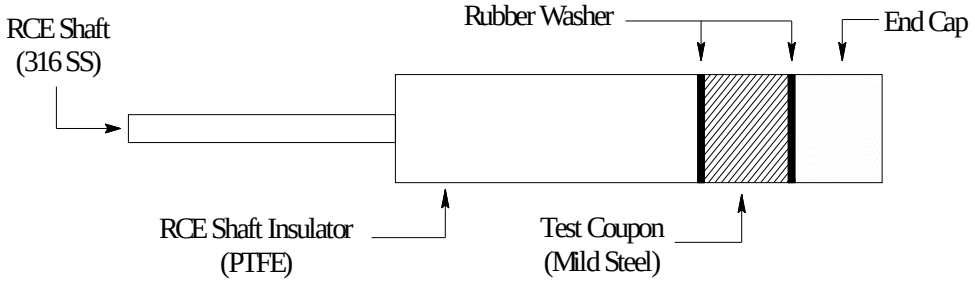


Figure 3.4 Details of the RCE specimen assembly with electrode diameter of 12 mm and length 8 mm.

### 3.2.4 Cell solutions

The total pressure was 1 bar, the glass cell was filled with 1 liter of deionized water with 3% wt NaCl, which was stirred with a magnetic stirrer. Then, $CO_2$ or $CO_2/H_2S/N_2$ gas was bubbled through the cell at least one hour prior to the experiments, in order to saturate and de-aerate the solution. Temperature was set using a hot plate. After the solution has been prepared, the pH was adjusted to the required pH using $NaHCO_3$ as a buffer solution. During the experiment, constant flow of gases at a fixed pressure was continuously bubbled through the electrolyte in order to maintain consistent water chemistry.

### 3.2.5 Composition of gases

Experiments was conducted in $CO_2$ gas and mixed $CO_2/H_2S$ gas environment. In $CO_2$ gas system, the experiments used saturation condition of $CO_2$ gas where concentration of $CO_2$ gas depends on temperature as presented in Table 3.8. Experiments in $CO_2/H_2S$ system used gas mixtures comprising 0.3 % $H_2S/N_2$ obtained commercially from MOX®. The mixture of $H_2S$ balanced with $N_2$ and $CO_2$ was adjusted using gas regulator and flow meter purged to the glass cell through a mixing tube. $N_2$ was used to substitute for methane for safety reasons. $N_2$ as an inert gas was also important to de-aerated the solution and maintenance the pressure. The compositions of the mixed gases are given in Table 3.9.

Table 3.8 Vapor pressure of water [61].

| T (°C) | Vapor pressure of water (mm Hg) | $CO_2$ (% mole) |
|---|---|---|
| 25 | 24 | 97 |
| 40 | 55 | 93 |
| 60 | 149 | 76 |

Table 3.9 Composition of gases used in the experiment.

| $CO_2$ (bar) | $H_2S$ (mbar) | $N_2$ (bar) | $H_2S$ (ppm) | $CO_2$ (ppm) | $CO_2/H_2S$ (ratio) |
|---|---|---|---|---|---|
| 0.7 | 0.3 | 0.2997 | 300 | 700000 | 2333 |

### 3.2.6 Preparation of solutions

The solutions were prepared using glacial HAc, NaAc, and sodium bicarbonate ($NaHCO_3$). All reagents were analytical grade chemicals. The 3% NaCl solution was saturated with $CO_2$ by purging for at least one hour prior to immerse the electrode in the solution. The pH of the solution was adjusted by adding a known amount of 1M $NaHCO_3$. The pH of the solution was checked by a microcomputer controlled pH-meter, METTLER-TOLEDO Model 320, which had been calibrated using standard buffer solutions.

### 3.2.7 Addition of HAc and acetate

The amount of HAc/acetate added to the solution was determined by the Handerson-Hasselbach equation in order to maintain the required pH.

Handerson-Hasselbach equation: ($pH = pKa + \log_{10}$ [Base]/[Acid])

For acetic buffer, this is given by:

$$pH = 4.76 + \log_{10}[CH_3COO^-]/[\ CH_3COOH] \quad (3.2)$$

The ratio of acetate ions and HAc at each pH is shown in Table 3.10 below.

Table 3.10 Calculated ratio of base and acid.

| pH Value | Ratio of Concentration (M) | |
|---|---|---|
| | $[CH_3COO^-]$ | $[CH_3COOH]$ |
| 4 | 1 | 5 |
| 5 | 2 | 1 |
| 5.5 | 5 | 1 |
| 6 | 17 | 1 |

The calculated concentration of the HAc species in solution are shown in Table 3.11. It is assumed that the concentration of the HAc species remained the same at different temperatures since the equilibrium constant for HAc $K_{HAc}$ varies a little with temperature.

Table 3.11 Concentration of HAc species (ppm) in NaCl-$CO_2$ saturated solution.

| Species | pH 4 | | | | pH 5.5 | | | |
|---|---|---|---|---|---|---|---|---|
| | 30 ppm | 72 ppm | 120 ppm | 132 ppm | 30 ppm | 66 ppm | 108 ppm | 138 ppm |
| HAc | 25 | 60 | 100 | 120 | 5 | 11 | 18 | 23 |
| NaAc | 5 | 12 | 20 | 12 | 25 | 55 | 90 | 115 |

### 3.2.8 Electrochemical measurement

The measurement used three types of electrodes (working electrode, reference electrode and counter electrode) connected to potentiostat. The electrodes are immersed in the electrolyte solution. Electrochemical technique records electrochemical process during oxidation and reduction in corroding solution. Electrochemical corrosion experiments measure current oxidation by controlling potential of the samples (working electrode). The measured current is plotted against potential in the Tafel plot where the slope of polarization resistance is determined.

This polarization resistance is assumed as corrosion resistance that can be used to calculate corrosion rate as presented by Equation 3.4 – 3.5.

### 3.2.8.1 Linear polarisation resistance (LPR)

LPR technique was used to determine the corrosion rates. The potential was swept from Ecorr to ± 10 mV at sweep rate 10 mV/minute. For calculation of the corrosion rates, Tafel constants was assumed to be 25 mV [61].

Polarization resistance (Rp) can be used to measure corrosion rate. Polarization reistance is resistance at the location very near to $E_{corr}$. At this point, the current versus voltage curve approximates a straight line. The Stern-Geary equation can be obtained to calculate corrosion rate is presented below [61]:

$$I_{corr} = \frac{b_a b_c}{R_p 2.303(b_a b_c)} \tag{3.3}$$

$$R_p = \frac{B}{I_{corr}} = \frac{(\Delta E)}{(\Delta i)_{\Delta E \to 0}} \tag{3.4}$$

$$B = \frac{b_a . b_c}{2.303(b_a . b_c)} \tag{3.5}$$

$$Corr.\ rate = I_{corr}\ 3272\ EW/\rho A \tag{3.6}$$

Where:

*Corr. rate* = Corrosion rate (mm/y)

$I_{corr}$ = Corrosion current (amps)

*Rp* = resistance polarisation

*EW* = The equivalent weight in grams/equivalent

$\rho$ = Metal density (grams/cm$^3$)

*A* = Sample area (cm$^2$)

$b_a$ = Anodic tafel slope

$b_c$ = Cathodic tafel slope

### 3.2.8.2. Electrochemical Impedance Spectroscopy (EIS)

EIS is one of the electrochemical methods to measure corrosion rate. EIS measures corrosion rate by applying an AC potential to an electrochemical cell and measuring the current through the cell without significantly disturbing the properties of the surface. EIS technique uses a small excitation signal ranging from 5 to 50 mV and the range of frequencies from 0.001 Hz to 100,000 Hz. Moreover, EIS presents a qualitative and quantitative analyses of surface characteristics. EIS also can give information about the process occurring on the metal surface during corrosion and further provides information of corrosion mechanisms on the surface.

## 3.3 Mechanistic Corrosion Model Prediction

A mechanistic model is a prediction model that uses fundamental theories. In corrosion, mechanistic theories include electrochemical reactions and thermodynamical processes occurring in the solution. The model also considers the role of chemical reactions and physical changes involved during the corrosion process such as standard state properties of species, thermodynamic model and activities of both ionic and molecular species to develop the mechanistic model. George et al. [86] has developed the mechanistic model for $CO_2$ corrosion as presented below (Equation 3.7 – 3.9). The model has been verified with many experimental data which showed reasonable results.

(i) Convective diffusion reactions through the mass transfer boundary layer.

$$Flux_i = k_{m,i}\left(c_{bi} - c_{o,i}\right) \tag{3.7}$$

(ii) Molecular diffusion through the liquid in the porous outer scale:

$$Flux_i = \frac{D_i \varepsilon \Psi}{\delta_{oc}}\left(c_{oi} - c_i\right) \tag{3.8}$$

(iii) Transfer ions through film by solid state diffusion can be formulated as:

$$Flux_i = A_i e^{\frac{B}{RT_K}} \ln\left(\frac{c_{i,i}}{c_{s,i}}\right) \tag{3.9}$$

### 3.3.1 $CO_2$ Corrosion in film free formation condition

The $CO_2$ corrosion mechanism involves electrochemical reaction and diffusion process that can be expressed mathematically. In these theories, the electron transfer is assumed as a corrosion rate. The electron transfer that passes through the film based on mechanistic theory provided by Nesic et al. [86] is expressed as:

$$CR_i = A_i e^{\frac{B}{RT_K}} \ln \frac{c_{b,i} - CR_i\left(\frac{\delta_{oc}}{D_i \varepsilon \Psi} + \frac{1}{k_{m,i}}\right)}{c_{s,i}} \tag{3.10}$$

Specific formula to calculate corrosion mechanism caused by $CO_2$ gas is formulated as follows [86]:

$$CR_{CO2} = A_i e^{\frac{B}{RT_K}} \ln \frac{c_{b_{CO2}} - CR_{CO2}\left(\frac{\delta_{oc}}{D_{co2} \varepsilon \Psi} + \frac{1}{k_{mCO2}}\right)}{CR_{CO2} \Big/ \left(D_{H_2CO_3} k_{hyd}^{f} K_{hyd}\right)^{0.5} f_{H_2CO_3}} \tag{3.11}$$

Where,

$K_m$ = mass transfer coefficient of species i (m/s),

$c_{b,}$ = bulk concentration of species i (mol/m$^3$),

$c_o$ = the interfacial concentration of species i at outer scale/solution interface (mol/m$^3$),

$D_i$ = diffusion coefficient for dissolved species i (m$^2$/s),

$\varepsilon$ = outer scale porosity,

$\psi$ = tortuosity factor,

$c_i$ = interfacial concentration of species I,

$\delta_{os}$ = the thickness of outer film scale,

$\delta_{hbl}$ = the thickness of turbulence boundary layer,

$\delta_{mbl}$ = the thickness of mass transfer boundary layer,

$\delta f$ = film thickness,

A = Arrhenius constant ,

$T_k$ = temperature (Kelvin),

$c_s$ = surface concentration,

R = universal gas constant.

### 3.4 Corrosion Predictions

There are corrosion model prediction software developed by industries namely ECE [75], Norsok [72], and Freecorp [88]. Those models calculate corrosion rate based on the experiences of the software designer and from experimental data. In this research, those models are used to validate experimental data and to evaluate the model performances.

This studies were conducted in order to formulate empirical corrosion prediction models based on RSM technique. The experiments were performed under conditions of varying temperature, rotation speed, and HAc concentration using LPR technique in $CO_2$ and $CO_2/H_2S$ environments. The corrosion rate data were structured in the matrices forms to find the model generation of empirical relationship among the variables tested.

The corrosion rate data base from literature review and from software calculations are required to quantify the RSM models. Comparison with corrosion rate data base have been conducted to evaluate the accuracy and precision in predicting corrosion rate. The details of the results are provided in the following chapter.

# CHAPTER 4

# EFFECTS OF HAc ON CARBON STEEL CORROSION IN $CO_2$ ENVIRONMENT

This chapter presents the results and discussions of the effect of HAc, temperature, flow condition indicated by rotation speed on carbon steel corrosion in $CO_2$ environment. The studies carried out in this work include: identifying initial of trending corrosion model, conducting experiments works based on design experiment selected, generating experimental data results to find empirical constant parameters used in the RSM model equation and evaluating the empirical model prediction. Empirical model and statistical analyses were calculated by Minitab program software [89]. In order to find a trending of the $CO_2$ corrosion as an effect of independent variable, $CO_2$ corrosion mechanistic theory was applied. Then, the trend model is used to fit the experimental data to obtain parametric relationships for the empirical model. To evaluate the accuracy and precision, the RSM model were compared against literature data from published papers and corrosion model calculated by commercial corrosion software.

## 4.1 Initial Identification of Corrosion Rate Model

Corrosion process can be constructed mathematically from mechanistic theory by using fundamental concepts of electrochemical reactions. The mathematical formulas describing corrosion process are formed based on several assumptions as described in Chapter 2. The trends of corrosion rate calculated by mechanistic theories are presented in Figure 4.1 to Figure 4.4. Based on the trends, the RSM corrosion models was fit using a second order model regression.

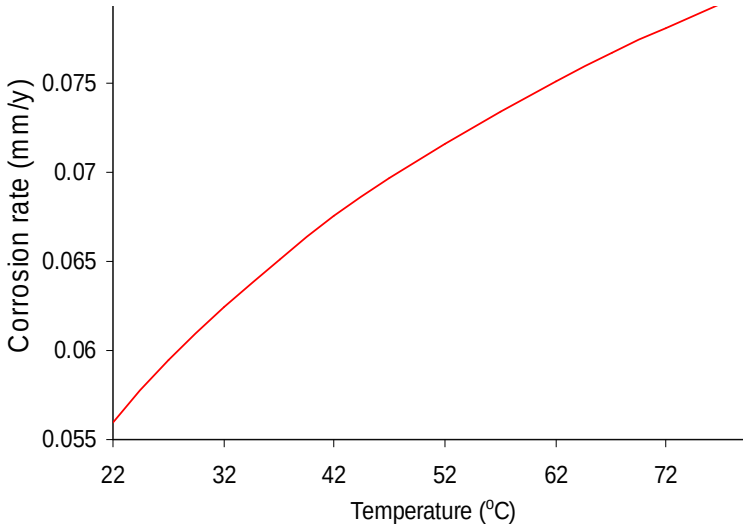


Figure 4.1 Simulated corrosion rate as a function of temperature from 22°C to 72°C, 1 bar and static in $CO_2$ environment without HAc.

Figure 4.1 presents the relationship between corrosion rate and temperature. From the graph, it is observed that corrosion rate increases exponentially with increasing temperature. This corrosion rate model is confirmed with other corrosion rate models as described by reference [28, 88].

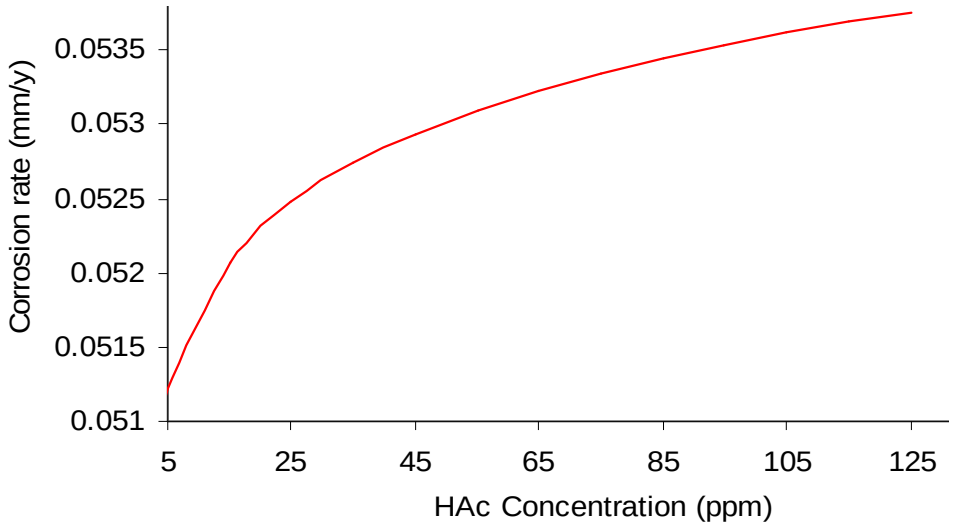


Figure 4.2 Simulated corrosion rate as a function of HAc concentration at 22°C, 1 bar and static.

Figure 4.2 presents the mechanistic model for calculating the effect of increasing HAc concentration on corrosion rate. From the figure, it can be observed that the corrosion rate increases exponentially with HAc concentrations.

The effect of rotation speed on corrosion rate is presented in Figure 4.3. The rotation speed is an important parameter to study the effect of flow conditions on corrosion rate. Figure 4.3 shows that there exists a condition when flow rate do not have significant impact on corrosion rate. As observed in Figure 4.3, the corrosion rate becomes constant after a certain flow value even though the flow continues to increase. Researchers define this condition as flow independent due to limiting current density [61].

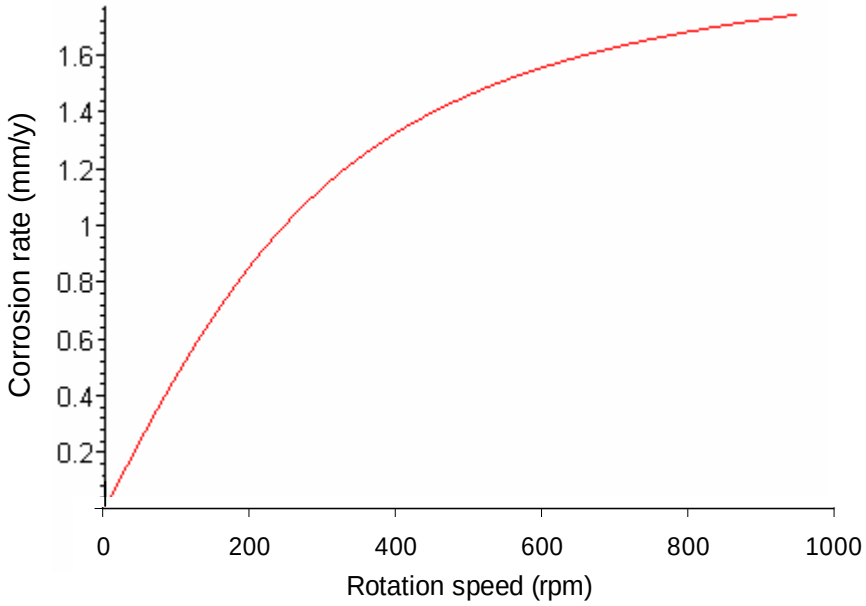


Figure 4.3 Simulated corrosion rate as a function of rotation speed for a range from stagnant to 1000 rpm at 22$^{o}$C and 1 bar.

### 4.2 Design of Experiment for Analyzing Corrosion Model at pH 4

The design selected for this experiment is a CCD with three independent variables. This design is used to study corrosion rate and to determine the combined effect of variables involved; temperature, HAc and rotation speed. It used a total of twenty observations, consisting of eight observations as a factorial design, six observations as axial points, and four points located in central points as repetitions.

Table 4.1 shows the effects of different concentration of HAc, temperature and flow conditions (indicated by rotation speed) using LPR technique at pH 4. The test was conducted for 1.5 hours and recorded the reading every 15 minutes. The corrosion rate measurements are calculated based on the average corrosion rate during 1.5 hours measurements. More detail about the corrosion rate data against time are presented in Appendix 1.

Table 4.1 CCD with observed values
for the response of experimental data (Yi).

| No | Coded variables | | | Natural variables | | | Exp. results (Yi) |
|---|---|---|---|---|---|---|---|
| | HAc (ppm) | T ($^{o}$C) | N (rpm) | HAc (ppm) | T ($^{o}$C) | N (rpm) | |
| 1 | 1 | 1 | 1 | 270 | 70 | 4000 | 10.7 |
| 2 | -1 | 1 | 1 | 70 | 70 | 4000 | 7.3 |
| 3 | 1 | -1 | 1 | 270 | 35 | 4000 | 6.5 |
| 4 | -1 | -1 | 1 | 70 | 35 | 4000 | 4.4 |
| 5 | 1 | 1 | -1 | 270 | 70 | 1000 | 10.7 |
| 6 | -1 | 1 | -1 | 70 | 70 | 1000 | 7.3 |
| 7 | 1 | -1 | -1 | 270 | 35 | 1000 | 6.4 |
| 8 | -1 | -1 | -1 | 70 | 35 | 1000 | 4.2 |
| 9 | √3 | 0 | 0 | 340 | 50 | 2000 | 9.6 |
| 10 | -√3 | 0 | 0 | 0 | 50 | 2000 | 4.6 |
| 11 | 0 | √3 | 0 | 170 | 80 | 2000 | 9.5 |
| 12 | 0 | -√3 | 0 | 170 | 22 | 2000 | 3.8 |
| 13 | 0 | 0 | √3 | 170 | 50 | 6000 | 8.5 |
| 14 | 0 | 0 | -√3 | 170 | 50 | 0 | 7.3 |
| 15 | 0 | 0 | 0 | 170 | 50 | 2000 | 8.4 |
| 16 | 0 | 0 | 0 | 170 | 50 | 2000 | 8.5 |
| 17 | 0 | 0 | 0 | 170 | 50 | 2000 | 8.3 |
| 18 | 0 | 0 | 0 | 170 | 50 | 2000 | 8.2 |

### 4.2.1 Generalization of corrosion predictions model at pH 4, HAc

Data from the CCD matrix (Table 4.1) were fit by the second–order polynomial (Equation 2.58) using the least sum squares method. A RSM constant parameter model was calculated using Equation 2.61 and 2.62 which yielded the regression Equation 4.1. The RSM regression model in Equation 4.1 represents an empirical relationship between HAc concentration, temperature and rotation speed.

$$Y= -6.1170 + 0.0230(HAc) + 0.3160\ (T) + 0.0005(N) -0.0001(HAc)^2 - 0.0023(T)^2 + 0.0002\ (HAc\times T) \quad (4.1)$$

Where;

$Y$ = corrosion rate (mm/y)

$HAc$ = concentration of HAc (ppm)

$T$ = temperature ($^oC$)

$N$ = rotation speed (rpm)

### 4.2.2 Prediction of $CO_2$ corrosion model at pH 4

The average corrosion rate obtained from the experiments (Yi) is compared to data from corrosion predictions ($\hat{y}$) as presented in Table 4.2. From the difference between experimental results and RSM model predictions, it can be seen that there is a reasonable results that indicates a satisfactory of the RSM model.

Table 4.2 Comparison between corrosion data experiments and corrosion data predictions

| No of run | Coded variables | | | Natural variables | | | Exp. results (Yi) | Predct. (ŷ) | Error (Yi-ŷ) |
|---|---|---|---|---|---|---|---|---|---|
| | HAc | T | N | HAc (ppm) | T ($^{o}$C) | N (rpm) | | | |
| 1 | 1 | 1 | 1 | 270 | 70 | 4000 | 10.7 | 10.7 | -0.0 |
| 2 | -1 | 1 | 1 | 70 | 70 | 4000 | 7.3 | 7.4 | -0.1 |
| 3 | 1 | -1 | 1 | 270 | 35 | 4000 | 6.5 | 6.8 | -0.3 |
| 4 | -1 | -1 | 1 | 70 | 35 | 4000 | 4.4 | 4.7 | -0.3 |
| 5 | 1 | 1 | -1 | 270 | 70 | 1000 | 10.6 | 10.4 | 0.2 |
| 6 | -1 | 1 | -1 | 70 | 70 | 1000 | 7.2 | 7.0 | 0.2 |
| 7 | 1 | -1 | -1 | 270 | 35 | 1000 | 6.4 | 6.4 | -0.0 |
| 8 | -1 | -1 | -1 | 70 | 35 | 1000 | 4.2 | 4.2 | -0.0 |
| 9 | √3 | 0 | 0 | 340 | 50 | 2000 | 9.6 | 9.1 | 0.5 |
| 10 | -√3 | 0 | 0 | 0 | 50 | 2000 | 4.6 | 4.5 | 0.1 |
| 11 | 0 | √3 | 0 | 170 | 80 | 2000 | 9.5 | 9.3 | 0.2 |
| 12 | 0 | -√3 | 0 | 170 | 22 | 2000 | 3.8 | 3.3 | 0.5 |
| 13 | 0 | 0 | √3 | 170 | 50 | 6000 | 8.5 | 8.1 | 0.4 |
| 14 | 0 | 0 | -√3 | 170 | 50 | 0 | 7.3 | 7.6 | -0.3 |
| 15 | 0 | 0 | 0 | 170 | 50 | 2000 | 8.4 | 8.2 | 0.2 |
| 16 | 0 | 0 | 0 | 170 | 50 | 2000 | 8.5 | 8.2 | 0.3 |
| 17 | 0 | 0 | 0 | 170 | 50 | 2000 | 8.3 | 8.2 | 0.1 |
| 18 | 0 | 0 | 0 | 170 | 50 | 2000 | 8.2 | 8.2 | -0.0 |

### 4.2.3 Variance Analysis

Table 4.3 shows the analysis of RSM regression model using variance analysis calculated by CCD matrix according to Reference [84]. The main factors for the coefficient of the linear and square models show a significant value at confidence level of $\alpha = 0.05$ ($p<0.5$). However, for the interaction effect of the model was insignificant ($p>0.5$). Furthermore, the high values (98%) of the correlation coefficients ($R^2$) for the responses suggest that the RSM model has a good fit.

Table 4.3 Analysis of variance (ANOVA) for the fitted models.

| Source | DF | Seq SS | Adj SS | Adj MS | F | P |
|---|---|---|---|---|---|---|
| Regression | 9 | 78.255 | 78.255 | 8.695 | 85.11 | 0.00 |
| Linear | 3 | 68.125 | 9.693 | 3.231 | 31.63 | 0.000 |
| Square | 3 | 9.368 | 9.364 | 3.122 | 30.55 | 0.000 |
| Interaction | 3 | 0.760 | 0.760 | 0.254 | 2.48 | 0.121 |
| Residual Error | 10 | 1.021 | 1.021 | 0.102 | | |
| Lack-of-Fit | 5 | 1.001 | 1.002 | 0.201 | 50.77 | 0.000 |
| Pure Error | 5 | 0.019 | 0.019 | 0.0039 | | |
| Total | 19 | 79.276 | | | | |
| R-Sq = 98.71% | | | | | | |

### 4.2.4 Model adequacy evaluation

The performance of the RSM model was checked using normal plots of the residual. As illustrated in Figure 4.4 to 4.6, it can be seen that all of the residual plots are in good agreement with the model's assumption of normal probability trend. The plot of residual vs. probability percent, Figure 4.4, shows a straight line pattern. This indicates that a normal distribution assumption has been satisfied and the coefficients estimated with the minimum variance are unbiased. Figure 4.5, plot of residual vs. order of data, is also identified as non-random error. This plot presents the assumption that the residuals are uncorrelated with each other. Residual vs. fitted values plot, Figure 4.6, shows a random pattern of residuals on both sides and no any recognizable pattern in the residual plot. Thus, this model was in random distributions.

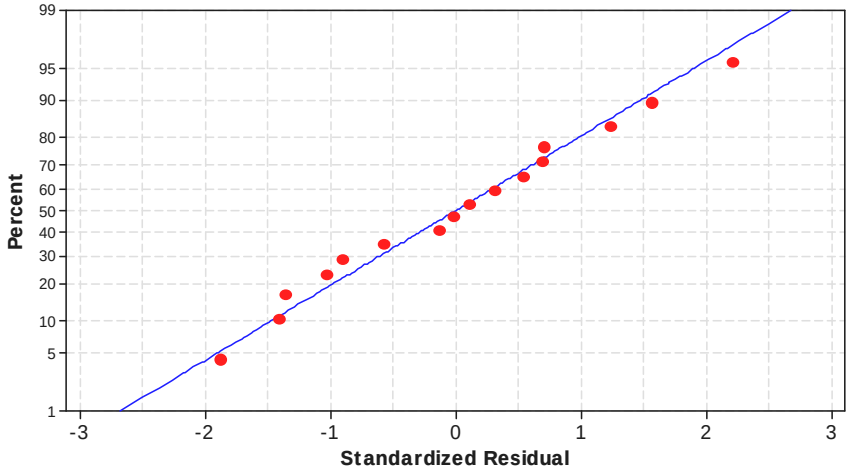


Figure 4.4 Normal plot of residuals.

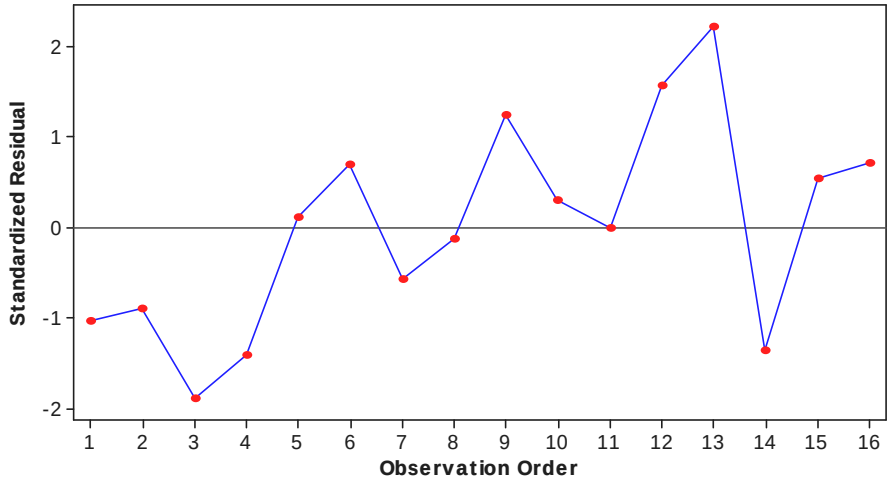


Figure 4.5 Residuals versus order of data.

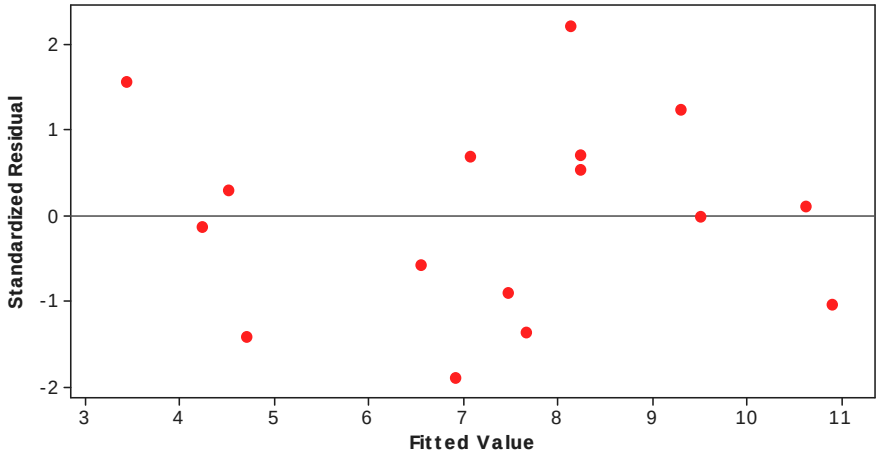


Figure 4.6 Residuals versus Fitted Values.

In further analysis, each of the observed value for the corrosion rate was compared with predicted values (Figure 4.7). Parity plot in Figure 4.7 shows a 98 % of acceptable level of agreement. All of these results present a satisfactory mathematical description of the corrosion rate data.

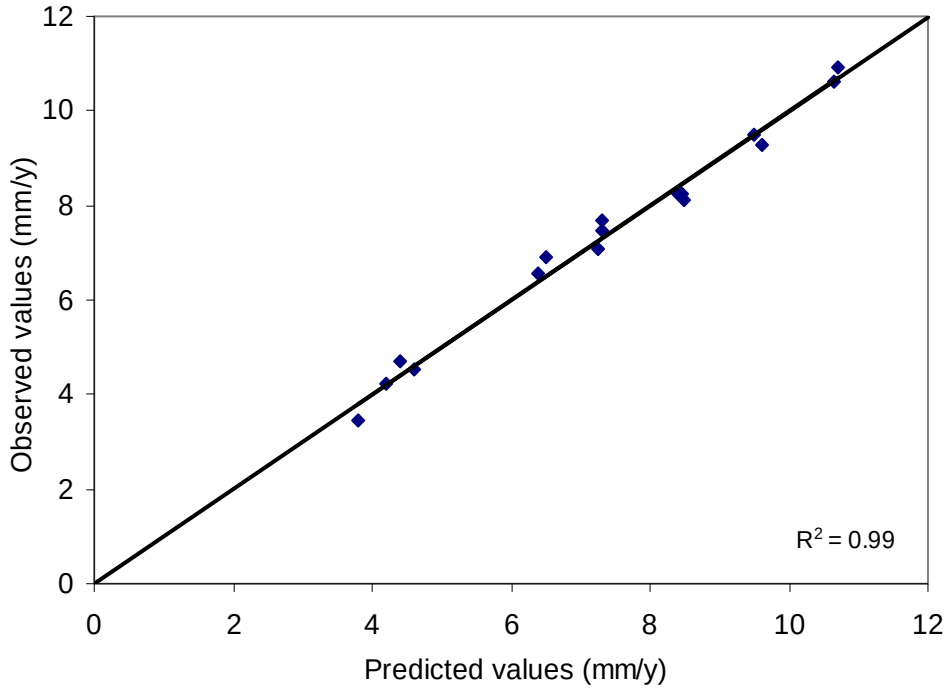


Figure 4.7 The relationship between observed and predicted values of corrosion rate model.

### 4.3 Verification with Experimental Data and Corrosion Prediction Software

The comparison of the resultant RSM model with Hedges's [22] and George's [86] experimental data are shown in Figure 4.8 and Figure 4.9, respectively. A good agreement between experimental and calculated data based on this corrosion prediction RSM model is observed. Comparing to Hedges's experiments at 60$^{o}$C, the RSM model has $R^2$ of 94%, correlation of 97% and standard error estimation deviation of 0.28 (± 0.22 mm/y). In comparison to George's experimental data, the RSM model shows a relationship with $R^2$ of 93%, correlation of 97%, and standard error estimation of 0.5 (± 0.4 mm/y). George's experiment showed a good relationship in correlation and regression relationship; but it provided less precision in standard error estimation.

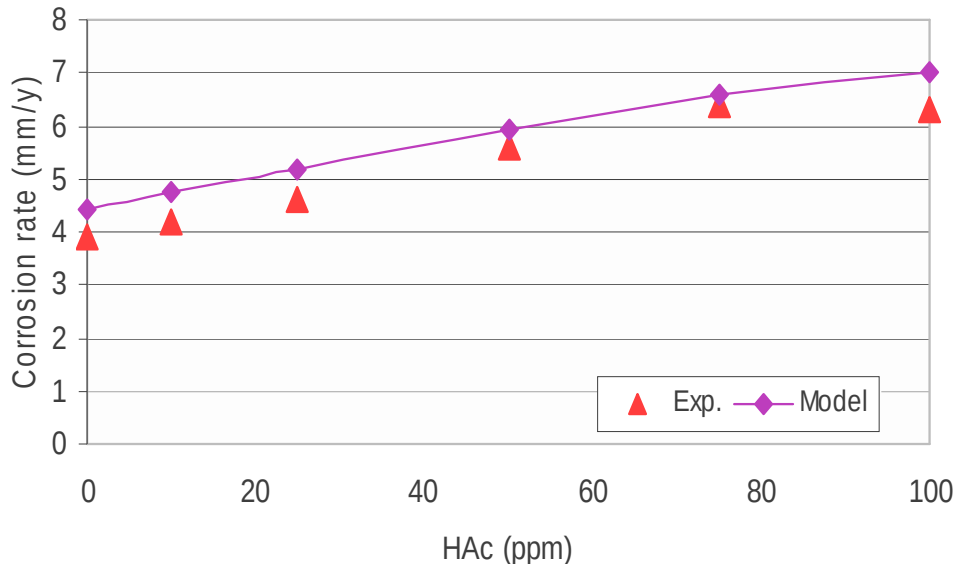


Figure 4.8 Comparison between the model and Hedges's experimental data in 1 bar $CO_2$, 60°C, and static condition.

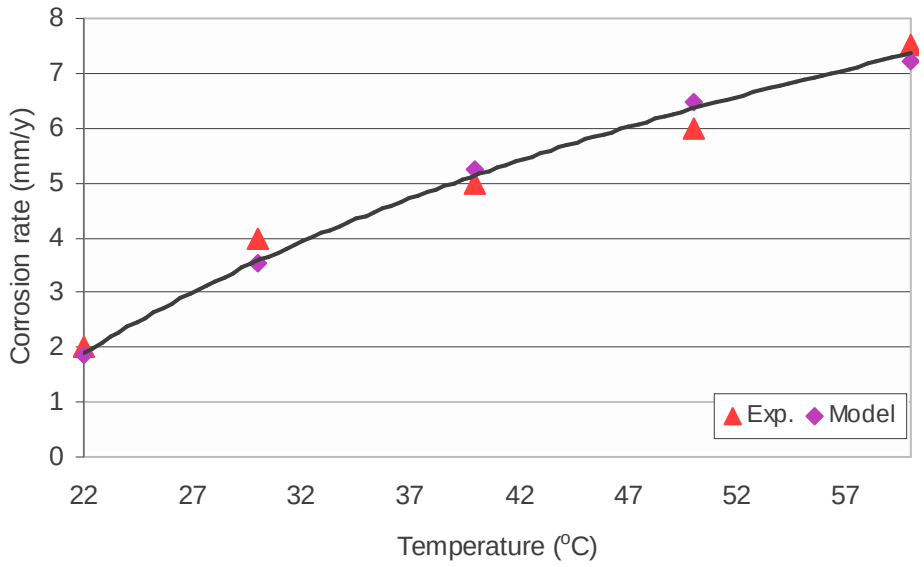


Figure 4.9 Comparison between the RSM model and George's electrochemical model in 1 bar $CO_2$, 100 ppm HAc, 300 rpm.

The comparison of the RSM model with corrosion prediction software Freecorp [88] at 35°C is shown in Figure 4.10. The results show $R^2$ of 90%, correlation of 94% and standard error of 0.3 (± 0.2 mm/y). A good fit was also found when comparing the RSM model with ECE [75] software as shown in Figure 4.11. The comparisons

show $R^2$ of 90%, correlation of 97%, and standard error estimation of 0.5 (± 0.43 mm/y).

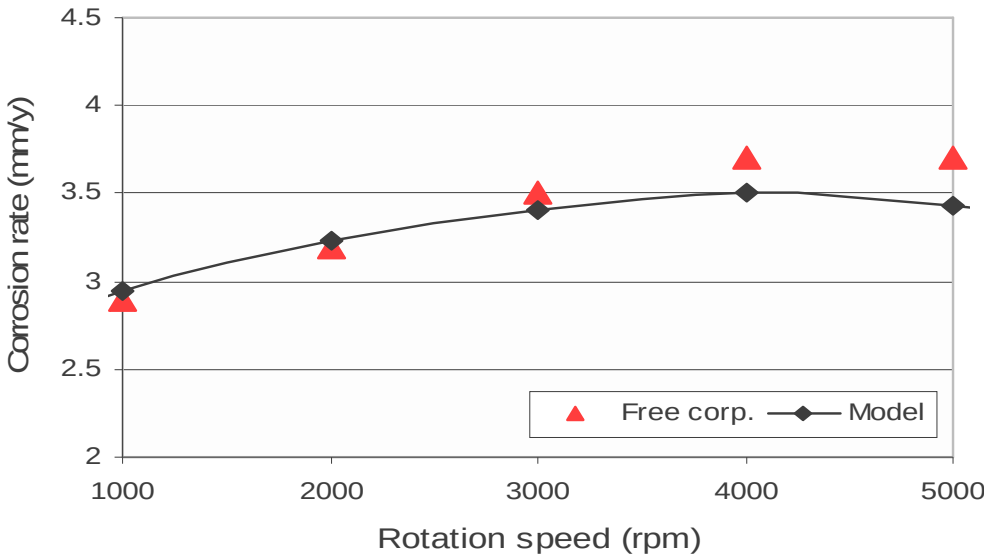


Figure 4.10 Comparison between the RSM model and Freecorp in 1 bar $CO_2$, and 35°C.

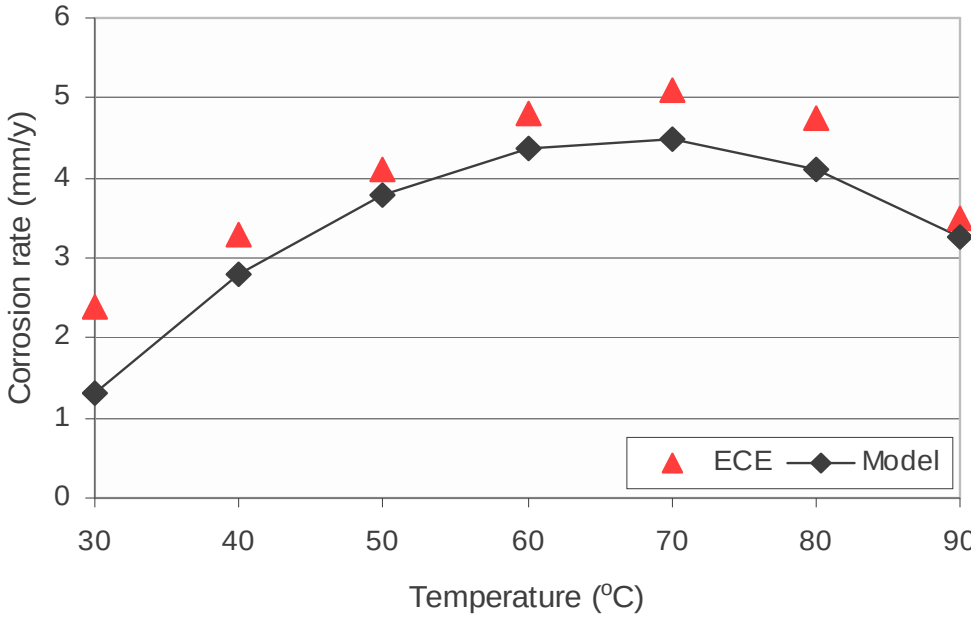


Figure 4.11 Comparison between the RSM model and ECE in 1 bar $CO_2$, and static condition.

The verification of the regression RSM model with this commercial software in a different cases is presented in Appendix 2. The model has a good correlation with

average coefficient determination 90%, correlation 95% and standard error estimation 0.2 (± 0.15 mm/y).

## 4.4 Analysis and Interpretation of Response Surface of $CO_2$ corrosion at pH 4

The RSM regression model can be graphically presented as response surface contour to show the simultaneous effects of variables tested. The following figures 4.12 - 4.15 present simultaneous effects of temperature, HAc, and rotation speed on corrosion rate at the pH 4 based on the RSM model. In further analyses, RSM model is also used to calculate maximum corrosion rate caused by scaling temperature and limiting current density indicated by critical values of the model.

### 4.4.1 Effects of temperature and HAc concentration

The effects of temperature and HAc concentration on the corrosion of carbon steel in $CO_2$ saturated solution is presented in Figure 4.12. The figure shows that an increase in temperature and HAc concentration leads to an increase in corrosion rate. The effects of HAc concentration on corrosion rate is smaller than the effects of temperature within the range tested. In the range of temperature from 22 to 70$^{o}$C, the corrosion rate reached to 12.0 mm/y. In the range of HAc concentration from 0 to 340 ppm, the corrosion rate increased from 2.0 mm/y to 4.0 mm/y.

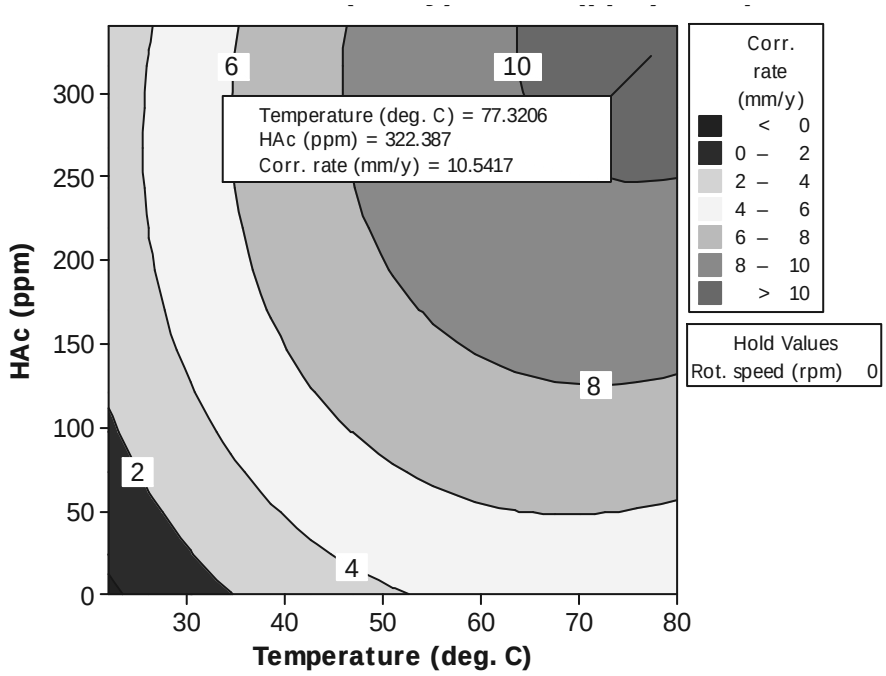


Figure 4.12 Response surface contours of corrosion rate as a function of temperature and HAc concentration at pH 4 and stagnant condition.

### 4.4.2 Effects of temperature and rotation speed

The effects of temperature and rotation speed on the corrosion of carbon steel in $CO_2$ environments, as modeled by RSM, is presented in Figure 4.13. In this conditions, corrosion rate increases with increasing temperature and rotation speed. From the figure, it can be seen effect of temperature has a greater effect than rotation speed. Corrosion rate increased from 1 mm/y to 5 mm/y with increasing temperature from 25$^{o}$C to 80$^{o}$C. But, corrosion rate only increase from 1 mm/y to 2 mm/y with increasing rotation speed from 1000 rpm to 6000 rpm. However, there was low dependence of rotation speed on temperature. At the higher temperature (80$^{o}$C), corrosion was higher compared to lower temperature with increasing rotation speed. For example, at 80$^{o}$C, the corrosion rate was in the range of 4 mm/y to 5 mm/y. While at the lower temperature (30$^{o}$C), the corrosion rate was from 1 mm/y to 2 mm/y when the rotation speed was increased from stagnant to 5000 rpm.

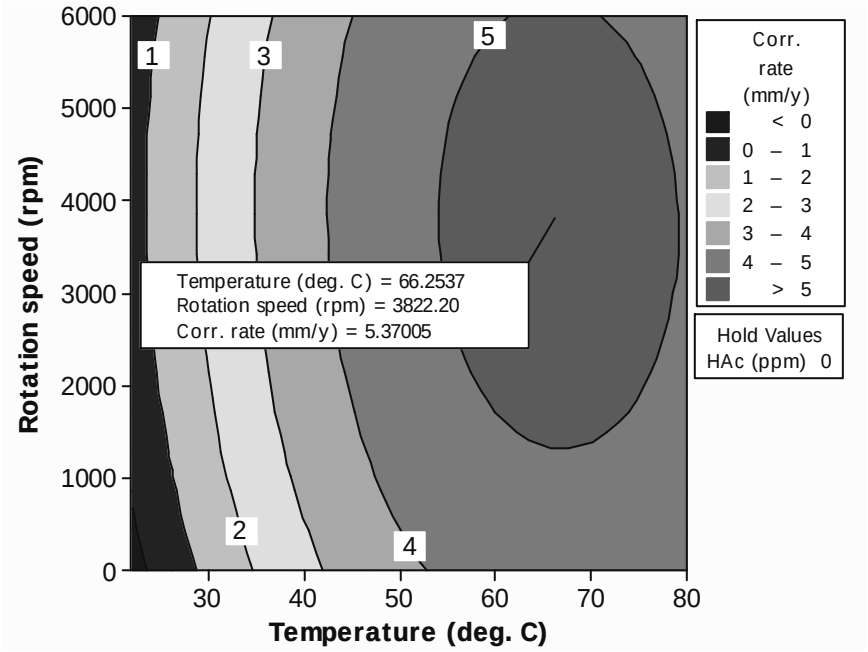


Figure 4.13 Response surface contours of corrosion rate as a function of temperature and rotation speed at pH 4 without HAc.

### 4.4.3 Effects of rotation speed and HAc concentration

Figure 4.14 presents the surface response graph showing to the combined effect of rotation speed and HAc concentration on the corrosion rate. The plot shows that different corrosion rate is influenced by HAc concentration and rotation speed. At higher HAc concentration (300 ppm), the corrosion rate increased from 3 to 3.5 mm/y when the rotation speed was set from 0 to 3000 rpm. While at lower HAc concentration (< 50 ppm), the corrosion rate increased from 0.1 to 1 mm/y in the range of rotation speed from 0 to 6000 rpm. This is in agreement with other researchers data that there is a minimum of HAc concentration to increase corrosion rate.

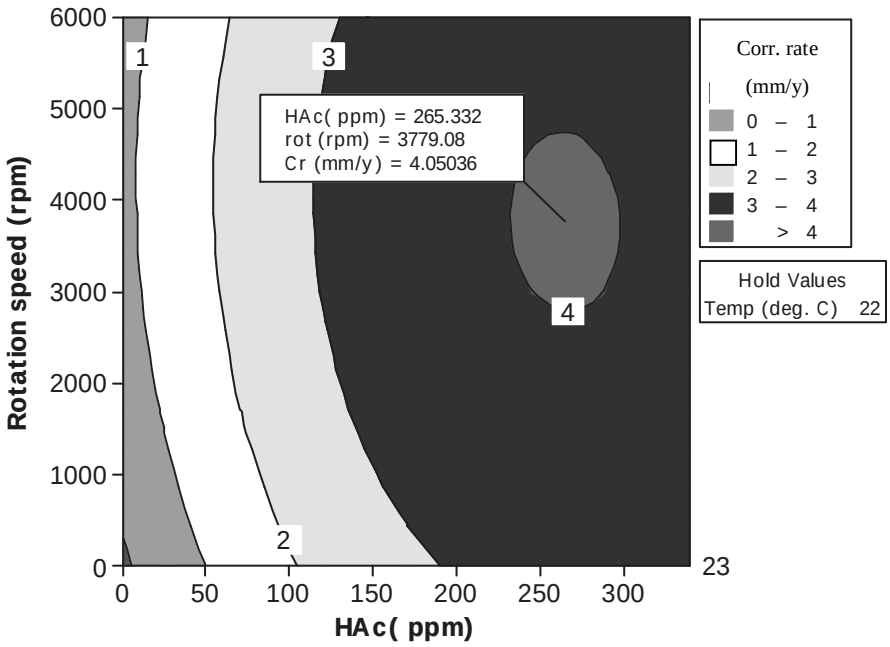


Figure 4.14 Response surface contours of corrosion rate as a function of HAc concentration and rotation rate at 22$^{o}$C at pH 4.

### 4.4.4 Maximum corrosion rate

As described previously, the response observation is useful to determine location of maximum corrosion rate which indicates scaling temperature. The use of RSM has been successful in visualizing the maximum corrosion rate along the range of variables setting. The contour plot in Figure 4.15 show that the maximum corrosion rate is dependent on the operating conditions.

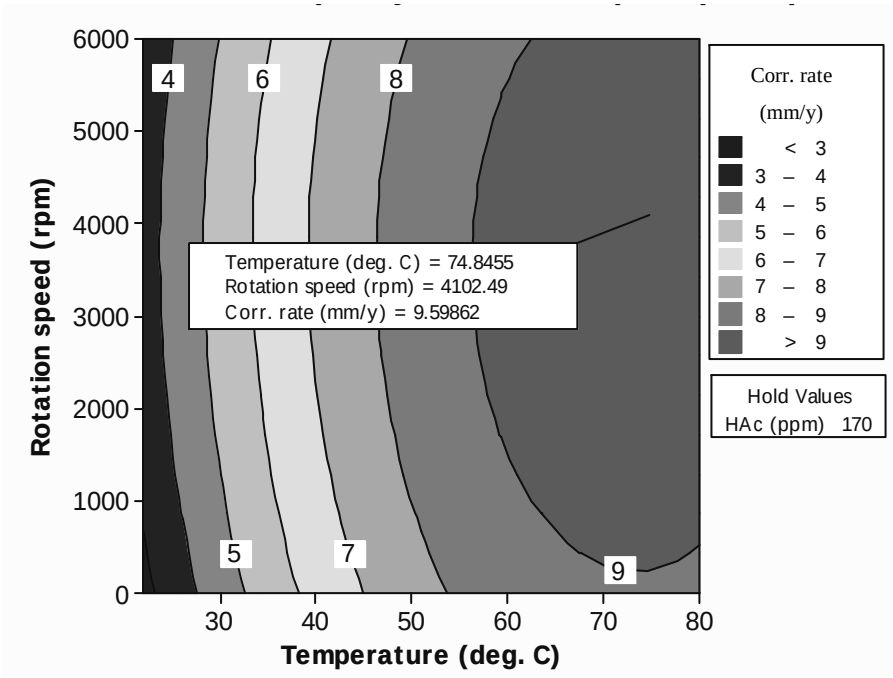


Figure 4.15 Response surface contours of corrosion rate as a function of temperature and rotation speed at 170 ppm HAc concentration at pH 4.

The response surfaces calculated by second order model can also be used to indicate the maximum point on the range of independent variable analytically. Calculations of the maximum point using the first derivative of the mathematical function gave the maximum corrosion rate. The maximum points are located in condition where the first derivative of the response surface equals to zero. Calculating first derivative of equation 4.1 to each independent variable (T, HAc, N) results:

$$\partial Y / \partial T = \quad 68.126 + 0.039(HAc) + 0.00017\,(N) - (T) = 0 \tag{4.2}$$

$$\partial Y / \partial HAc = 231.58 + 1.89(T) - 0.002(N) - (HAc) = 0 \tag{4.3}$$

$$\partial Y / \partial N = \quad 4417.33 - 1.84(HAc) - 7.45(T) - (N) = 0 \tag{4.4}$$

Thus, to calculate the coordinate of the critical point, it is necessary to solve those three equations and to find the T, HAc and N values. By solving the equations, the maximum corrosion rate of the model was found to occur at HAc 380 ppm, rotation speed 3000 rpm, and temperature 80$^{o}$C. The corrosion rate at this condition is 11.0 mm/y.

## 4.5 Design of Experiment for Analyzing Corrosion Rate Model at pH 5.5

The design of experiment selected for this experiment was CCD. This design methodology has been found as the best methodology as discussed previously for experiments at pH 4. The CCD used in this experiment is presented in Table 4.4. A total of eighteen observations were involved in this design. The independent variables used in these experiments are temperature, rotation speed and HAc concentration to predict corrosion rate model at pH 5.5.

Table 4.4 CCD experimental design for $CO_2$ corrosion at pH 5.5.

| No of run | Variable code | | | Experimental variables | | | Exp. results (Yi) |
|---|---|---|---|---|---|---|---|
| | HAc | T | N | HAc (ppm) | T ($^oC$) | N (rpm) | |
| 1 | 1 | 1 | 1 | 270 | 70 | 4000 | 7 |
| 2 | -1 | 1 | 1 | 70 | 70 | 4000 | 5.2 |
| 3 | 1 | -1 | 1 | 270 | 35 | 4000 | 4.2 |
| 4 | -1 | -1 | 1 | 70 | 35 | 4000 | 3.2 |
| 5 | 1 | 1 | -1 | 270 | 70 | 1000 | 5.2 |
| 6 | -1 | 1 | -1 | 70 | 70 | 1000 | 4 |
| 7 | 1 | -1 | -1 | 270 | 35 | 1000 | 3.1 |
| 8 | -1 | -1 | -1 | 70 | 35 | 1000 | 2.4 |
| 9 | √3 | 0 | 0 | 340 | 50 | 2000 | 5.9 |
| 10 | -√3 | 0 | 0 | 0 | 50 | 2000 | 2 |
| 11 | 0 | √3 | 0 | 170 | 80 | 2000 | 5.3 |
| 12 | 0 | -√3 | 0 | 170 | 22 | 2000 | 2.4 |
| 13 | 0 | 0 | √3 | 170 | 50 | 6000 | 5.9 |
| 14 | 0 | 0 | -√3 | 170 | 50 | 0 | 2.3 |
| 15 | 0 | 0 | 0 | 170 | 50 | 2000 | 4.5 |
| 16 | 0 | 0 | 0 | 170 | 50 | 2000 | 4.6 |
| 17 | 0 | 0 | 0 | 170 | 50 | 2000 | 4.7 |
| 18 | 0 | 0 | 0 | 170 | 50 | 2000 | 4.7 |

### 4.5.1 Generalization of corrosion prediction model at pH 5.5

The corrosion prediction model at pH 5.5 was fitted using second-order polynomial equation (Equation 2.68). The model proposed as calculated by Equation 2.71 and 2.72 for the response is given below.

$$Y = -2.3890 + 0.0090(HAc) + 0.1064(T) + 0.0006(N) - 0.0007(T)^2 + 0.0001(HAc)(T) \quad (4.5)$$

Where;

$Y$ = corrosion rate (mm/y)

$HAc$ = concentration of HAc (ppm)

$T$ = temperature ($^oC$)

$N$ = rotation speed (rpm)

### 4.5.2 Prediction of $CO_2$ corrosion model at pH 5.5

The average corrosion rate obtained from the experiments (Yi) is compared to data from corrosion predictions (ŷ) as presented in Table 4.5. From the difference, it can be seen that there is a reasonable predictions between corrosion data experiments and predictions.

Table 4.5 Comparison between corrosion data experiments and corrosion data predictions for $CO_2$ corrosion at pH 5.5.

| No of run | Variable code | | | Experimental variables | | | Exp. results (Yi) | Predct. (ŷ) | Error (Yi-ŷ) |
|---|---|---|---|---|---|---|---|---|---|
| | HAc (ppm) | T ($^oC$) | N (rpm) | HAc (ppm) | T ($^oC$) | N (rpm) | | | |
| 1 | 1 | 1 | 1 | 270 | 70 | 4000 | 7 | 7.2 | -0.2 |
| 2 | -1 | 1 | 1 | 70 | 70 | 4000 | 5.2 | 5.2 | -0.0 |
| 3 | 1 | -1 | 1 | 270 | 35 | 4000 | 4.2 | 4.7 | -0.5 |
| 4 | -1 | -1 | 1 | 70 | 35 | 4000 | 3.2 | 3.2 | -0.0 |
| 5 | 1 | 1 | -1 | 270 | 70 | 1000 | 5.2 | 5.2 | -0.0 |
| 6 | -1 | 1 | -1 | 70 | 70 | 1000 | 4 | 3.4 | 0.6 |
| 7 | 1 | -1 | -1 | 270 | 35 | 1000 | 3.1 | 3.3 | -0.2 |
| 8 | -1 | -1 | -1 | 70 | 35 | 1000 | 2.4 | 1.9 | 0.5 |
| 9 | √3 | 0 | 0 | 340 | 50 | 2000 | 5.9 | 5.3 | 0.6 |
| 10 | -√3 | 0 | 0 | 0 | 50 | 2000 | 2 | 2.6 | -0.6 |
| 11 | 0 | √3 | 0 | 170 | 80 | 2000 | 5.3 | 5.5 | -0.2 |
| 12 | 0 | -√3 | 0 | 170 | 22 | 2000 | 2.4 | 2.2 | 0.2 |
| 13 | 0 | 0 | √3 | 170 | 50 | 6000 | 5.9 | 5.6 | 0.3 |
| 14 | 0 | 0 | -√3 | 170 | 50 | 0 | 2.3 | 2.9 | -0.6 |
| 15 | 0 | 0 | 0 | 170 | 50 | 2000 | 4.5 | 4.4 | 0.1 |
| 16 | 0 | 0 | 0 | 170 | 50 | 2000 | 4.6 | 4.4 | 0.2 |
| 17 | 0 | 0 | 0 | 170 | 50 | 2000 | 4.7 | 4.4 | 0.3 |
| 18 | 0 | 0 | 0 | 170 | 50 | 2000 | 4.6 | 4.4 | 0.2 |

### 4.5.3 Analysis variance

Table 4.6 shows the analysis of variance for corrosion in saturated $CO_2$ solution using CCD methodology for corrosion rate at pH 5.5 as calculated from Reference [84].

Table 4.6 Analysis of variance for CCD model regression for the fitted models.

| Source | DF | Seq SS | Adj SS | Adj MS | F | P |
|---|---|---|---|---|---|---|
| Regression | 9 | 32.3158 | 32.3158 | 3.59064 | 10.13 | 0.005 |
| Linear | 3 | 31.4462 | 26.5343 | 8.84476 | 24.95 | 0.001 |
| Square | 3 | 0.5830 | 0.5711 | 0.19035 | 0.54 | 0.674 |
| Interaction | 3 | 0.2866 | 0.2866 | 0.09552 | 0.27 | 0.845 |
| Residual Error | 6 | 2.1266 | 2.1266 | 0.35443 | | |
| Lack-of-Fit | 5 | 2.1216 | 2.1216 | 0.42431 | 84.86 | 0.082 |
| Pure Error | 1 | 0.0050 | 0.0050 | 0.00500 | | |
| Total | 15 | 34.4423 | | | | |
| R-Sq = 97.29% | | | | | | |

### 4.6 Evaluation of Model Adequacy

As shown in Figure 4.16 to Figure 4.18, it can be seen that the normal plotting of the residual meets the model's assumptions for normal probability (Figure 4.16), independency (Figure 4.17) and uncorrelated variance (Figure 4.18). Figure 4.19 shows the correlation between observed experimental data and predicted values with an acceptable level of 94%. These results imply a satisfactory mathematical description of the corrosion rate data.

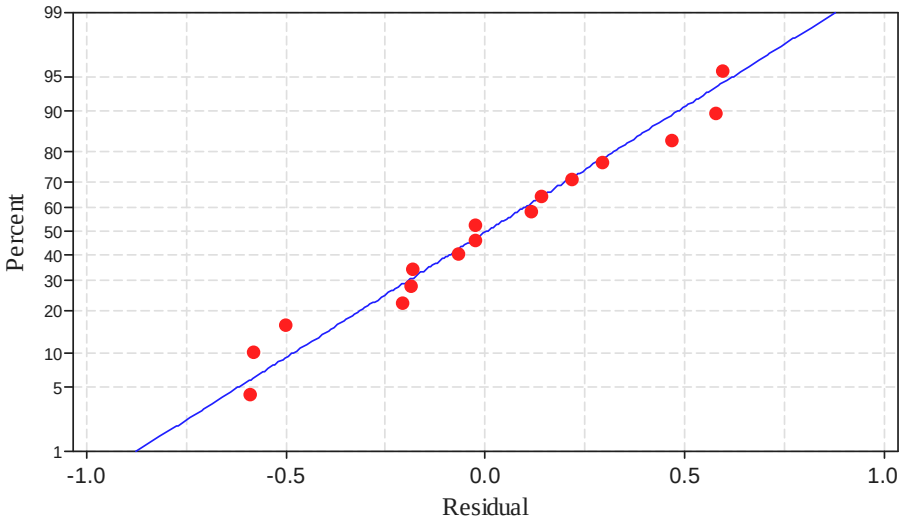


Figure 4.16 Normal plot of residuals.

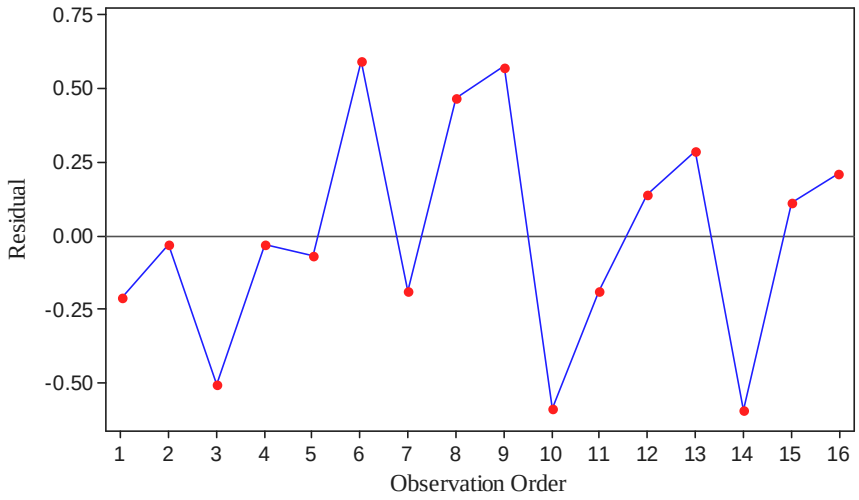


Figure 4.17 Residuals versus order of data.

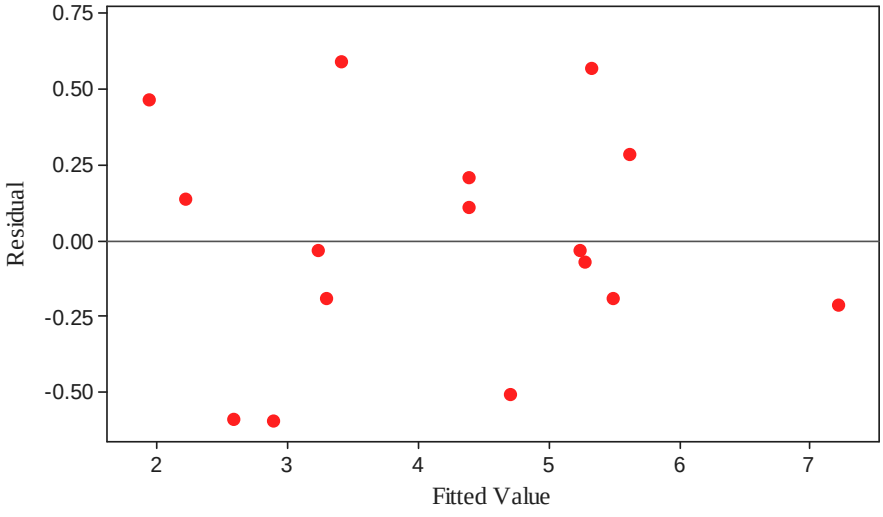

Figure 4.18 Residuals versus fitted values.

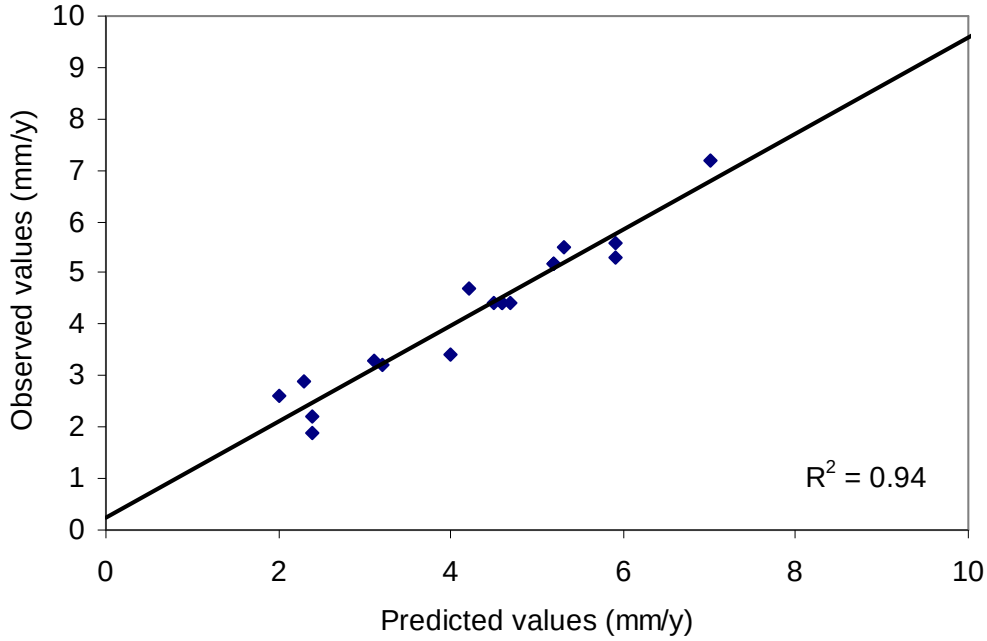


Figure 4.19 The relationship between observed and predicted values of the corrosion rate model at pH 5.5.

### 4.7 Verification with Experimental Data and Corrosion Prediction Software

Experimental data of Ismail [61] is used for the range of HAc concentration from 0 – 300 ppm. The comparison between the RSM model and the experiment data is shown in Figure 4.20 and Figure 4.21. A good fit was observed of the effects of HAc concentration and temperature.

The effect of temperature on corrosion rate for the case of HAc concentration 20 ppm was also verified using ECE [75] software (Figure 4.22). The predicted corrosion rate calculated by ECE software has $R^2$ of 95%, correlation of 97% and standard error of 0.2 (± 0.15 mm/y). A HAc comparison between the RSM model and those calculated by Freecorp software [88] is presented in Figure 4.23. It shows a coefficient determination of 99%, correlation of 99%, and standard error estimation of 0.05 (± 0.03 mm/y). The summaries of statistical performances of the models are presented in Appendix 2.

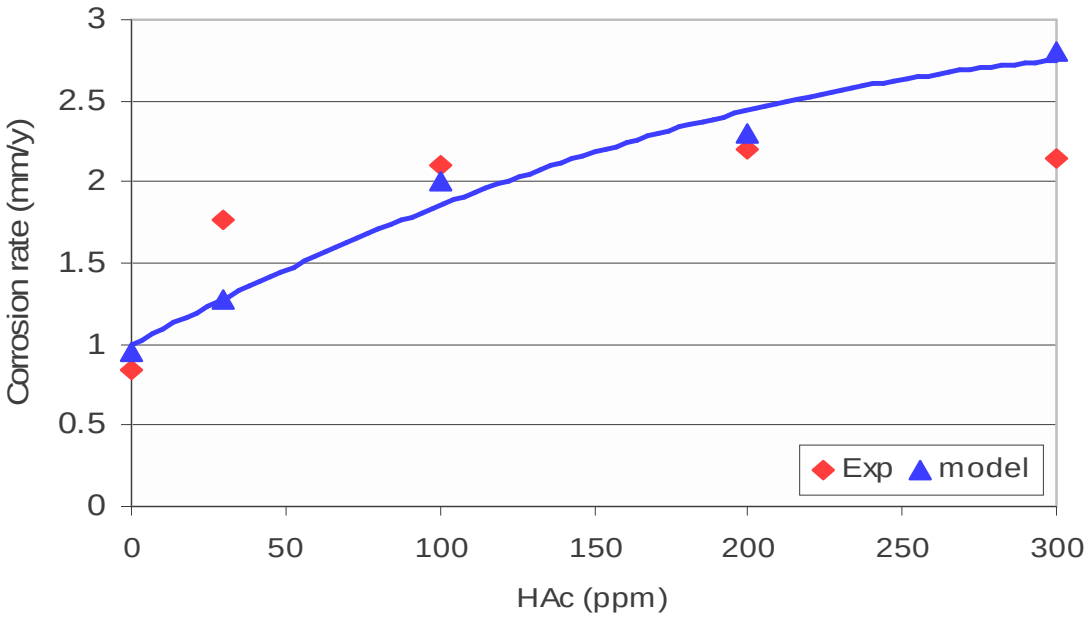


Figure 4.20 Corrosion rate at varying concentrations of HAc; a comparison between RSM model and Ismail's experimental data in 1 bar $CO_2$, 22°C, pH 5.5, and 1000 rpm.

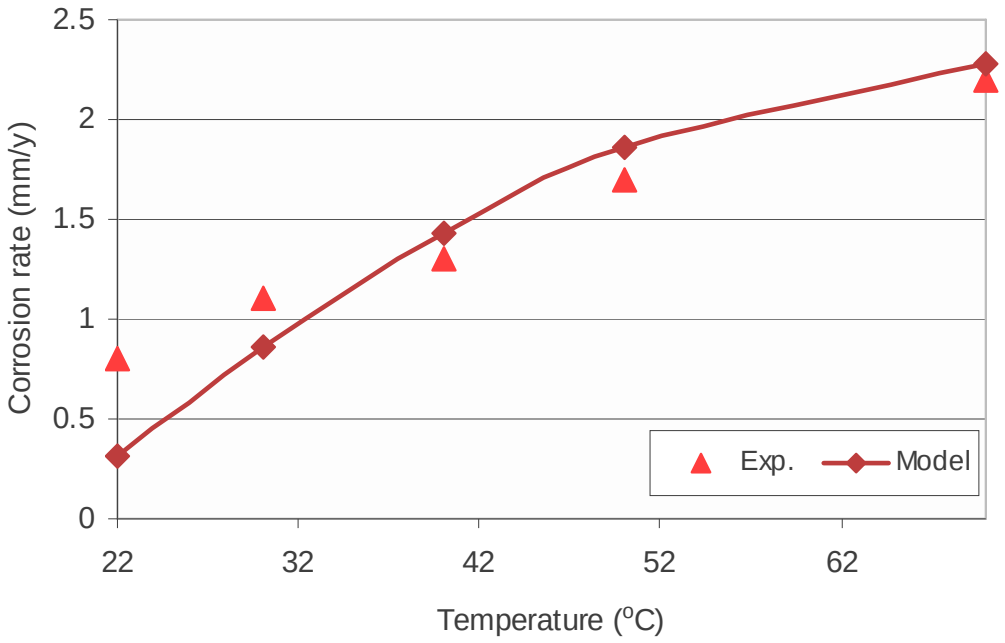


Figure 4.21 Corrosion rate at varying temperature; a comparison between RSM model and Ismail's experimental data in 1 bar $CO_2$, blank solution, pH 5.5, and stagnant condition.

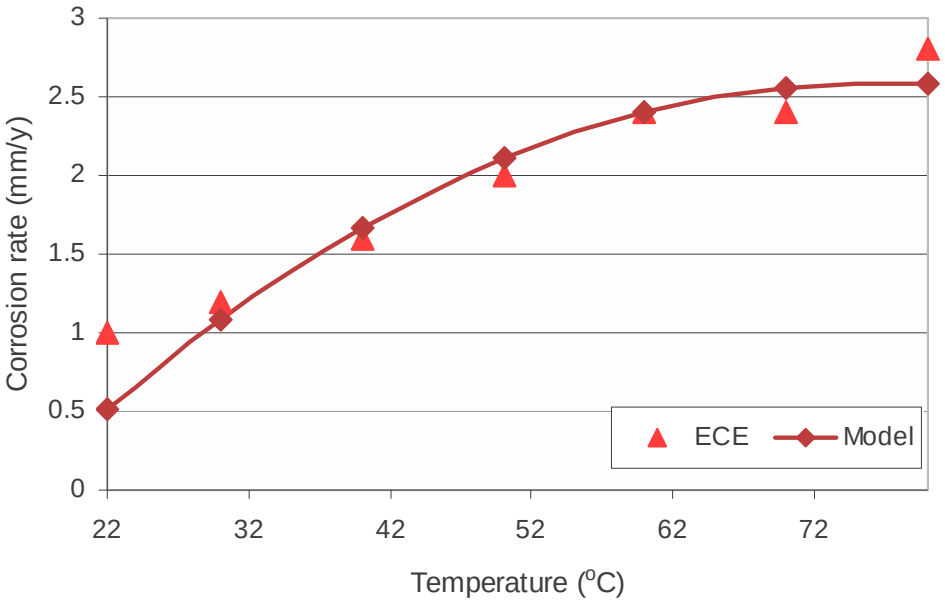


Figure 4.22 Corrosion rate at varying temperature; a comparison between RSM model and ECE in 1 bar $CO_2$, 20 ppm HAc, pH 5.5, and stagnant condition.

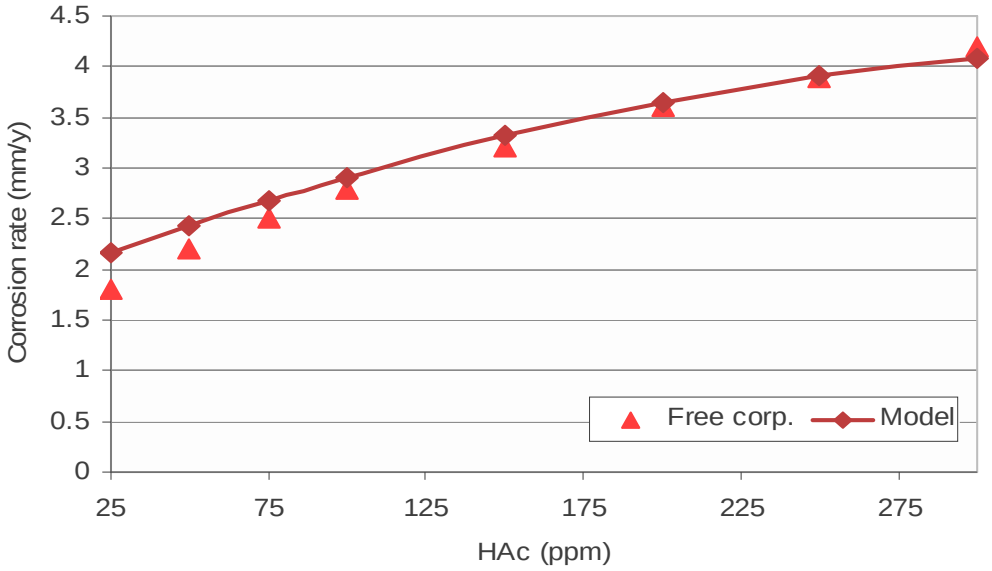


Figure 4.23 Corrosion rate at varying concentrations of HAc, a comparison between Model and Freecorp in 1 bar $CO_2$, 35°C, pH 5.5, and 1000 rpm rotation speed.

### 4.8 Analysis and Interpretation of Response Surface of $CO_2$ Corrosion at pH 5.5

Response of corrosion rate at pH 5.5 can be seen in the form of surface contour to show the simultaneous effects of variables tested as presented in Figures 4.24 - 4.26. RSM model equations are also used to calculate maximum corrosion rate caused by scaling temperature and limiting current density indicated by critical values of the model.

#### 4.8.1 Effects of temperature and HAc concentration

The interaction between HAc concentration and temperature was studied using contour plot as presented in Figure 4.24. From Figure 4.24, it can be observed that there is an increase in corrosion rate due to increase in temperature and HAc concentration and temperature. At the higher temperature (80$^{o}$C), an increase in HAc concentration causes a significant increase in the corrosion rate.

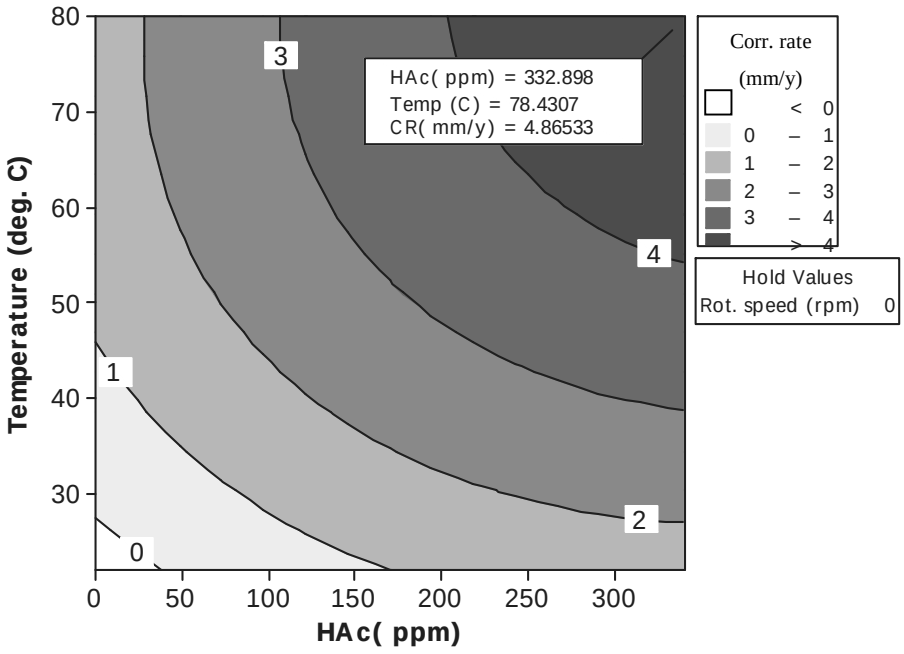


Figure 4.24 Response surface contours of corrosion rate as a function of temperature and HAc concentration at pH 5.5 and stagnant condition.

### 4.8.2 Effects of temperature and rotation speed

Figure 4.25 shows the effects of temperature and rotation speed on corrosion rate. As can be seen in Figure 4.25, corrosion rate increases with increasing temperature and rotation speed. The corrosion rate increases sharply at high temperature (80$^{o}$C). At 30$^{o}$C, increasing the rotation speed from 1000 to 6000 rpm caused the corrosion rate to increase from 1 to 2 mm/y. However at 80$^{o}$C, there is an increase of corrosion rate by 2 mm/y. These observations indicate that there was a synergism effect between temperature and rotation speed.

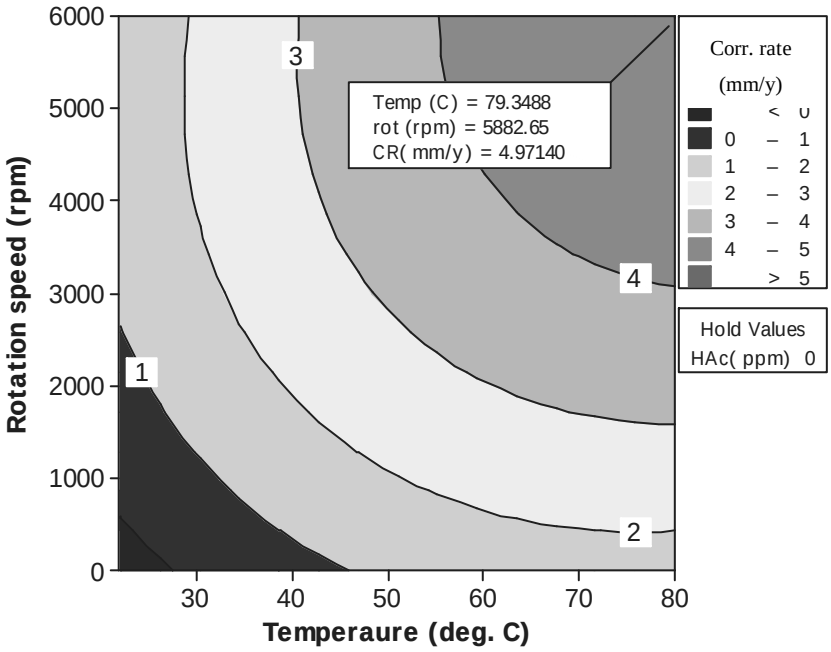


Figure 4.25 Response surface contours of corrosion rate as a function of temperature and rotation speed at pH 5.5 without HAc.

### 4.8.3 Effects of HAc concentration and rotation speed

The relationship between HAc concentration and rotation speed presented in contour graph is as shown in Figure 4.26. At the specified test conditions, corrosion rate shows an increase with increasing HAc concentration and rotation speed. Similarly, an increase in temperature and rotation speed (Figure 4.25) also causes corrosion rate to increase. From the contour graph in Figure 4.26, it can be concluded that the effect of HAc concentration and rotation speed on corrosion rate is to cause corrosion rate to

reach a stationary (maximum values) which shows the effect of limiting current density and film formation.

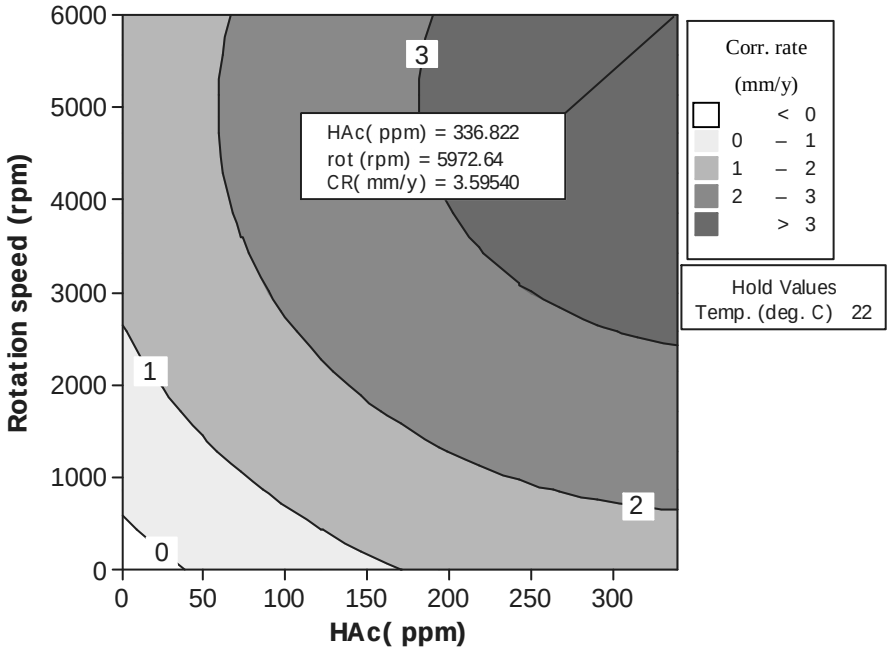


Figure 4.26 Response surface contours of corrosion rate as a function of temperature and rotation speed at temperature 22$^{o}$C and pH 5.5.

### 4.8.4 Maximum corrosion rate

The response surfaces calculated by second order model as explained previously (corrosion at pH 4) is applied to predict the maximum corrosion rate at pH 5.5. The first derivate of the mathematical function of corrosion model at pH 5.5 gives the following results:

$$\partial Y / \partial T = \quad 75.01 + 0.051(HAc) + 0.004(N) - (T) = 0 \tag{4.6}$$

$$\partial Y / \partial N = \quad 4134.22 + 1.37(HAc) + 34.107(T) - (N) = 0 \tag{4.7}$$

$$\partial Y / \partial HAc = 304.49 + 2.434(T) + 0.007(N) - (HAc) = 0 \tag{4.8}$$

By solving the equations, the maximum corrosion rate obtained from the model is 10 mm/y. These results have shown that the response surface has a maximum point

outside the experimental range of the independent variables. The maximum coordinates for three independent variables can be found beyond these experimental variables.

### 4.9 Design of Experiment to Predict Corrosion Rate at varying pH

The RSM regression model was used to study simultaneous effects of variables tested (HAc, T, N, pH). The model used FFD to find empirical relationship among variables. The first step was conducted by identifying historical data variables to find the trending of the $CO_2$ corrosion model. In order to evaluate the model performance, the model was verified with published experimental data and corrosion software calculation.

#### 4.9.1 Identification corrosion trend

The relationship between corrosion rate and $H^+$ ions concentration from 0.1 to 0.001 mol/$m^3$ based on mechanistic theory is shown in Figure 4.27. This concentration of $H^+$ ions corresponds to conditions at pH 4 to pH 6. It is shown that corrosion rate will increase exponentially when $H^+$ concentration increases. At the low concentration of $H^+$ ions, the corrosion rate increases significantly; while at the higher concentration of $H^+$ ions, the corrosion rate increases slowly.

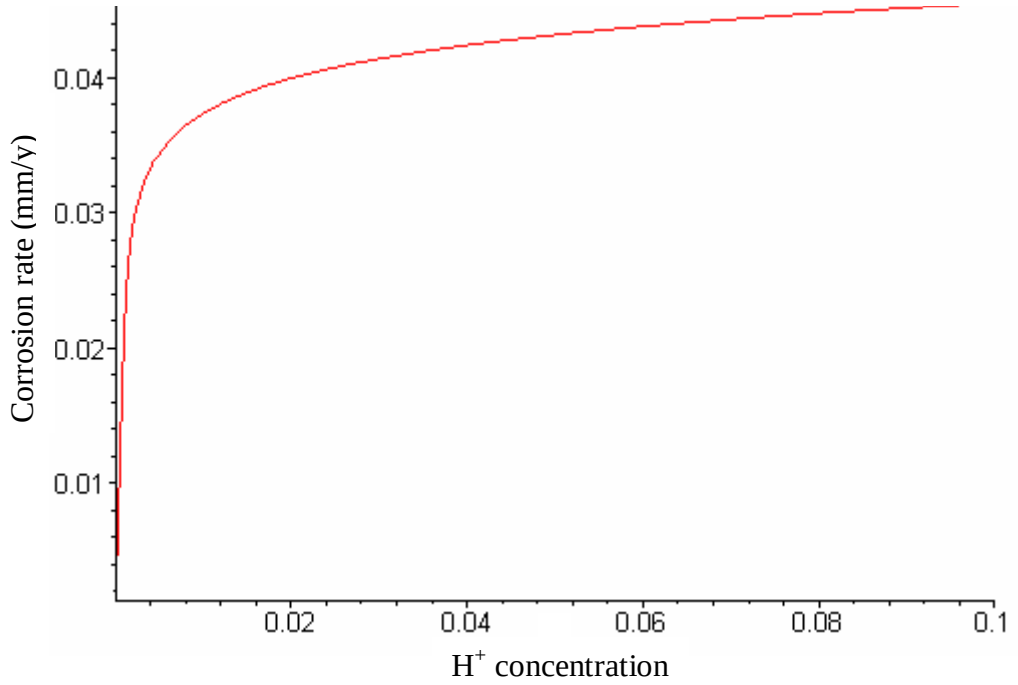


Figure 4.27 Simulated corrosion rate for a range of ions $H^+$ concentration from 0.1 mol/m $^3$ to 0,001 mol/m$^3$ (corresponds to pH 4 to pH 6) at 1 bar and static.

A design experiment involving four independent variables where full factorial design methodology was applied to predict the effect of pH on corrosion rate. The factors that were analyzed were: pH, temperature, HAc concentration and rotation speed. Table 4.7 shows the matrix arrangement used to study the effects of those four independent variables on corrosion rate using 3 % NaCl saturated $CO_2$ solution. The selected design experiment model was based on the most adequate model fitting. It was found that second order model had the best fitting of the corrosion rate data.

### 4.10 Design of Experiment to Study Effect of pH on Corrosion Rate

Table 4.7 shows the corrosion rate as effects of different concentration of HAc, T and N at various pH 4. The test was conducted for 1.5 hours and recorded the reading every 15 minutes. The corrosion rate measurements are calculated based on the average corrosion rate during 1.5 hours measurements.

Table 4.7 Experimental design to calculate model regression constant.

| No of run | Coded variables | | | | Natural variables | | | | Exp. results (mm/y) |
|---|---|---|---|---|---|---|---|---|---|
| | pH | Temp | HAc | Rot | pH | Temp ($^oC$) | Hac (ppm) | N (rpm) | |
| 1 | -1 | -1 | -1 | -1 | 4 | 22 | 0 | 1000 | 1.3 |
| 2 | 1 | -1 | -1 | -1 | 5.5 | 22 | 0 | 1000 | 1.2 |
| 3 | -1 | 1 | -1 | -1 | 4 | 60 | 0 | 1000 | 5.2 |
| 4 | 1 | 1 | -1 | -1 | 5.5 | 60 | 0 | 1000 | 2.9 |
| 5 | -1 | -1 | 1 | -1 | 4 | 22 | 60 | 1000 | 2.6 |
| 6 | 1 | -1 | 1 | -1 | 5.5 | 22 | 60 | 1000 | 1.8 |
| 7 | -1 | 1 | 1 | -1 | 4 | 60 | 60 | 1000 | 6.9 |
| 8 | 1 | 1 | 1 | -1 | 5.5 | 60 | 60 | 1000 | 3.8 |
| 9 | -1 | -1 | -1 | 1 | 4 | 22 | 0 | 6000 | 2.8 |
| 10 | 1 | -1 | -1 | 1 | 5.5 | 22 | 0 | 6000 | 2.3 |
| 11 | -1 | 1 | -1 | 1 | 4 | 60 | 0 | 6000 | 5.1 |
| 12 | 1 | 1 | -1 | 1 | 5.5 | 60 | 0 | 6000 | 4.9 |
| 13 | -1 | -1 | 1 | 1 | 4 | 22 | 60 | 6000 | 3.1 |
| 14 | 1 | -1 | 1 | 1 | 5.5 | 22 | 60 | 6000 | 2.9 |
| 15 | -1 | 1 | 1 | 1 | 4 | 60 | 60 | 6000 | 6.8 |
| 16 | 1 | 1 | 1 | 1 | 5.5 | 60 | 60 | 6000 | 5.8 |
| 17 | -1 | 0 | 0 | 0 | 4 | 35 | 40 | 3000 | 5.0 |
| 18 | 1 | 0 | 0 | 0 | 5.5 | 35 | 40 | 3000 | 3.7 |
| 19 | 0 | -1 | 0 | 0 | 5 | 22 | 40 | 3000 | 2.8 |
| 20 | 0 | 1 | 0 | 0 | 5 | 60 | 40 | 3000 | 5.4 |
| 21 | 0 | 0 | -1 | 0 | 5 | 35 | 0 | 3000 | 4.0 |
| 22 | 0 | 0 | 1 | 0 | 5 | 35 | 60 | 3000 | 4.3 |
| 23 | 0 | 0 | 0 | -1 | 5 | 35 | 40 | 1000 | 3.0 |
| 24 | 0 | 0 | 0 | 1 | 5 | 35 | 40 | 6000 | 4.9 |

### 4.10.1 Generalization of model

The application of RSM to study effects of pH on $CO_2$ corrosion using $2^4$ factorial design taken from Table 4.7 yields the following regression equation. This equation is an empirical relationship between independent variables as given in the following equation:

$$Y = -9.5966 + 1.5759(pH) + 0.4585(T) + 0.0361(HAc) + 0.0001(N) - 0.1720(pH)^2 - 0.0032(T)^2 - 0.0230(pH)(T) - 0.0067(pH)(HAc) + 0.0002(pH)(N) + 0.0001(T)(HAc) \quad (4.9)$$

Where;

$Y$ = corrosion rate (mm/y)

$pH$ = pH

$HAc$ = concentration of HAc (ppm)

$T$ = temperature ($^oC$)

$N$ = rotation speed (rpm)

### 4.10.2 Prediction of $CO_2$ corrosion model at various pH

The corrosion rate measured from the experiments (Yi) is compared with data from corrosion predictions ($\hat{y}$) is presented in Table 4.8. From the difference, it can be seen that there is a reasonable agreement between the experimental corrosion data and predicted values.

Table 4.8 Comparison between corrosion data experiments and corrosion data predictions

| No of run | Experimental variables | | | | Exp. results (Yi) | Predct. (ŷ) | Error (Yi-ŷ) |
|---|---|---|---|---|---|---|---|
| | pH | Temp($^{o}$C) | HAc (ppm) | N (rpm) | | | |
| 1 | 4 | 22 | 0 | 1000 | 1.3 | 1 | 0.3 |
| 2 | 5.5 | 22 | 0 | 1000 | 1.2 | 0.4 | 0.8 |
| 3 | 4 | 60 | 0 | 1000 | 5.2 | 5 | 0.2 |
| 4 | 5.5 | 60 | 0 | 1000 | 2.9 | 3.1 | -0.1 |
| 5 | 4 | 22 | 60 | 1000 | 2.6 | 2 | 0.6 |
| 6 | 5.5 | 22 | 60 | 1000 | 1.8 | 0.8 | 1 |
| 7 | 4 | 60 | 60 | 1000 | 6.9 | 6.6 | 0.3 |
| 8 | 5.5 | 60 | 60 | 1000 | 3.8 | 4 | -0.2 |
| 9 | 4 | 22 | 0 | 6000 | 2.8 | 1.7 | 1.1 |
| 10 | 5.5 | 22 | 0 | 6000 | 2.3 | 2.3 | 0 |
| 11 | 4 | 60 | 0 | 6000 | 5.1 | 5.4 | -0.3 |
| 12 | 5.5 | 60 | 0 | 6000 | 4.9 | 4.7 | 0.2 |
| 13 | 4 | 22 | 60 | 6000 | 3.1 | 2.5 | 0.6 |
| 14 | 5.5 | 22 | 60 | 6000 | 2.9 | 2.4 | 0.5 |
| 15 | 4 | 60 | 60 | 6000 | 6.8 | 6.9 | -0.1 |
| 16 | 5.5 | 60 | 60 | 6000 | 5.8 | 5.5 | 0.3 |
| 17 | 4 | 35 | 40 | 3000 | 5.0 | 4.8 | 0.2 |
| 18 | 5.5 | 35 | 40 | 3000 | 3.7 | 3.8 | -0.1 |
| 19 | 5 | 22 | 40 | 3000 | 2.8 | 2.1 | 0.7 |
| 20 | 5 | 60 | 40 | 3000 | 5.4 | 5.5 | -0.1 |
| 21 | 5 | 35 | 0 | 3000 | 4.1 | 3.8 | 0.3 |
| 22 | 5 | 35 | 60 | 3000 | 4.3 | 4.5 | -0.2 |
| 23 | 5 | 35 | 40 | 1000 | 3 | 3.3 | -0.3 |
| 24 | 5 | 35 | 40 | 6000 | 4.9 | 4.6 | 0.3 |

### 4.10.3 Analysis variance

Table 4.9 shows the analysis of variance for corrosion in saturated $CO_2$ solution using two level of full factorial designs (FFD) methodology for studying corrosion rate. The analyses of variance (ANOVA) described the confidence level of predicted parameters involved in the regression model. According to the ANOVA, the effect of linear and square in model regression has a significant value (for significance of 95%). But, the effect of interaction is significant at 93% significance level. Overall, the RSM model represents 97 % of experimental data.

Table 4.9 Analysis of variance for FFD model regression for the fitted models.

| Source | DF | Seq SS | Adj SS | Adj MS | F | P |
|---|---|---|---|---|---|---|
| Regression | 14 | 0.940032 | 0.940032 | 0.067145 | 23.06 | 0.000 |
| Linear | 4 | 0.740227 | 0.831772 | 0.207943 | 71.43 | 0.000 |
| Square | 4 | 0.148696 | 0.148747 | 0.037187 | 12.77 | 0.001 |
| Interaction | 6 | 0.051109 | 0.051109 | 0.008518 | 2.93 | 0.072 |
| Residual Error | 9 | 0.026202 | 0.026202 | 0.002911 | | |
| Total | 23 | 0.966234 | | | | |
| R-Sq = 97.29% | | | | | | |

### 4.11 Prediction and Verification of Corrosion Rate at pH 5

The effects of rotation speed on corrosion rate of carbon steel in solutions containing 3% sodium chloride, pH 5, temperature 60$^{o}$C at different HAc concentration from both experimentation and calculation are shown in Figure 4.28 to Figure 4.30. The results show that the corrosion rate for both experimental and predictions increase with increasing rotation speed and HAc concentration. All figures show good agreement with each other. The results also reveal that at higher rotation speed, corrosion rate reaches a plateau that may be associated to limiting current density.

This shows that electrochemical reactions and diffusion reaction may govern the corrosion rate.

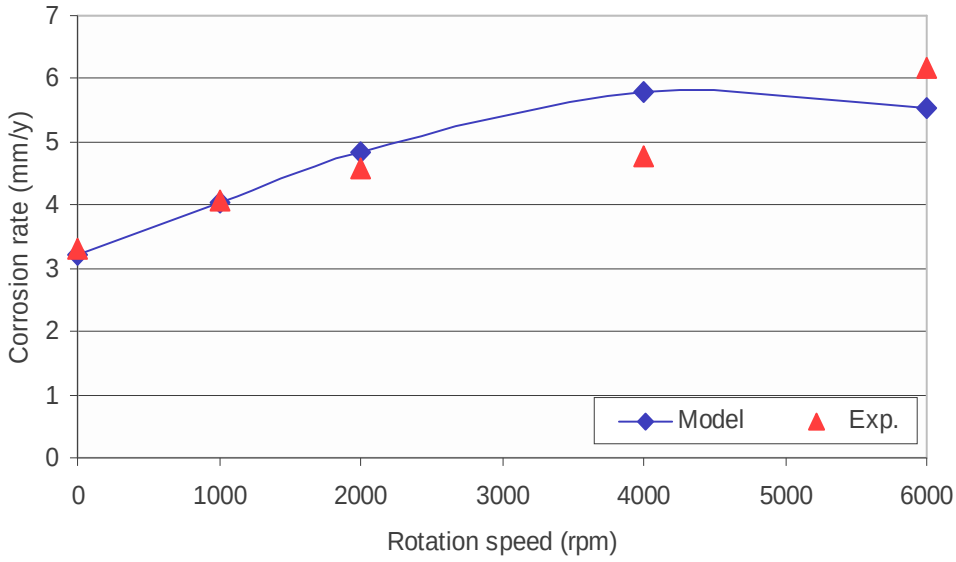


Figure 4.28 Effect of rotation speed on corrosion rate; a comparison between RSM model and Martin's experiments in 1 bar $CO_2$, 60°C, 20 ppm HAc, and pH 5.

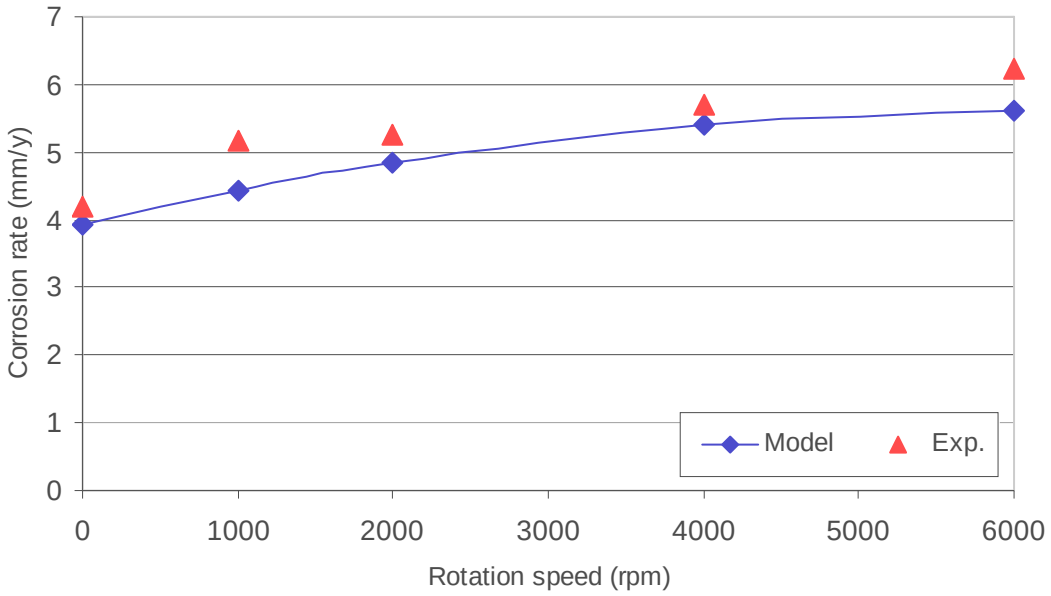


Figure 4.29 Effect of rotation speed on corrosion rate; a comparison between RSM model and Martin's experiments in 1 bar $CO_2$, 60°C, 40 ppm and HAc, pH 5.

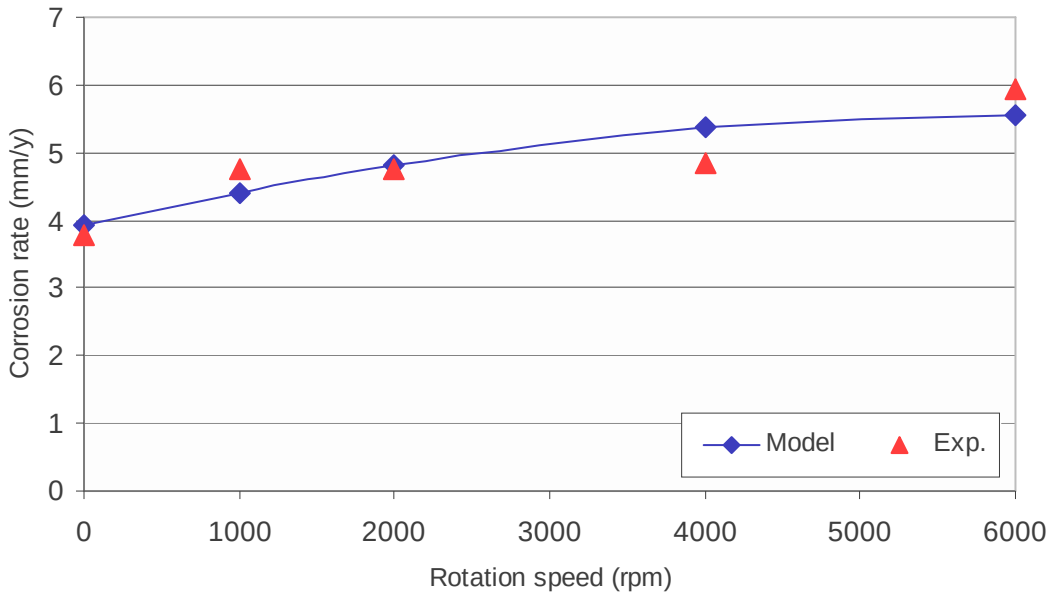


Figure 4.30 Effect of rotation speed on corrosion rate; a comparison between RSM model and Martin's experiments in 1 bar $CO_2$, 60$^{o}$C, 60 ppm HAc, and pH 5.

## 4.12 Prediction and Verification of Corrosion Rate at pH 6.

The effects of rotation speed on corrosion rate of carbon steel in 3% sodium chloride solutions at pH 6 and temperature 60°C, at varying HAc concentration from both experimentation and calculation are shown in Figure 4.31 to Figure 4.33. The corrosion rate is observed to increase with the increase in rotation speed and HAc concentration. Both, data predicted by the RSM model and experimental data show a steady corrosion increase at higher rotation speed. This trend is similar to the corrosion rate at pH 5. This shows that corrosion rate is not only controlled by charge transfer, but also by mass transfer.

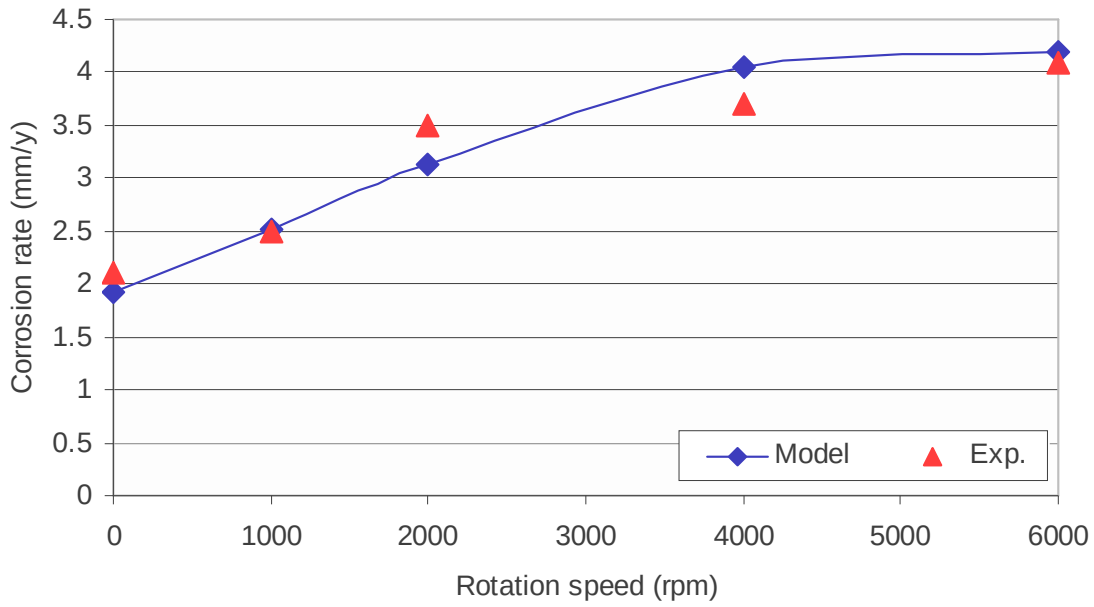


Figure 4.31 Effect of rotation speed on corrosion rate; a comparison between RSM model and Martin's experiments in 1 bar $CO_2$, 60°C, 20 ppm HAc, and pH 6.

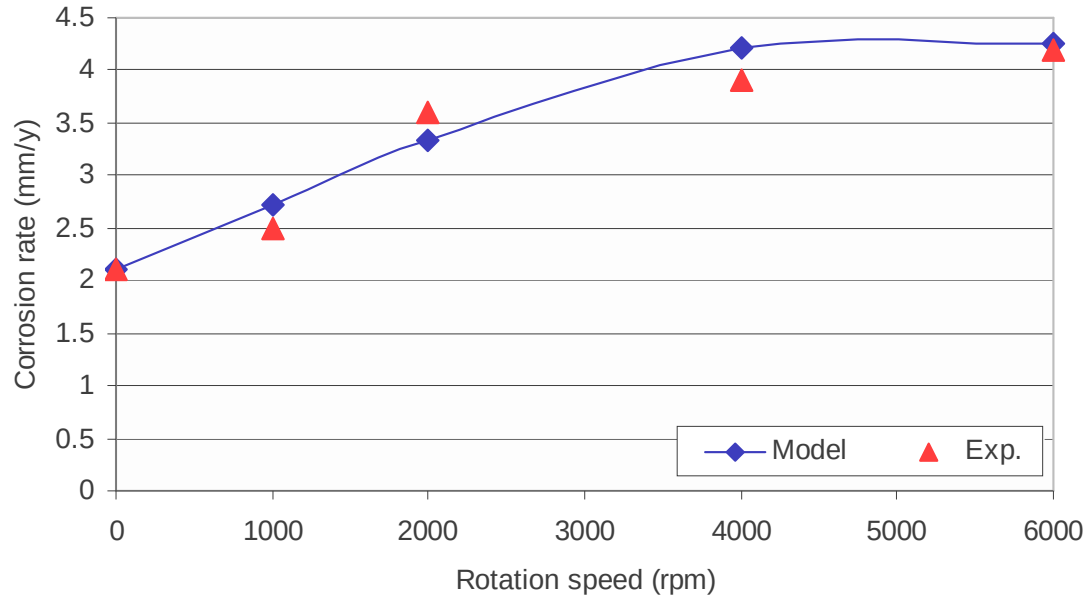


Figure 4.32 Effect of rotation speed on corrosion rate; a comparison between RSM model and Martin's experiments in 1 bar $CO_2$, 60°C, 40 ppm HAc, and pH 6.

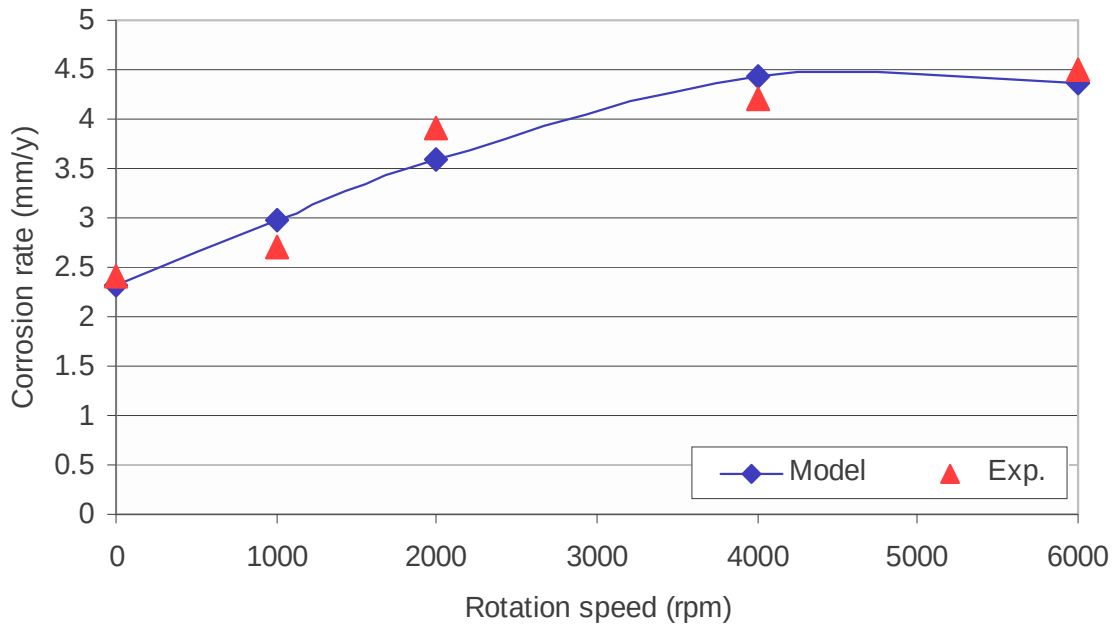


Figure 4.33 Effect of rotation speed on corrosion rate; a comparison between RSM model and Martin's experiments in 1 bar $CO_2$, 60°C, 60 ppm HAc, pH 6.

### 4.13 Prediction of the Effect of pH on Corrosion rate

The effect of pH on corrosion rate was studied in solutions saturated with $CO_2$ with the addition of HAc in the pH range from 4 to 5.5 using RSM. The results are shown in Figure 4.34 to Figure 4.37. The RSM model is compared to Nesic's experimental data, which had shown a good fit. As the pH was increased from 4 to 6, the corrosion rate decreased from 0.8 mm/y to 0.5 mm/y.

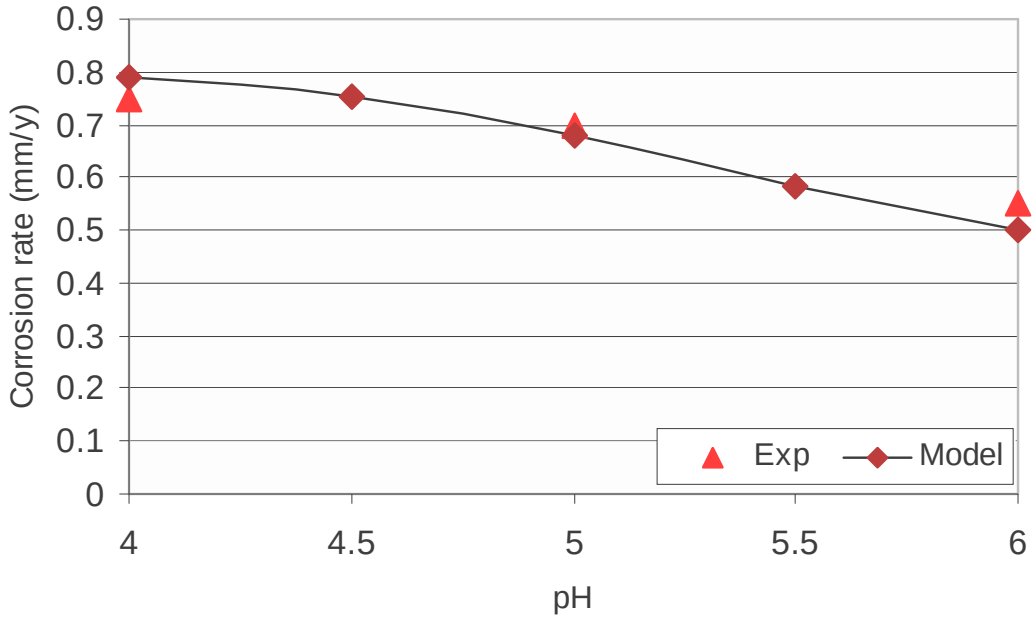


Figure 4.34 Corrosion rate at varying pH; a comparison RSM model with Nesic's experimental data in1 bar, 20°C, and stagnant condition.

### 4.13.1 Effect of pH and temperature on $CO_2$ corrosion

Figure 4.35 shows the result of corrosion prediction by RSM at various pH and temperature. These calculations were performed at temperatures from 25 to 60°C at varying pH in the range of 4 to 5.5. From the figure, it is observed that corrosion rate increases rapidly at the temperature of around 50°C. While at lower temperatures (25°C), the corrosion rate increases slowly (from 3 to 3.5 mm/y). Corrosion rate seems to be affected more by temperature rather than pH.

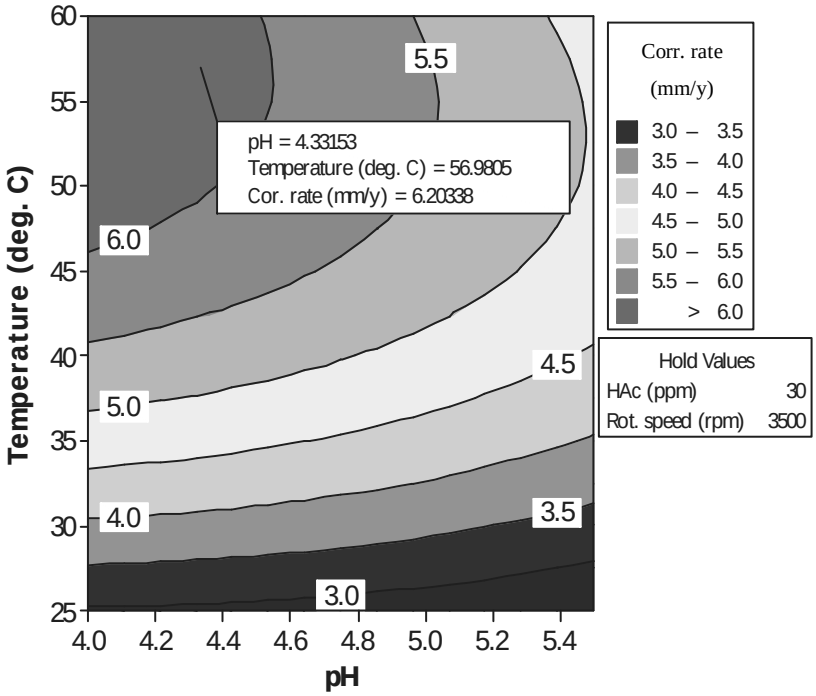


Figure 4.35 Response surface contours for corrosion rate as a function of temperature and pH at HAc at 30 ppm and rotation speed at 3500 rpm.

### 4.13.2 Effect of pH and HAc on $CO_2$ corrosion

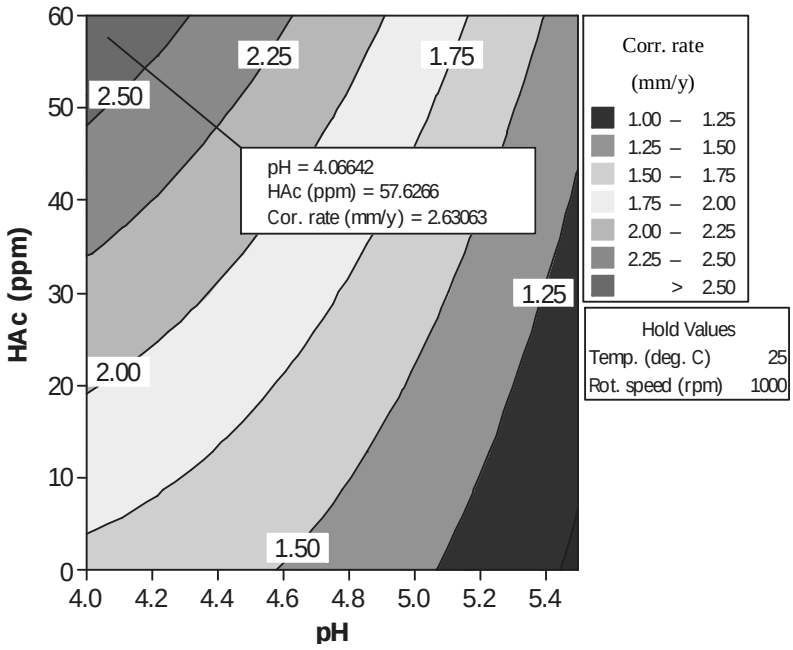


Figure 4.36 Response surface contours for corrosion rate as a function of HAc and pH at 25$^{o}$C and rotation speed at 1000 rpm.

Figure 4.36 presents the corrosion rate obtained using RSM model for varying HAc concentration and pH in the range 4 to 5.5. In general, the corrosion rate increases with increasing HAc concentration in the specified range of pH. The graph shows that corrosion rate decreases with increasing pH. In this prediction, the maximum corrosion rate is at pH 4 and 60 ppm HAc.

### 4.13.3 Effect of pH and rotation speed on $CO_2$ corrosion

Figure 4.37 shows a correlation between pH, rotation speed and corrosion rate. In Figure 4.37, it can be seen that corrosion rate increases with increasing rotation speed. The corrosion rate increases faster at pH 4 compared to pH 5. It is also observed that at higher rotation speed (4000 – 6000 rpm), the corrosion rate is almost constant even though pH increases. This indicates the flow independent limiting current region caused by rotation speed.

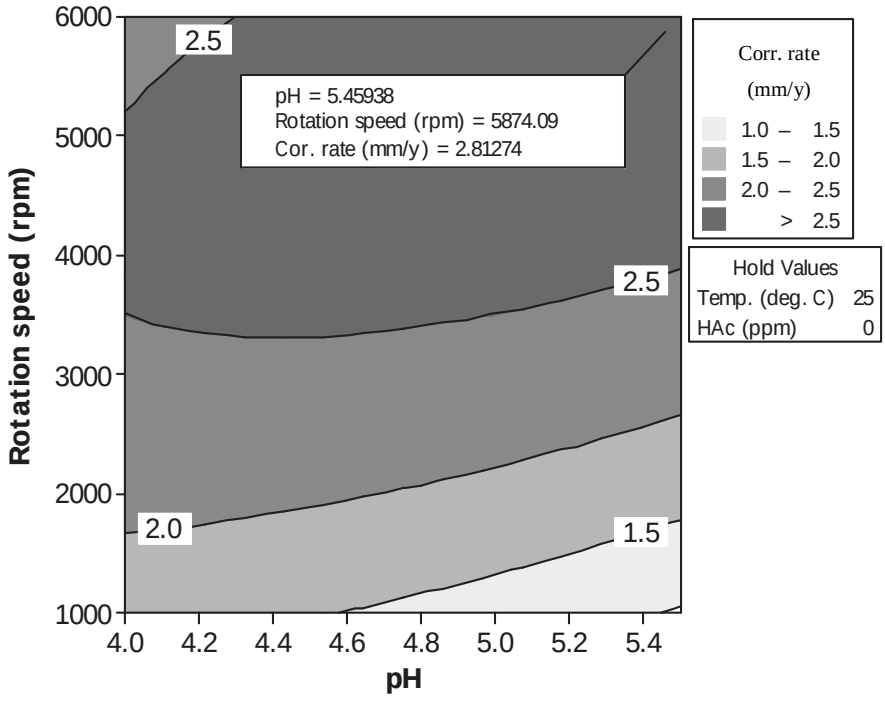


Figure 4.37 Response surface contours for corrosion rate as a function of rotation speed and pH at 25°C and blank solution.

### 4.14 Discussions: $CO_2$/HAc Corrosion

The results of the various concentrations of HAc with different variables tested such as T and N in $CO_2$ saturated solution are discussed in these sections below.

#### 4.14.1 Effects of temperature and HAc concentration on corrosion rate

The effects of temperature and HAc concentration on carbon steel in $CO_2$ environments, as modeled by RSM, are presented in Figure 4.12 and Figure 4.24. The figures show that an increase in temperature and HAc concentration leads to an increase in corrosion rate. The increase in corrosion rate is related to the role of HAc as a source of additional species providing protons and a new cathodic reaction via the direct reduction of undissociated HAc [62]. The mechanism of the dissolved HAc in $CO_2$ corrosion can also be correlated to the concentration of undissociated HAc present in the solution as described by Nafday [17]. The effects of HAc in low concentration (6-60 ppm) had been proposed by Crolet et al. [64] to inhibit the anodic (iron dissolution). They argued that the increase in the rate of corrosion was due to an inversion in the bicarbonate/acetate ratio. At this inversion point, HAc is the predominant acid compared to carbonic acid, and becomes the main source of acidity. Several researchers who have conducted experiments involving HAc confirmed that the presence of HAc in the range of 10 – 340 ppm causes higher corrosion rate compared to without HAc [61]. The increased corrosion as an effect of temperature and HAc concentration was also observed by Ismail [61], James [5] and Nesic et al. [6].

The electrochemical behavior of carbon steel with the presence of HAc resulted: decreasing pH, increasing cathodic limiting current, and decreasing $E_{corr}$. Further, Nesic et al. [6] argued that the cathodic reaction will become the rate determining step and the limitation was due to diffusion of proton to the steel surface rather than electron transfer. There is a proof that HAc can increase the cathodic reaction rate by hydrogen evolution reaction process if the concentration is significant.

As shown by the RSM model, the corrosion rate at pH 4 is higher than at pH 5.5. The effect is proportional to the amount of HAc presented. At pH 5.5, the corrosion rate also increases when HAc concentration is increased. However, the average

corrosion rate at pH 5.5 is lower than the average corrosion rate at pH 4. These observations suggest that $H^+$ ions are the predominant factor that contributes to corrosion rate.

### 4.14.2 Effects of temperature and rotation speed.

As observed in the Figure 4.13, corrosion rate increases with increasing temperature and rotation speed. It can be seen that at 80$^o$C, increasing the rotation speed did not produce significant effect on corrosion rate. These observations indicate that increasing temperature will eliminate the effect of rotation speed on corrosion rate. This is due to the formation of limiting current density as the effect of interaction with temperature.

It has been recognized that temperature strongly influences corrosion rate. It can increase or decrease corrosion rate depending on films properties produced during corrosion reactions. As can be seen from Figure 4.13, the corrosion rate is higher at lower temperatures (< 60 °C) compared to the higher temperatures. An increase of the corrosion rate can be related to the degree of solubility of the species in solution since higher solubility of $FeCO_3$ slows down the formation of the protective film. Song [90] stated that, at temperatures below 60$^o$C, hydrogen evolution took part as a rate determining step and carbonate scale did not form well. The film was detached and porous, which gave little protection and cannot be detected. In this condition, the kinetics of film formation was faster and corrosion rate was under charge-transfer control. Above 60°C, the protectiveness of the iron carbonate layer increases with temperature as the solubility of iron carbonate decreases. Thus, the corrosion rate is reduced. However, at higher temperatures, there is a direct reaction between steel and water to produce dense and protective films [91]. Therefore, in this condition corrosion rate may be governed by film formation.

### 4.14.3 Scaling temperature

Based on the literature reviews [61, 91], temperature is known to increase corrosion rate until the temperature reaches a maximum value called scaling temperature. Beyond this temperature, the corrosion rate will decrease or becomes constant. Factors affecting the scaling temperature are pH, HAc concentration and rotation speed. The scaling temperature as an effect of pH predicted by the RSM model is presented in Figure 4.38 and 4.39 below.

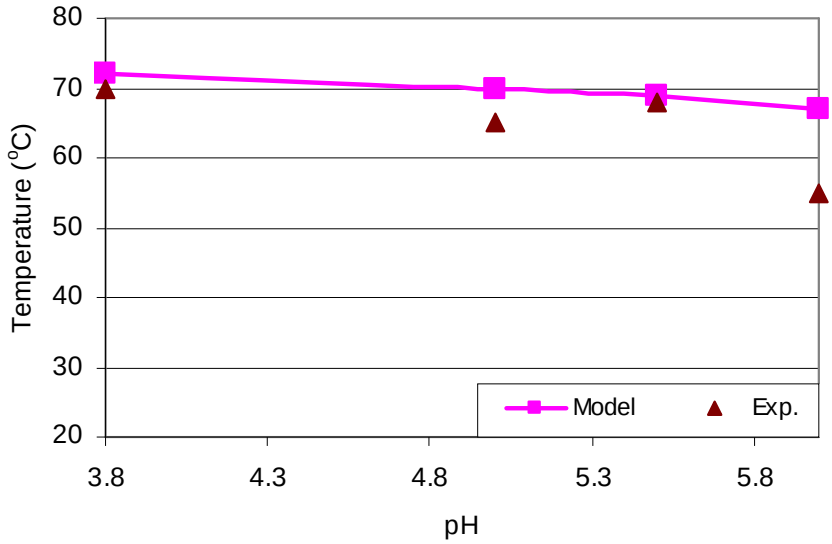


Figure 4.38 Effects of pH on scaling temperature as calculated by RSM in 1 bar and stagnant (Experimental data were taken from reference [61]).

From Figure 4.38 and Figure 4.39, it can be seen that higher pH tend to decrease scaling temperature. This observation is supported by several researchers [6, 17], who related this phenomena to film formation where higher pH tend to favor film precipitation.

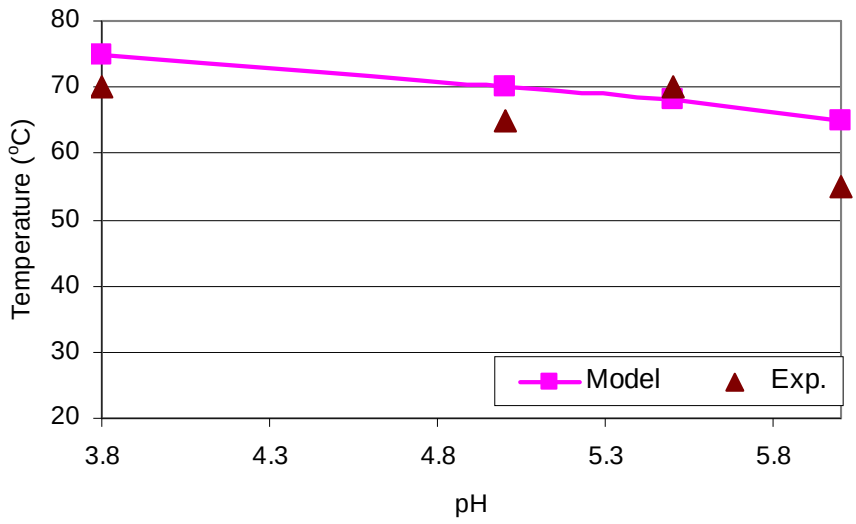


Figure 4.39 Effects of pH on scaling temperature as calculated by RSM in 1 bar $CO_2$, 360 ppm HAc, and stagnant (Experimental data were taken from reference [61]).

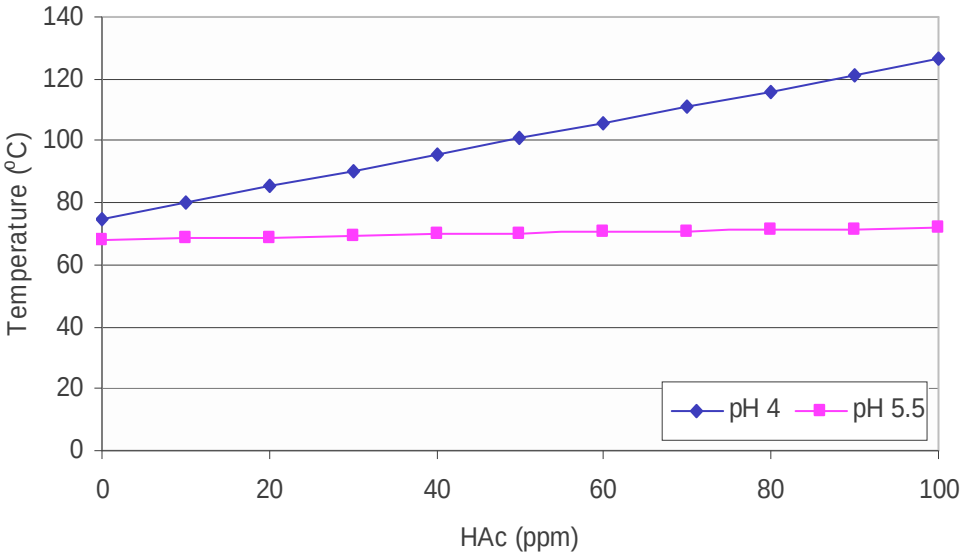


Figure 4.40 Effects of HAc on scaling temperature as calculated by RSM in 1 bar $CO_2$, and stagnant.

Scaling temperature is also influenced by HAc concentration. As shown in Figure 4.40 and Figure 4.41, higher HAc concentration will increase scaling temperature. Figure 4.40 shows that the influence of pH on scaling temperature, where lower pH causes the scaling temperature to increase. The finding are also supported by M.C. Ismail [61]. A comparison between calculations from RSM and Ismail's experimental data is presented in Figure 4.41. George [62] explained that the presence of HAc can

interrupt the film formation and increase scaling temperature. Surface analyses investigation indicated that HAc concentration has decreased the thickness of the film.

Vennesa et al. [66] observed that HAc can retard the time to reach scaling temperature. She related this effect to an increase in the area of corrosion. She argued that the prime factor which influences film formation is the degree of solubility. However, since the solubility of iron acetate is much higher than iron carbonate's, therefore, the protective film formation by iron acetate cannot readily occur. Without the formation of a stable protective film, the corrosion rate of steel in $CO_2$ environment can remain high [14].

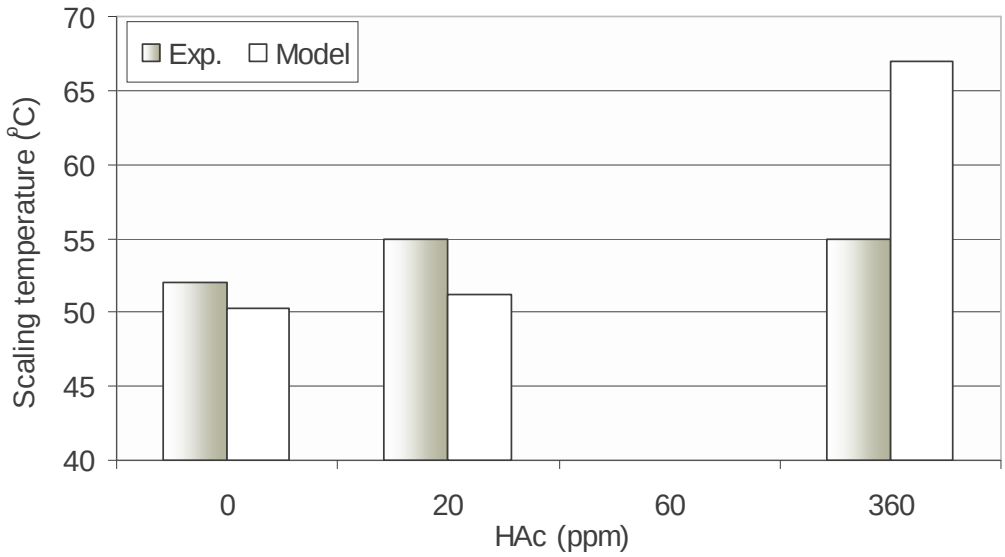


Figure 4.41 Effects of HAc on scaling temperature as calculated by RSM in 1 bar $CO_2$, stagnant, and pH 6 (Experimental data were taken from reference [61]).

### 4.14.4 Effects of rotation speed on corrosion rate

Figure 4.14 (pH 4) and Figure 4.26 (pH 5.5) present a second order model of response surface relating the effect of rotation speed and HAc concentration on corrosion rate. Different corrosion rate are observed at different HAc concentration and rotation speed, for both pH conditions.

The effect of flow on corrosion rate has been studied by Silverman et al.[33-35]. They explained that flow increases corrosion due to a combination of mechanical

effects due to water motion, and electrochemical effects of corrosion. Higher velocity is directly associated with higher turbulence that promotes mixing in the solution. This affects both the corrosion rate of the bare steel surface and the precipitation rate of iron carbonate. Prior to any film formation, high velocity will lead to increased corrosion rate. The transport of cathodic species toward the steel surface is enhanced by turbulent transport. At the same time the transport of $Fe^{2+}$ ions away from the steel surface also increases, leading to a lower concentration of $Fe^{2+}$ ions at the steel surface. This results in higher surface supersaturation and thus precipitation rate becomes lower [34].

Further, Singer [51] explained that flow-induced corrosion is a type of corrosion that is caused by a combination between mechanical and electrochemical effects. Mechanical effect due to water motion causes impingement that leads to metal removal and material abrasion, and increases wall shear stress as shown in Figure 4.42. Water that flows to the surface can also wear the corrosion product film or create shear stress to the surface. In conclusion, the researchers [33, 34, 51] found that parameters influenced flow induced corrosion are hydrodynamic boundary layer and rate of momentum transfer which affects on mass transfer of reactants.

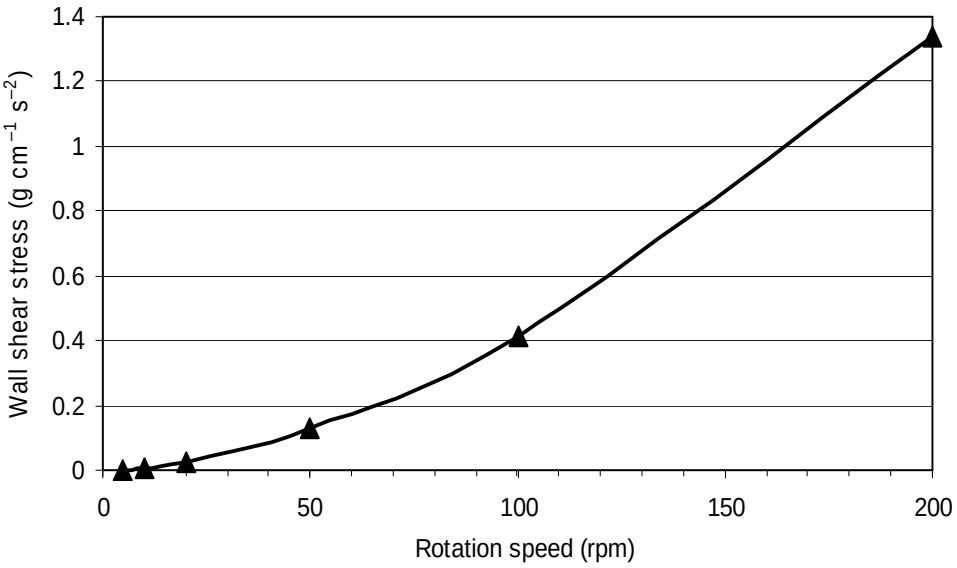


Figure 4.42 Effect of rotation speed on wall shear stress [74].

### 4.14.5 Flow independent limiting current

There is also threshold value of rotation speed. These phenomena can be studied by using cathodic scan polarization. Through cathodic polarization, Martin [60] observed that at specific rotation value the cathodic current behavior will show diffusion behavior termed as limiting current density. In this case, Rothman and Mendoza as cited by Ismail [61] classified the effect of flow in two regions; flow dependent limiting current and flow independent limiting current. Flow dependent limiting current is correlated with diffusion of main electrochemical species of $H^+$, $H_2CO_3$, and HAc; while flow independent limiting current is related to chemical reaction product as an effect of corrosion process. The effect of temperature and HAc concentration on rotation speed threshold is presented in Figure 4.43. This graph was obtained by solving RSM equations 4.2 to 4.4.

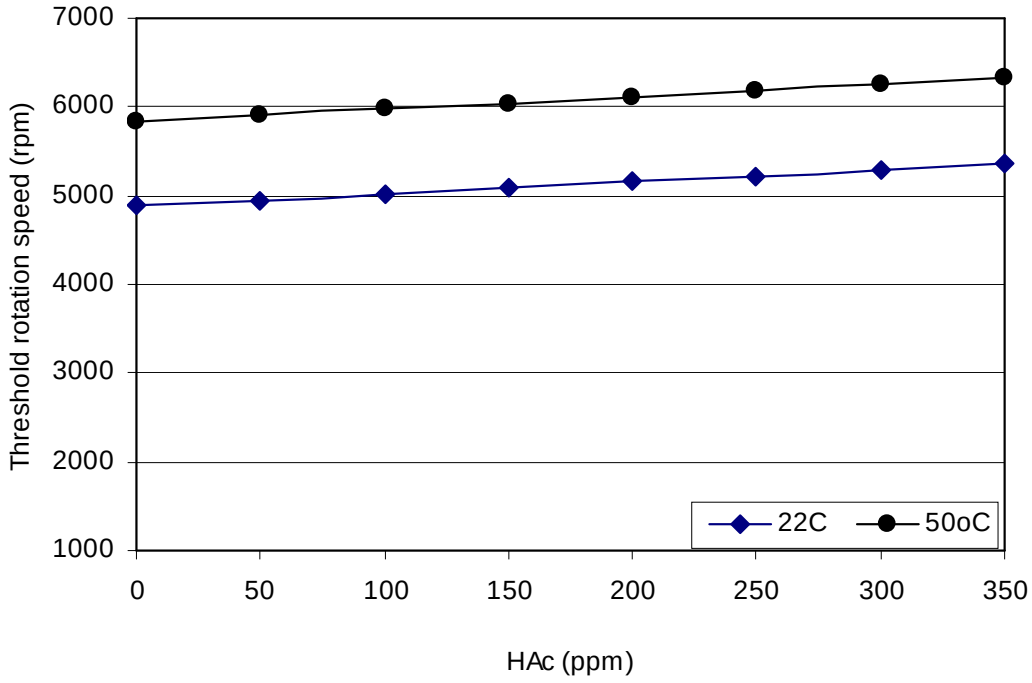


Figure 4.43 Effects of HAc on threshold rotation speed as calculated by RSM in 1 bar $CO_2$, pH 4 and stagnant.

### 4.14.6 Effects of pH

The effects of pH on corrosion rate as calculated by RSM can be seen in Figure 4.36 and Figure 4.37. At low pH, corrosion rate increases sharply. According to Garsany et al. [65], in relating to HAc, the increase of corrosion rate will increase proportionally to the concentration of undissociated HAc in the brine solution. Joosten et al. [2], also examined the effect of pH on corrosion rate in synthetic seawater solution with HAc. They found a localized corrosion when 600 ppm HAc was added.

In $CO_2$ environments, pH is influenced by changing the $H^+$ ions concentration, temperature, pressure, and ionic strength [17]. pH is affected by dissolved iron bicarbonate; pH will increase when there is an increase of ion bicarbonate, The reduction in corrosion rate pH increases can be explained by the properties of the protective film. At higher pH, the carbonate film becomes thicker, more dense and protective. Thus, the passivity of carbon steel lies within the pH range of the carbonate/bicarbonate formation [92]. Observations as described by Figure 4.37 show that as pH increases from 4 to 5, the anodic reaction rate also increases; this observation is consistent with Bockris's iron dissolution mechanism [12]. However a further increase of pH from 5 to 6, did not increase either the anodic reaction rate or corrosion rate. At higher pH, the cathodic reaction and the limiting current was retarded by the increasing pH. Hoffmeister [29] recorded that at pH 5.8 the corrosion rate did not reduce significantly, which reflected a relatively porous, detached and un-protective carbonate film. These properties may be related to fast formation of the film. Thus, the effect of concentration of dissolved iron bicarbonate, as an initial corrosion product is important to predict corrosion rate at certain pH value [50].

## 4.15 Comparison between Experimental Corrosion Rates and Commercial Predictive Models

The results from the experiments are compared to Freecorp [88], which is a commercial prediction software. The Freecorp combines electrochemical theories which consist of partial cathodic and anodic processes on the metal surface. This model provides the most realistic conditions of aqueous $CO_2$ system. The total corrosion rate is calculated based on the mixed-potential theory under activation or

mass control by taking account the oxidation of iron and reduction of hydrogen ions, water reductions, carbonic acid and acetate ions reductions. The comparisons are shown in Table 4.10 (pH 4) and Table 4.11 (pH 5.5). Based on the comparison results on Table 4.10 at conditions: 20 ppm HAc concentration, temperature 60 – 70$^{o}$C and low rotation speed, it shows that the corrosion rate calculated by the RSM model is less precise compared to blank solution, middle temperature and high rotation speed conditions. At the middle temperature, high rotation speed conditions, the Freecorp and RSM model shows precise values (st. error 0.1). Table 4.11, conditions at pH 5.5, shows that Freecorp does not show a good standard error of corrosion rate at low temperature and high rotation speed condition. While good agreements of standard error occurred in middle and high temperature as well as 20 ppm HAc concentration conditions.

Table 4.10 Summary of the performance of predictive model pH 4

| Test Conditions | Level | RSM models Predictions vs Freecorp | | |
|---|---|---|---|---|
| | | $R^2$ | Correlation | Standard error |
| Temperature ($^{o}$C) | High | 0.80 | 0.88 | 0.4 |
| | Medium | 0.83 | 0.90 | 0.18 |
| | Low | 0.87 | 0.94 | 0.27 |
| Rotation speed (rpm) | High | 0.90 | 0.97 | 0.30 |
| | Medium | 0.90 | 0.97 | 0.30 |
| | Low | 0.90 | 0.97 | 0.18 |
| HAc (ppm) | High | 0.85 | 0.8 | 0.10 |
| | Medium | 0.82 | 0.94 | 0.20 |
| | Low | 0.89 | 0.98 | 0.37 |

Table 4.11 Summary of the performance of predictive model at pH 5.5

| Test Conditions | Level | RSM models Predictions vs Freecorp | | |
|---|---|---|---|---|
| | | $R^2$ | Correlation | Standard error |
| Temperature ($^oC$) | High | 0.81 | 0.89 | 0.30 |
| | Medium | 0.90 | 0.95 | 0.18 |
| | Low | 0.80 | 0.88 | 0.18 |
| Rotation speed (rpm) | High | 0.95 | 0.94 | 0.22 |
| | Medium | 0.96 | 0.93 | 0.28 |
| | Low | 0.96 | 0.93 | 0.44 |
| HAc (ppm) | High | 0.85 | 0.80 | 0.20 |
| | Medium | 0.82 | 0.94 | 0.20 |
| | Low | 0.89 | 0.98 | 0.15 |

In general, the RSM models consider a feasible comparable with the Freecorp model calculation as described by statistics performance attached in Appendix 2. It can be summarized that the models, in average, have coefficient determination of 87 % that shows 87 % of the software prediction can be explained by the RSM model. The trend similarity indicated by correlation provides a value of 92%. However, the scatter observed between RSM model and predictive model contribute to predictive error of 24%. Comparing RSM model with experimental data from reference [61] (Appendix 2c – 2d), the results does not show a significant different to the comparison with Freecorp. It has coefficient determination 88 %, correlation 94% and standard error 0.26.

From the statistical data explained above it can be seen that it is found uncertainties indicated by standard error between RSM and Freecorp or experimental data. Those errors come from the following:

- Freecorp calculates corrosion rate under activation control of cathodic reactions. It will show a higher results when corrosion is controlled by film formation.

- The total rate of corrosion involving several species is equal to the sum of the corrosion caused by those individual species. This will cause the higher value corrosion rate due to interactions between the species that change the electrochemical behavior.
- Freecorp model does not consider carbon content of specimen, scan rate polarization, surface roughness of specimen, and Tafel slope. Although those parameters are often neglected, those parameters, in fact, have effects in corrosion rate.
- Limitations of the LPR test methodology, test parameters setting and experimental set up. The uncertainties of corrosion measurements based on this electrochemical method have been recorded to significant value (27 %) [17].
- $Fe^{2+}$ concentration, $Cl^-$ ions concentrations, and actual water chemistry are not known in detail. The effect of $Fe^{2+}$ concentration and water chemistry properties influence iron carbonate precipitation which can affect corrosion rate.

Those factors that affect the error have been recorded to contribute absolute experimental error of 34% as calculated by O. A. Nafday [17].

### 4.16 Conclusion

Based on the experimental predictions using response surface methodology, the following conclusion can be made:

#### 4.16.1 Experimental design

- Second order polynomial regression model is adequate to represent the data for all responses obtained. The RSM corrosion model, which includes the effects of temperature, HAc and rotation speed has a quadratic function and can be fitted well with the literatures and corrosion program software.
- The mathematical models obtained by RSM can be used to calculate stationary value analytically. The stationary values are useful to determine mechanistic

corrosion process such as scaling temperature, flow independent limiting current and flow dependent limiting current.

- The RSM is capable in predicting corrosion rate by using limited numbers of experiments.

### 4.16.2 Regression model relationship

A second order relationship has been found between HAc concentration, rotation speed and temperature on corrosion rate; while an exponential relationship is found between pH, HAc concentration, rotation speed and temperature on corrosion rate. As expected, all dependent variables have a high positive correlation with corrosion rate. While pH, and interaction between pH and HAc concentration show a negative correlation. The curve describes that a high HAc concentration and temperature will increase corrosion rate.

### 4.16.3 Effects of HAc, temperature and rotation speed based on RSM model

- Increasing HAc concentration causes increased corrosion rate for a given temperature and rotation speed at both pH 4 and pH 5.5.
- Increasing temperature causes increased corrosion rate for a given HAc concentration and rotation speed at both pH 4 and pH 5.5.
- Increasing rotation speed causes increased corrosion rate for a given temperature and HAc concentration at both pH 4 and pH 5.5.
- Highest corrosion rate occurred at the middle of temperature, HAc concentration and rotation speed at pH 4. While at pH 5.5, the maximum corrosion rate located on the high temperature, high rotation speed and high HAc concentration.
- At low rotation speed, the effect of temperature is more dominant as compared to the effects of HAc concentration at pH 4. The dominant effect of temperature compared to rotation speed was also observed at low HAc concentration at pH 5.5. These trends did not find in pH 5.5 where both

temperature and HAc concentration have the same role in contributing corrosion rate.

- Corrosion product formation is an important parameter in defining corrosion model regression that can be used to determine initial identification for corrosion predictions.
- Based on RSM data and supported by the works of previous researches, rotation speed has little effect on the corrosion rate of carbon steel in $CO_2$ environment (at pH 4 and pH 5.5).
- Corrosion rate has a weak dependence on combination rotation speed with HAc concentration and temperature at both pH 4 and pH 5.5.
- Interaction simultaneously between HAc concentration, temperature and rotation did not have a significant value in contributing corrosion rate.

# CHAPTER 5

# EFFECTS OF HAc AND $H_2S$ IN $CO_2$ ENVIRONMENT

The results and discussions of the effect of $H_2S$ and HAc are presented in the following sections. The experimental studies carried out in this work include: identify initial of $H_2S$ corrosion model, conduct experimental works based on design of experiment, generate experimental data to find empirical constant parameters used in the RSM model equation and evaluate the empirical RSM model prediction. In order to find a trending of experimental data, it was used $H_2S$ corrosion mechanistic theory developed by Nesic et al. [62] and Song et al. [90]. Then, the data trend is used to fit the experimental data to obtain parametric relationships for the empirical model.

## 5.1 Initial Identification of Corrosion Rate Model

Figure 5.1 presents the simulated corrosion rate of carbon steel due to the presence of $H_2S$ in $CO_2$ environment, calculated based on Equation 3.9. The individual effects of $H_2S$ on corrosion rate under two different conditions were simulated i.e. free of film formation and with film formation. In film free formation (dot line), the corrosion is found to be controlled by activation process. On the other hand, when film formation exists, corrosion is controlled by diffusion limiting current. As can be seen in the graph, in film free condition (straight line) the corrosion rate will increase if $H_2S$ concentration increases. In contrast to film formation condition, an increase in $H_2S$ concentration will reduce the corrosion rate. These results are in agreement with Gaute et al. [93] who predicted in parabolic model represent carbon steel metal loss in the $CO_2/H_2S$ environments. Heusler [94] also proposed a parabolic model to predict a model for the relationship metal loss with exposure time in aqueous $H_2S$ conditions.

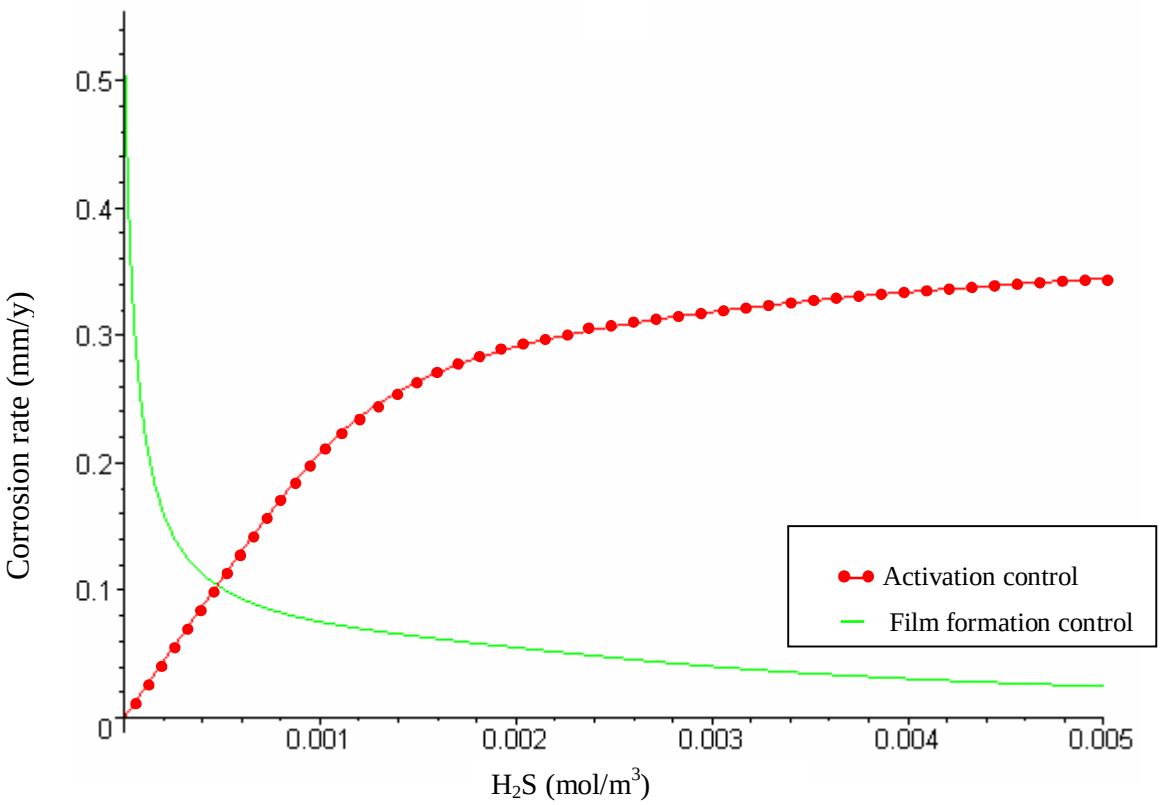


Figure 5.1 Simulated corrosion rate as a function of $H_2S$ concentration in conditions where film dominated reaction or activation dominated reaction.

## 5.2 Design of experiment for Analyzing $CO_2/H_2S$/HAc Corrosion Model

This study proposes the use of RSM to construct a $CO_2/H_2S$/HAc corrosion model. A CCD with RSM has been applied to study the effects of $H_2S$ and HAc in $CO_2$ corrosion. An experimental design matrix as presented in Table 5.1 was used to study the effects of independent variables such as, HAc, rotation speed, and temperature to predict the corrosion rate of carbon steel in $CO_2/H_2S$ environments.

Table 5.1 Experimental design matrix of independent variables to study corrosion rate in $CO_2/H_2S$/HAc environment (at 300 ppm $H_2S$).

| Coded variables | | | Natural variables | | | Corrosion rate (mm/y) |
|---|---|---|---|---|---|---|
| HAc | T | N | HAc (ppm) | T ($^oC$) | N (rpm) | Exp. results (Yi) |
| 1 | 1 | 1 | 108 | 70 | 4000 | 3.9 |
| -1 | 1 | 1 | 28 | 70 | 4000 | 3.0 |
| 1 | -1 | 1 | 108 | 35 | 4000 | 3.2 |
| -1 | -1 | 1 | 28 | 35 | 4000 | 2.2 |
| 1 | 1 | -1 | 108 | 70 | 1000 | 3.7 |
| -1 | 1 | -1 | 28 | 70 | 1000 | 2.9 |
| 1 | -1 | -1 | 108 | 35 | 1000 | 3.0 |
| -1 | -1 | -1 | 28 | 35 | 1000 | 2.0 |
| 1.7 | 0 | 0 | 136 | 50 | 2000 | 4.0 |
| -1.7 | 0 | 0 | 0 | 50 | 2000 | 2.0 |
| 0 | 1.7 | 0 | 68 | 80 | 2000 | 3.4 |
| 0 | -1.7 | 0 | 68 | 22 | 2000 | 2.4 |
| 0 | 0 | 1.7 | 68 | 50 | 6000 | 2.8 |
| 0 | 0 | -1.7 | 68 | 50 | 500 | 2.4 |
| 0 | 0 | 0 | 68 | 50 | 2000 | 2.8 |
| 0 | 0 | 0 | 68 | 50 | 2000 | 2.5 |
| 0 | 0 | 0 | 68 | 50 | 2000 | 2.6 |
| 0 | 0 | 0 | 68 | 50 | 2000 | 2.7 |

**5.3 Parameter Estimation**Based on mechanistic identification, the corrosion rate in $CO_2/H_2S$/HAc model was assumed to be a second-order polynomial as the best fitting. Thus, by fitting this curve to the experimental data, a regression model of the following equation was obtained:

$$Y = 1.6612 + 0.0046(HAc) - 0.0103(T) + 0.0001(N) + 0.0001(HAc)^2 + 0.0001(T)^2 \quad (5.1)$$

Where;

$Y$ = Corrosion rate (mm/y)

$T$ = temperature ($^oC$)

$HAc$ = concentration of HAc (ppm)

$N$ = rotation speed (rpm)

Table 5.2 presents variant analysis of the second order model regression model used to fit corrosion behavior calculated RSM theory. From the Table5.2, it can be seen that overall the regression models have significant values of 97%. The regression effects of temperature, HAc, and rotation speed show a significant level of F-test (p-value <0.05). There are also significant effects of square RSM model (92%) while interaction model is less significant in modeling this regression. Therefore it can be concluded that in general, there is a significant correlation between the RSM model and experimental result.

Table 5.2 Analysis of variance for CCD RSM model regression.

| Source | DF | Seq SS | Adj SS | Adj MS | F | P |
|---|---|---|---|---|---|---|
| Regression | 9 | 5.864 | 5.862 | 0.651 | 28.94 | 0.00 |
| Linear | 3 | 5.600 | 0.044 | 0.0146 | 0.65 | 0.61 |
| Square | 3 | 0.248 | 0.247 | 0.082 | 3.65 | 0.08 |
| Interaction | 3 | 0.016 | 0.016 | 0.005 | 0.24 | 0.86 |
| Residual Error | 6 | 0.136 | 0.135 | 0.022 | | |
| Lack-of-Fit | 5 | 0.091 | 0.090 | 0.018 | 0.40 | 0.8 |
| Pure Error | 1 | 0.045 | 0.045 | 0.045 | | |
| Total | 15 | 6 | | | | |
| R-Sq = 97.7% | | | | | | |

### 5.4 Prediction of $CO_2$ corrosion model at pH 4

The average corrosion rate of carbon steel observed from the experiments (Yi) is compared with data from corrosion predictions (ŷ) as presented in Table 5.3. From the difference, it can be seen that there is a reasonable predictions between corrosion data experiments and predictions.

Table 5.3 Comparison between corrosion data from experiments and predicted corrosion data

| Coded variables | | | Natural variables | | | Corrosion rate (mm/y) | | |
|---|---|---|---|---|---|---|---|---|
| HAc | T | N | HAc (ppm) | T ($^oC$) | N (rpm) | Exp. results (Yi) | Predicted (ŷ) | Error Yi – ŷ |
| 1 | 1 | 1 | 108 | 70 | 4000 | 3.9 | 4.0 | -0.1 |
| -1 | 1 | 1 | 28 | 70 | 4000 | 3 | 3.0 | 0 |
| 1 | -1 | 1 | 108 | 35 | 4000 | 3.2 | 3.3 | -0.1 |
| -1 | -1 | 1 | 28 | 35 | 4000 | 2.2 | 2.1 | 0.1 |
| 1 | 1 | -1 | 108 | 70 | 1000 | 3.7 | 3.7 | 0 |
| -1 | 1 | -1 | 28 | 70 | 1000 | 2.9 | 2.7 | 0.2 |
| 1 | -1 | -1 | 108 | 35 | 1000 | 3 | 3.1 | -0.1 |
| -1 | -1 | -1 | 28 | 35 | 1000 | 2 | 1.9 | 0.1 |
| 1.7 | 0 | 0 | 136 | 50 | 2000 | 4 | 4.0 | 0 |
| -1.7 | 0 | 0 | 0 | 50 | 2000 | 2 | 2.1 | -0.1 |
| 0 | 1.7 | 0 | 68 | 80 | 2000 | 3.4 | 3.5 | -0.1 |
| 0 | -1.7 | 0 | 68 | 22 | 2000 | 2.4 | 2.3 | 0.1 |
| 0 | 0 | 1.7 | 68 | 50 | 6000 | 2.8 | 2.9 | -0.1 |
| 0 | 0 | -1.7 | 68 | 50 | 500 | 2.4 | 2.5 | -0.1 |
| 0 | 0 | 0 | 68 | 50 | 2000 | 2.8 | 2.6 | 0.2 |
| 0 | 0 | 0 | 68 | 50 | 2000 | 2.5 | 2.6 | -0.1 |
| 0 | 0 | 0 | 68 | 50 | 2000 | 2.6 | 2.6 | 0 |
| 0 | 0 | 0 | 68 | 50 | 2000 | 2.7 | 2.6 | 0.1 |

Relationship between observed experimental data and predicted values is shown in Figure 5.2 that shows a correlation with an acceptable level of 98%. These results imply a satisfactory mathematical description of the corrosion rate data.

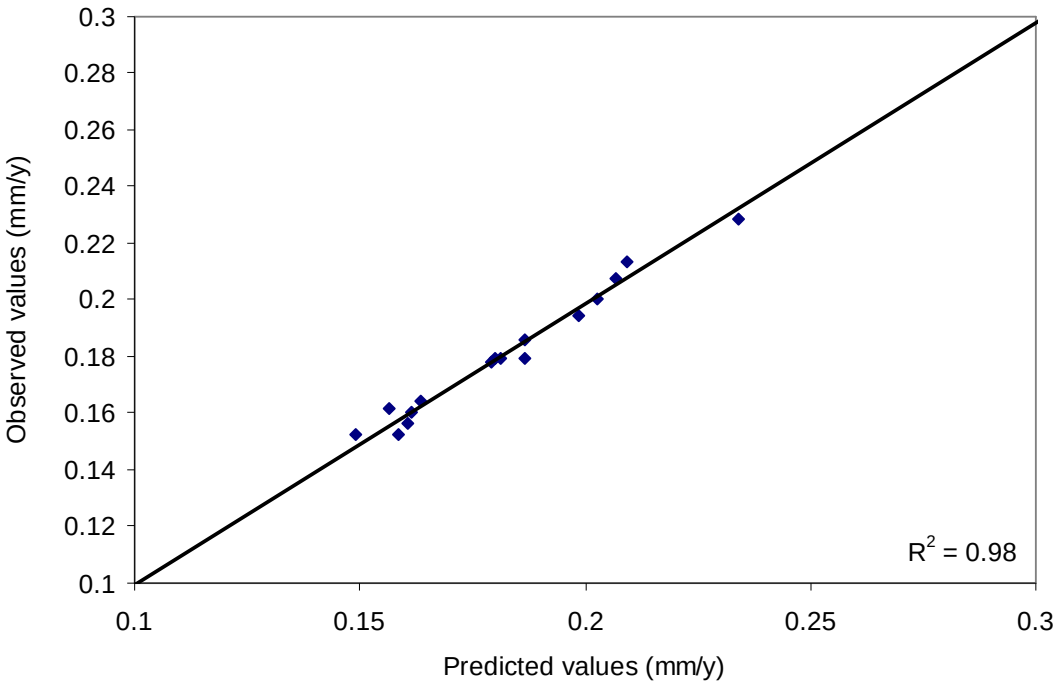


Figure 5.2 A relationship between observed and predicted values of the RSM corrosion rate model.

## 5.5 Verification of the RSM Model with Experimental Data and Corrosion Prediction Software

### 5.5.1 Effect of HAc concentration on corrosion rate in $CO_2/H_2S$/HAc environments

The corrosion rate of various concentrations of HAc obtained from RSM model is presented in Figure 5.3. A comparison of the corrosion rate calculated by the RSM model to the predicted corrosion rate by Freecorp software [88] at 35°C, 300 ppm $H_2S/CO_2$ saturated solution and 10 rpm rotation speed shows a good relationship in the range 40 to 160 ppm of HAc . The results show a standard error of 0.23 (0.18 mm/y). The correlation is 0.98 and the $R^2$ is 0.97.

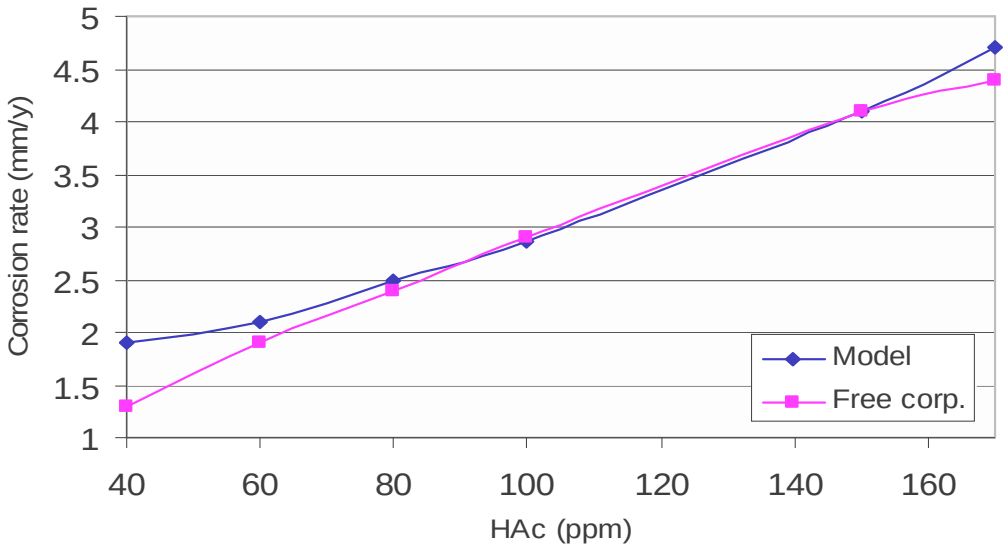


Figure 5.3 Corrosion rate at varying concentrations of HAc. A comparison between RSM model and Freecorp. corrosion software in 1 bar, 300 ppm $H_2S$, 35$^oC$, and 10 rpm.

### 5.5.2 Effect of temperature on corrosion rate in $CO_2/H_2S$/HAc environments

Effect of temperature on corrosion rate in $CO_2/H_2S$/HAc environments is presented in Figure 5.4. The effect of temperature on linear polarization sweep was studied using 3% NaCl solutions saturated with 300 ppm $H_2S/CO_2$, pH 4, 1000 rpm and of the temperature was varied from 30$^oC$ to 80$^oC$. The results calculated by RSM model and those predicted by ECE [75] are shown in Figure 5.4. The comparison between the RSM model and ECE shows $R^2$ of 97, correlation of 98 and standard error estimation of 0.1 (0.08 mm/y).

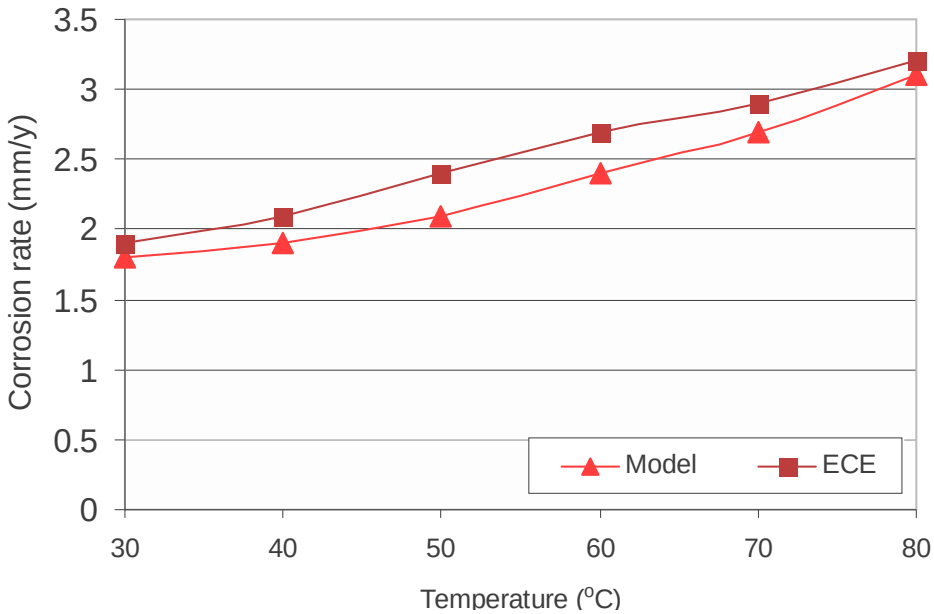


Figure 5.4 Corrosion rate at various temperature. A comparison between RSM model and ECE in 1 bar, 300 ppm $H_2S$, 10 ppm HAc, and 1000 rpm.

### 5.5.3 Effect of rotation speed on corrosion rate in $CO_2/H_2S$/HAc environments

Corrosion rates of carbon steel at various rotation speed for exposures up to 1 hour is also shown in Figure 5.5. Looking at corrosion values predicted by the software, it can be observed that an increase in the rotation speed from 200 to 4000 rpm has increased the corrosion rate from 1.9 to 2.4 mm/y. The graph also shows that the values calculated by the RSM model are lower than the values predicted by Freecorp [88], however, the values are still reasonable. A comparison between the predicted and calculated values shows an $R^2$ of 0.80, standard error estimation of 0.07 and correlation of 0.90. This indicates that the RSM model's prediction is less accurate.

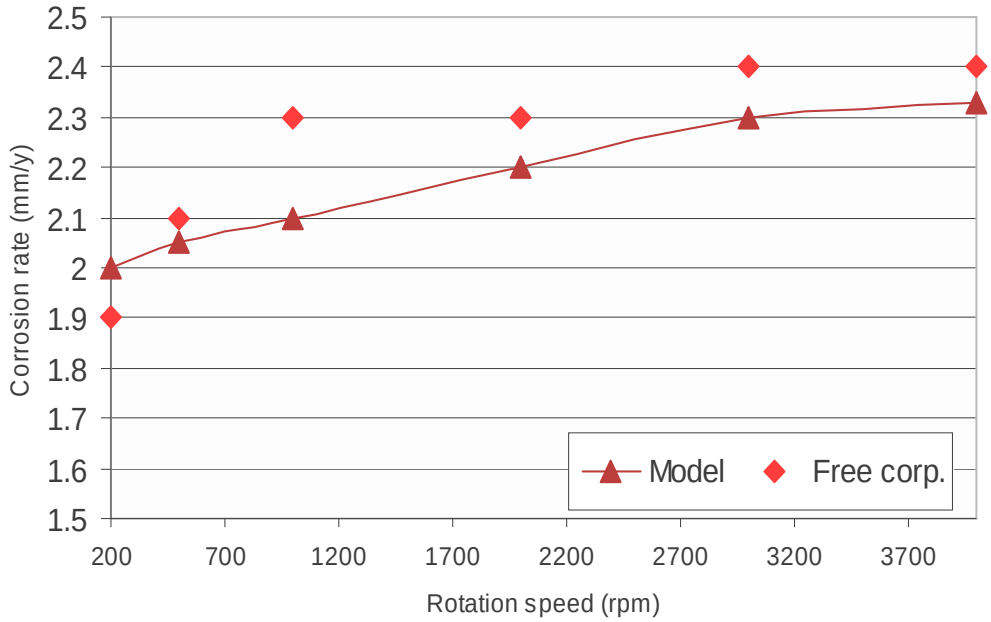


Figure 5.5 Corrosion rate at various rotation speed. A comparison between RSM and Freecorp in 1 bar, 300 ppm $H_2S$, 50$^oC$, and 5 ppm HAc.

## 5.6 Analysis and Interpretation of Response Surface of $CO_2/H_2S$/HAc Corrosion

The following results present the contour surface that shows effects of combinations variables tested on $CO_2/H_2S$/HAc corrosion model.

### 5.6.1 Combined effects of rotation speed and HAc on corrosion rate

The simultaneous combined effect of rotation speed and HAc on corrosion rate is presented in Figure 5.6. As illustrated in the figure, the corrosion rate increased slowly in the presence of low concentration of HAc (0 – 60 ppm). In the presence of 10 ppm of HAc, rotation speed does not seem to have a very strong influence on corrosion rate. The corrosion rate increased to 2.5 mm/y in the range of HAc concentration from 0 to 60 ppm. While the corrosion rate increased to 4 mm/y in the presence of 120 ppm of HAc. These observations are in good agreement with previous study [60, 61, 63] where the increase of corrosion rate were related with extra cathodic reaction and direct reduction of HAc.

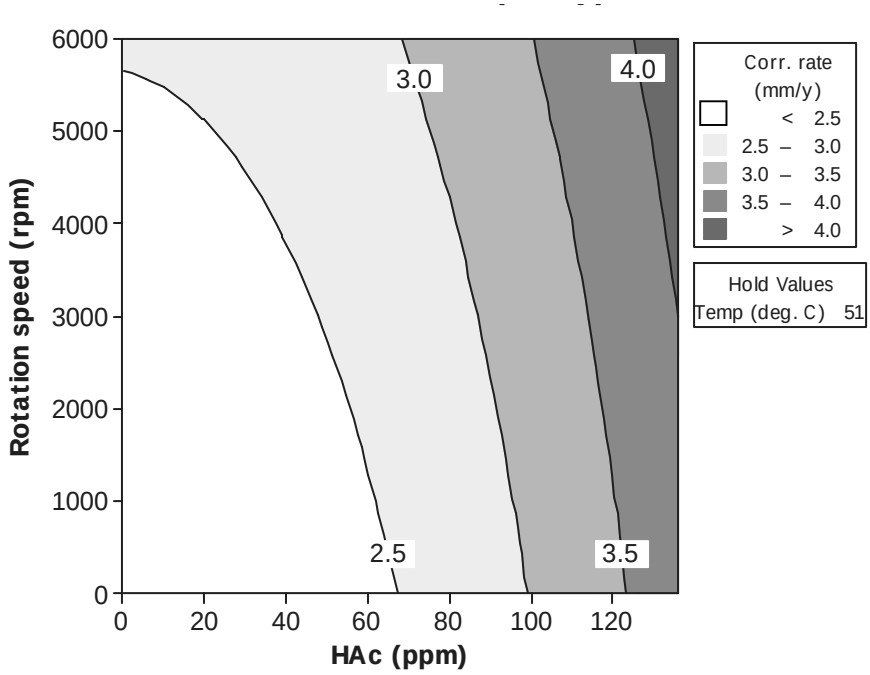


Figure 5.6 Response surface contours for corrosion rate as a function of HAc and rotation speed at 51$^{o}$C and 300 ppm $H_2S$.

### 5.6.2 Combined effects of rotation speed and temperature on corrosion rate

The effect of rotation speed and temperature is presented in Figure 5.7 as calculated by RSM. The combined effect of rotation speed and temperature has increased the corrosion rate to 3.6 mm/y. The combined effects of rotation speed and temperature on corrosion rate indicates a logarithmic model. At lower temperature (25$^{o}$C), the effect of rotation speed shows an increase in the corrosion rate up to 2.7 mm/y. The same trends are observed at all of the temperature conditions.

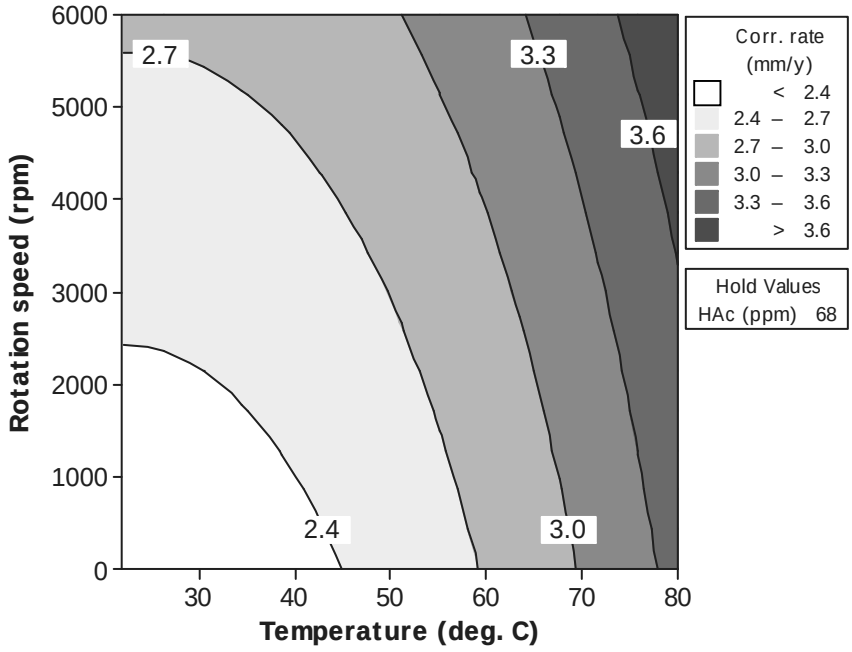


Figure 5.7 Response surface contours of corrosion rate as a function of rotation speed and temperature at 68 ppm HAc concentration and 300 ppm $H_2S$.

### 5.6.3 Combined effects of HAc and temperature on corrosion rate

The combined effect of temperature and HAc on corrosion rate in 300 ppm $H_2S/CO_2$ environment is presented in Figure 5.8. The figure shows that effects of HAc concentration on corrosion rate follow the same trend as the effects of temperature. Both temperature and HAc concentration increase corrosion rate according to a polynomial pattern.

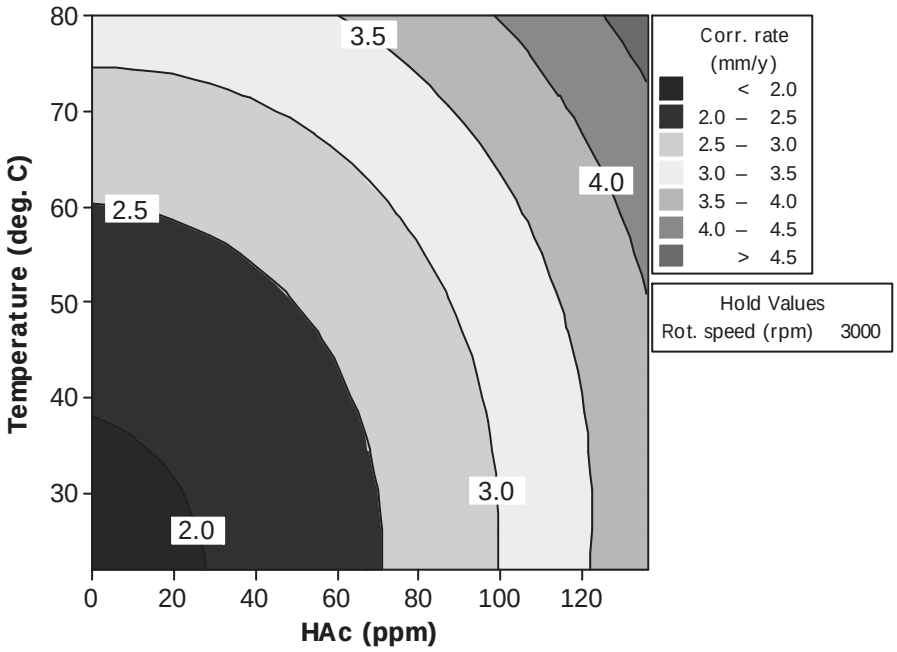


Figure 5.8 Response surface contours for corrosion rate as a function of HAc and temperature at 3000 rpm rotation speed.

### 5.7 Mechanistic Study of $CO_2/H_2S$/HAc Corrosion

The corrosion rate of carbon steel at various HAc concentration in the $CO_2/H_2S$ system was also studied by LPR and EIS technique and the results are presented in Figure 5.9. As observed in the graph, the corrosion rate increases consistently at the experimental conditions of HAc concentration ranging from 0 – 180 ppm. In other words, HAc controls the corrosion rate. At 180 ppm of HAc, the corrosion rate increases by 0.5 times.

The study of surface characteristics of $H_2S/CO_2$/HAc corrosion was carried out using EIS technique and the results are presented in Figure 5.10. Figure 5.10 illustrates characteristics of the Nyquist plot at 80 ppm and 130 ppm of HAc in a 3% NaCl solution with 300 ppm $H_2S$ and saturated $CO_2$. As seen in the graph, there is a depressed semi-circle at high frequencies, which indicates a double layer capacitance.

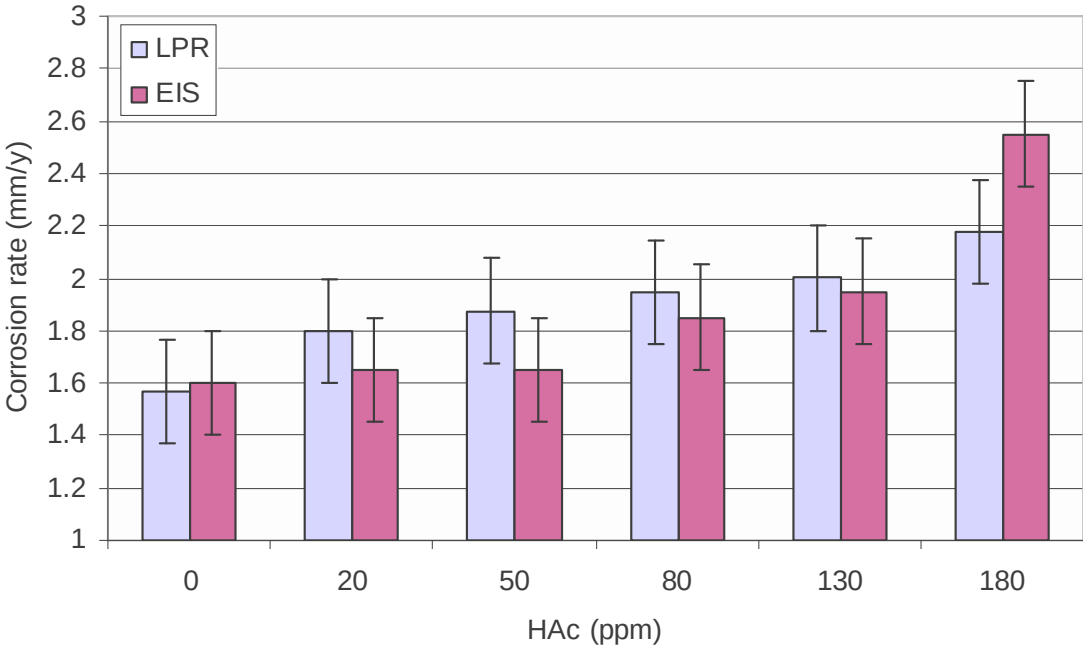


Figure 5.9 Corrosion rate at various HAc concentration in 1 bar, 300 ppm $H_2S$, and 22°C. (A comparison between LPR and EIS results).

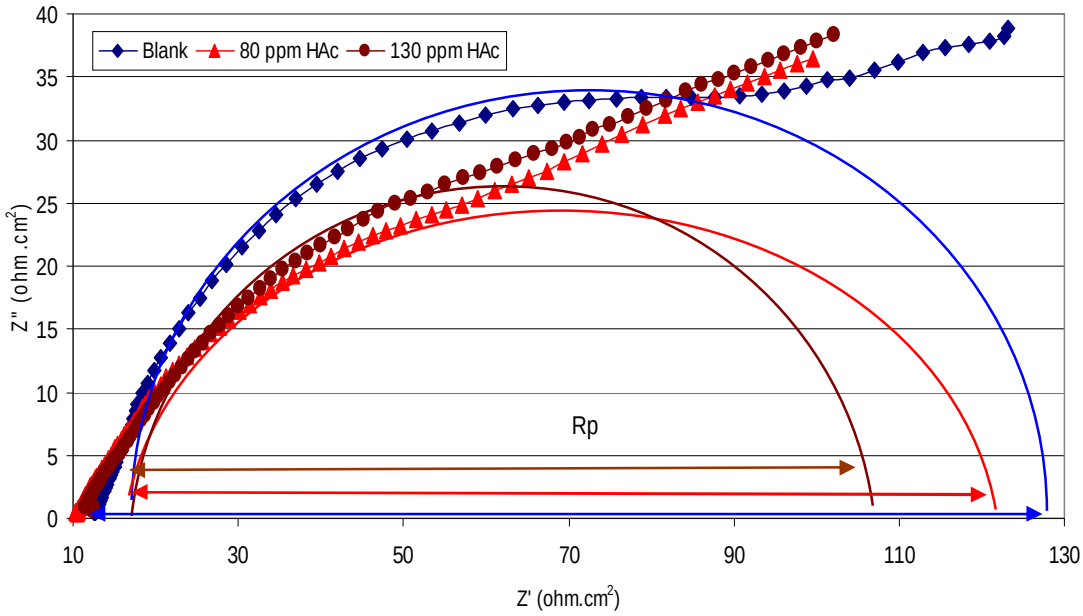


Figure 5.10 Nyquist plot to calculate corrosion rate as a function of HAc concentration in 1 bar, 300 ppm $H_2S$, and 22°C.

The Nyquist plot shows a decreasing charge transfer resistance with increasing of HAc concentration. This means that corrosion rate increases as the concentration of

HAc is increased (Figure 5.10) and the effect is proportional to the amount of HAc added. As shown in Figure 5.10, the charge transfer resistance decreases from 129 to 99 when 130 ppm of HAc is introduced into solution.

From the EIS data, several values of solution resistance, charge transfer resistance, capacitance film formed and corrosion rate can be described in the form of equivalent circuit parameters as presented in Figure 5.11. Table 4.55 shows the parameters values of solution resistance, charge transfer resistance, capacitance film formed and corrosion rate obtained from the experiments using EIS technique.

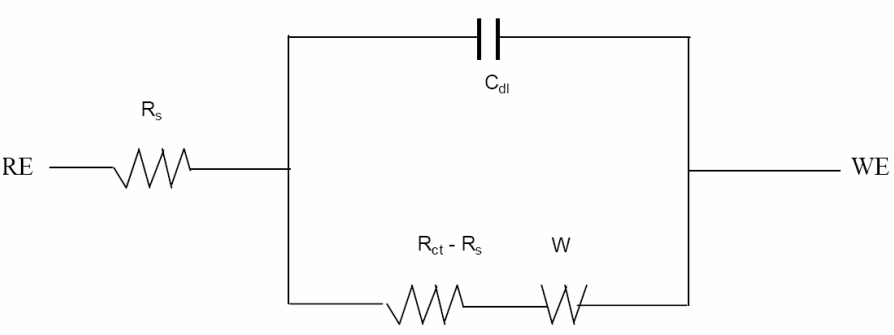


Figure 5.11 Typical equivalent circuit for a mixed diffusion and charge transfer control used to represent the experimental conditions.

Table 5.4 Circuit parameters result for $CO_2/H_2S$/HAc corrosion at various HAc concentration.

| Electrical circuit | Blank | 80 (ppm) | 130 (ppm) |
|---|---|---|---|
| Rp (ohms.cm²) | 104 | 88 | 74 |
| Capacitance (F) | $3.32x10^{-3}$ | $6.18x10^{-3}$ | $6.92x10^{-3}$ |
| Depression angle | 30.56 | 38.23 | 35.23 |
| Corr. rate (mm/y) | 1.3 | 1.5 | 1.6 |

## 5.8 Potentiodynamic Polarization Test

The polarization sweeps were conducted to study the effect of $H_2S$ on $CO_2$ corrosion. The result is presented in Figure 5.12. The figure shows that there are some differences between the polarization graphs of carbon steel corrosion in $CO_2$ and in

300 ppm $H_2S/CO_2$ system. $H_2S$ gas increases $CO_2$ corrosion rate and also increases cathodic Tafel slope. This finding was also observed by Zang et al. [95] when they conducted experiments in conditions with a constant $H_2S/CO_2$ partial pressure ratio of 1.7.

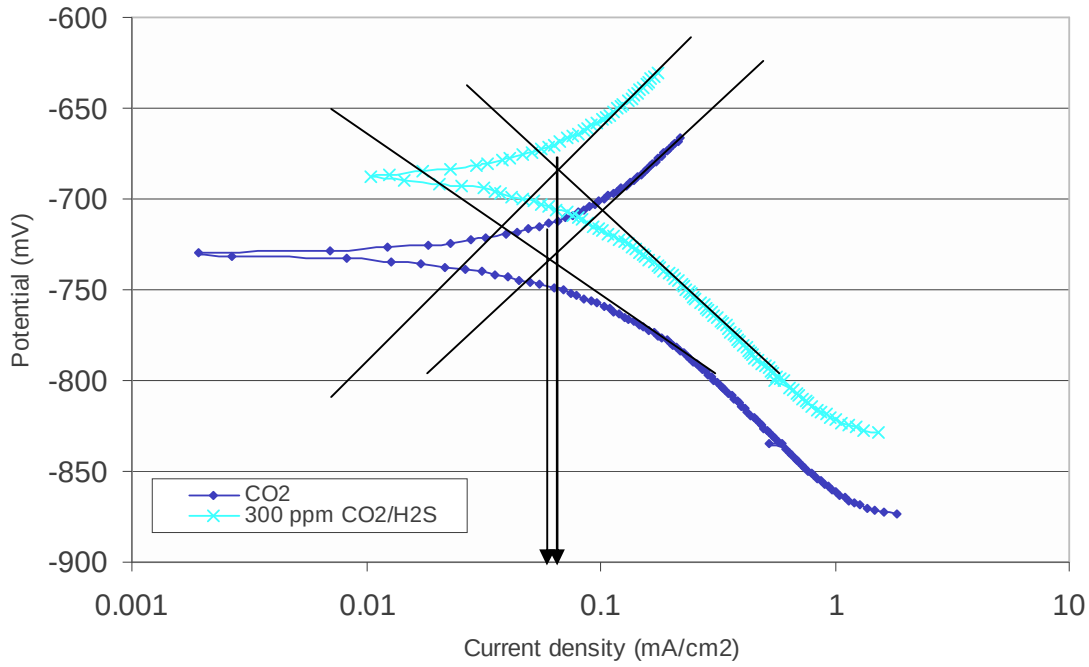


Figure 5.12 Potentiodynamic sweeps in $CO_2$ solution with/without $H_2S$ in 1 bar, 22°C, 300 ppm $H_2S$, pH 4, and stagnant.

Effects of HAc addition on Tafel slope can be seen in Figure 5.13. Observations from Figure 5.13 indicates that there is no significant effect of HAc addition on anodic Tafel slopes in 300 ppm $H_2S/CO_2$ system. However, the cathodic slope shows an increase of reaction process in the presence of HAc.

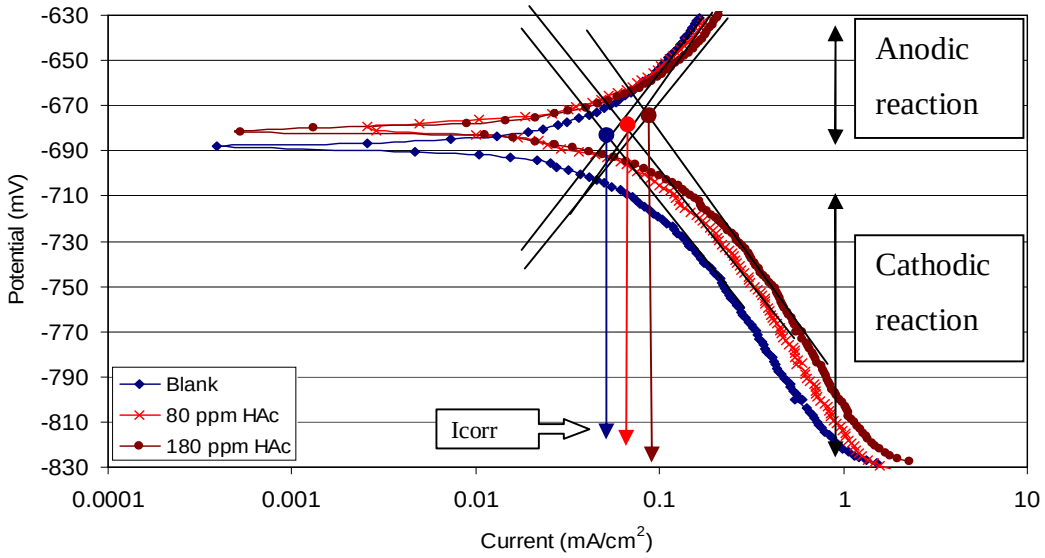


Figure 5.13 Potentiodynamic sweeps in 300 ppm $H_2S/CO_2$ saturated solution at various HAc concentrations in 1 bar, 22°C, 300 ppm $H_2S$, pH 4, and stagnant.

## 5.9 $CO_2/H_2S$/HAc Corrosion Discussions

Based on data calculations using RSM model, the following sections are discussed effects of the variables tested on corrosion in $H_2S/CO_2$ environment.

### 5.9.1 Model evaluation

In these experiments, the results show that second-order polynomial model is the most appropriate model to predict $CO_2/H_2S$/HAc corrosion pattern. Using the polynomial model, the curve pattern such as linear or exponential pattern can be obtained. Figure 5.3 shows a linear pattern at low HAc concentration, while a polynomial model is shown at higher concentrations of HAc. Flow rate influences corrosion rate in a linear pattern in the range of rotation speed tested from 0 to 6000 rpm. The effect of temperature shows a similar trend as the effects of HAc on corrosion rate. Temperature shows a linear pattern at lower temperature range and a polynomial pattern at higher temperature range (Figure 5.4).

Residual analysis method was applied to validate all proposed RSM models. It was simplified by analyzing the *p*-value of each RSM model as presented in the ANOVA (Table 5.2). The *p*-value for the 2nd polynomial model is 0.08. The

confidence level of all RSM models is within 97 %, which indicates that the RSM models represent 97% of the experimental data.

### 5.9.2 Combined effect of rotation speed and HAc

The corrosion rate as a function of different rotation speed and HAc is shown in Figure 5.6. As observed in the graph, corrosion rate increases significantly with increasing speed and the effect is more dominant at higher HAc concentration. At lower HAc concentration, the corrosion rate increases slowly.

At higher rotation speed and higher HAc concentration, the effect of rotation speed is to cause the corrosion rate to increase significantly. The higher corrosion rate may be related to electrochemical and hydrodynamic effects of the solution. Increasing the HAc concentration and rotation speed accelerate the electrochemical reaction transfer in agreement with George [86]. A faster rotation speed can also reduce thickness of the boundary layer of water next to a metal surface. This thinner boundary layer allows the dissolved species to corrode the metal surface more quickly in agreement with Gaute [93].

### 5.9.3 Combined effect of temperature and rotation speed

From Figure 5.7, it has shown that the maximum corrosion rate of carbon steel increases by 50% with increasing temperature from 20 to 80°C. However, the corrosion rate starts to reach a plateau as temperature increases, especially in the temperature range more than 70$^{o}$C. This observation may be related to the formation of FeS and $FeCO_3$ film. The corrosion rate, which is charge-transfer controlled at room temperature (22°C) becomes mass-transfer limiting current controlled at higher temperatures.

The combined effect of rotation speed and temperature on both the corrosion rate and the scaling temperature can be visually illustrated by RSM model. As can be observed in Figure 5.7, at 300 ppm of $H_2S$ gas concentration, the corrosion rate varies with rotation speed. As predicted by RSM, at the lower rotation speed, there is minimum effect of

temperature on corrosion rate. When the rotation speed is higher, the corrosion rate increases significantly with increasing temperature. This finding is in agreement with the findings by Fragiera et al. [96], who also found that at higher temperature, localized corrosion tend to occur.

### 5.9.4 The combined effect of HAc and Temperature

The potentiodynamic experimental results for different HAc concentrations in and temperature in $CO_2/H_2S$/HAc mixed corrosion environments are given in Figure 5.8. The experimental results show that as HAc concentration increases, the corrosion rate also increases. The HAc acts as a provider of protons and at the same time adds a new cathodic reaction via direct reduction of undissociated HAc [86]. The effect is proportional to the amount of HAc added. Thus, it can be concluded that HAc concentration is a dominant factor in determining corrosion behavior. In addition, the increase of cathodic reaction caused by HAc concentration do not change cathodic Tafel slope.

### 5.9.5 Flow independent and flow dependent limiting current

It has been commonly accepted that the increase in corrosion rate due to an increase in rotation speed will become stagnant at a certain rotation speed called flow independent limiting current. But, at this condition, there is no significant effect of rotation speed on limiting current density. A mathematical relationship of temperature, HAc concentration and rotation speed was obtained using RSM model. Equation 5.1, which was obtained by fitting the experimental matrices in Table 5.1 shows that a curved slope pattern that corresponds to flow independent limiting current cannot be obtained. The equation shows a constant relationship between rotation speed and curved slope.

### 5.9.6 Scaling temperature and chemical reaction limiting current in $H_2S/CO_2$/HAc corrosion

The response surfaces calculated by quadratic models can also be used to indicate the maximum point on the range of independent variable analytically. The determination of scaling temperature can be performed by calculated using first derivate of the mathematical function of Equation 5.1. The maximum points are located at conditions where the first derivative of the response surface equals to zero as presented in Equation 5.2 and Equation 5.3. Figure 5.14 below shows the dependency of scaling temperature on HAc concentration. Based on the RSM model in Figure 5.14, the scaling temperature did not form. The corrosion rate continues to increase as temperature increases. It can be concluded that within 1 hours of exposure time, there was no film formation. The corrosion process was under activation control.

$$\frac{\partial}{\partial T}(1.661+0.0046(HAc) - 0.0103(T)+ 0.0001(N) + 0.0001(HAc)^2 + 0.0001(T)^2) = 0 \quad (5.2)$$

$$T = -14.7143 - 0.11471(HAc) = 0 \quad (5.3)$$

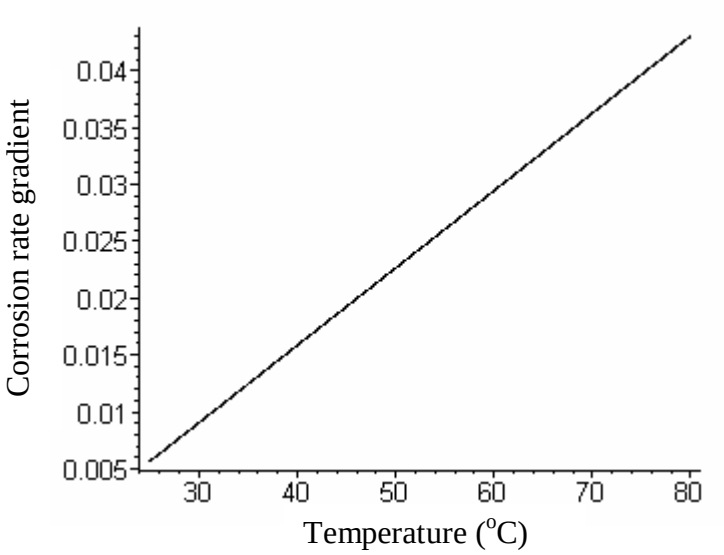


Figure 5.14 Corrosion rate gradient of RSM model at varying temperature and without HAc.

Chemical reaction limiting current can be obtained using RSM model, by calculating first derivative of the mathematical function of the RSM model (Equation 5.1 ).

$$\frac{\partial}{\partial HAc}(1.661+0.0046(HAc)- 0.0103(T) + 0.0001(N) + 0.0001(HAc)^2 + 0.0001(T)^2)= 0 \quad (5.4)$$

$$HAc = 0.0023) - 0.00005(T) \quad (5.5)$$

Analytical observation from Equations 5.4 and 5.5 indicates that chemical reaction limiting current did not happen in this range of experiments. The slope of the mathematical function shows a tendency to increase with increasing HAc concentration. This means that the corrosion rate will increase continuously within the tested variables (Figure 5.15)

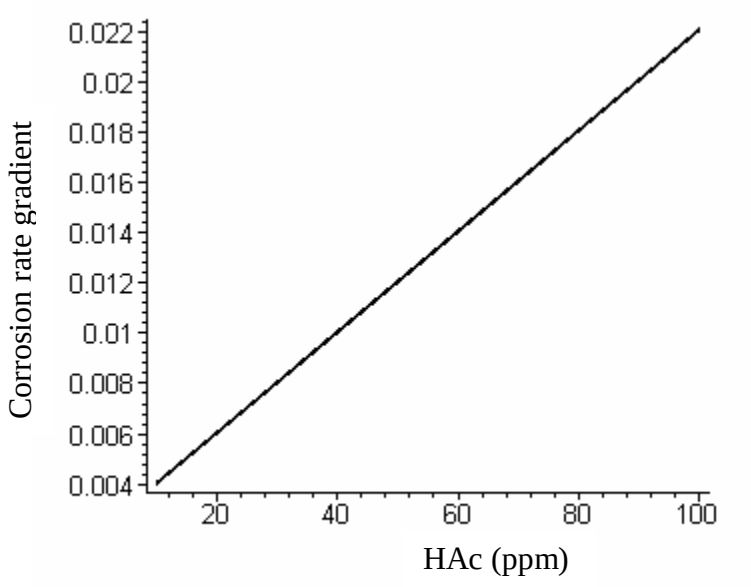


Figure 5.15 Corrosion rate gradient of the RSM model at varying HAc concentration and 22$^{o}$C.

### 5.9.7 Effects of $H_2S$ on $CO_2$ corrosion mechanism

Effects of $H_2S$ on $CO_2$ corrosion are presented in Figure 5.12. It is observed that corrosion rate increases in the presence of $H_2S$ gas. In pure $CO_2$ solution, corrosion rate is controlled by charge transfer reaction. The addition of 300 ppm of $H_2S$ caused

the corrosion rate to increase. $H_2S$ can accelerate corrosion rate by increasing cathodic reaction rate. Kvarekval [50] explained that the increased corrosion rate is caused by sulfide ions or by $H_2S$ acting as a catalyst for hydrogen evolution and governs diffusion of proton donors. Further, he reported that $H_2S$ can also increase hydrogen evolution rate without taking part in the net reaction. The $H^+$ ions from $H_2S$ molecule can penetrate steel surface to create a pitting corrosion which can increase corrosion rate [95]. Figure 5.13 also reveals that anodic polarization behavior does not change significantly with the addition of hydrogen sulfide. Anodic Tafel slope is consistent with iron dissolution in $CO_2$ solution. However, cathodic Tafel slope has increased significantly.

The addition of $H_2S$ also gives impact to diffusion limiting current density of $CO_2$ corrosion. From the experiments using EIS technique (Figure 5.10), the presence of tail in the Nyquist plot has been detected, which indicates mass transfer effect in the process. However, the scan polarization analyses show activation control reaction. Thus, the behavior of cathodic limiting current density consists of chemical reaction and diffusion process.

### 5.9.8 Effects of HAc on $CO_2$/$H_2S$ corrosion mechanisms

EIS corrosion measurement technique was used to study the effects of HAc concentration on $CO_2$/$H_2S$ corrosion. Figure 5.10 demonstrates the effects of adding 80 ppm and 180 ppm of HAc into a 300 ppm $H_2S$/$CO_2$ saturated solution at pH4. As can be seen from the figure, the impedance diagram shows a depressed semi-circle at high frequencies, which indicates a double layer capacitance. This condition, as quoted by Bai [97], suggests that there are heterogeneous surface and non-uniform distribution of current density.

At 80 ppm and 180 ppm HAc, the steady state impedance diagram demonstrates a smaller depressed semi-circle with similar characteristics. The decrease in polarization resistance Rp from EIS measurements indicates an increase in corrosion rate with increasing HAc concentration. Moreover, there was a tail observed in the experiments (Figure 5.10). These results suggest that the corrosion mechanism is a diffusion process control in the presence of HAc. The same characteristic is found in

the experiments without HAc. From the description in Figure 5.10, it can be concluded that the corrosion reaction of $H_2S/CO_2$ system is dominated by HAc reactions.

The effects of adding HAc was also studied using potentiodynamic test. From the test, it has been shown that additional HAc concentration do not have significant effect on anodic Tafel slope (Figure 5.13). Figure 5.13 indicates that cathodic slope increases the reaction process with increasing HAc concentration, but do not change cathodic Tafel slope. This means that HAc is the dominant factor that governs the reaction process.

## 5.10 Conclusion

### 5.10.1 Mechanism corrosion rate in $CO_2/H_2S$/HAc system

- The presence of 0.3 mbars of $H_2S$ in 0.7 bars of $CO_2$ causes an average of approximately 10% increase in the corrosion rate compared to $H_2S$ free.
- $H_2S$ accelerates corrosion rate by increasing the cathodic Tafel slope.
- The introduction of 180 ppm of HAc to the $H_2S/CO_2$ gaseous mixture causes the corrosion rate to increase sharply in the temperature range 40–80°C.
- The anodic polarization behavior did not change significantly with the addition of hydrogen sulfide.
- HAc is the dominant factor that governs the reaction process in $CO_2/H_2S$ system. The behavior of cathodic reaction consists of chemical reaction and diffusion process.
- Based on RSM model, the scaling temperature, limiting current density and limiting chemical reaction did not form in the range of experiments.
- HAc has the most dominant effect on corrosion process followed by temperature and rotation speed.
-

### 5.10.2 Model regressions

The results have shown that second-order polynomial model can be used to predict $CO_2/H_2S$/HAc corrosion pattern adequately. This study has proven that CCD can be applied to predict $CO_2$ corrosion process with reasonable planning and execution. Thus, the statistical analysis and evaluations of data could be proved analytically. The results from the experiments are compared to Freecorp [88] as provided in the appendix 2.e. It can be summarized that the models, in average, have coefficient determination 70 % correlation 82% and predictive error 18 % relative to the Freecorp model.

# CHAPTER 6

# CONCLUSION AND RECOMMENDATION

## 6.1 Conclusion

The RSM regression models for the carbon steel corrosion in $CO_2$ environments involving HAc, temperature and rotation speed as parameters have been successful developed and validated with experimental data and commercial predictive models. The RSM is efficient in determining empirical relationship of the variables tested simultaneously. In the form of mathematical equations, the effects of independent variables will be easily identified and developed. Furthermore, using mathematical operations, certain conditions such as stationary conditions can be calculated analytically to identify scaling temperature, limiting current density and independent flow conditions.

The results have shown that second-order polynomial model can be used to predict $CO_2/H_2S$/HAc corrosion pattern adequately. CCD is appropriate to design experiments in $CO_2/H_2S$ environments. The comparison results show that all of the RSM models are acceptable statistically with average $R^2$ of 93%, average standard error 0.2 and average correlation of 95%.

In general, effects of individual variables can be concluded as follows:

- Increasing HAc concentration causes increased corrosion rate for a given temperature and rotation speed at both pH 4 and pH 5.5.
- Increasing temperature causes increased corrosion rate for a given HAc concentration and rotation speed at both pH 4 and pH 5.5.
- Increasing rotation speed causes increased corrosion rate for a given temperature and HAc concentration at both pH 4 and pH 5.5.

## 6.2 Scope of Model

Since the model is developed based on experimental data only, there are several limitations of the RSM that makes it suitable only for parameters used in the experiments conditions. The presented RSM model is for uniform corrosion in experimental test conditions; therefore it does not predict localized corrosion in other environments. The RSM model does not account for higher partial pressure of $CO_2$, film formations, the effect of high chloride concentrations, oxygen, elemental sulfur or any other conditions that may contribute to corrosion rate. Therefore, it is recommended to use this RSM model under corrosion prediction at testing conditions.

## 6.3 Future Research

The RSM model considers pH, temperature and rotation speed in combination with HAc concentration to predict corrosion at atmospheric parameters. However, in field conditions, there are other operating variable at higher pressure such as oxygen, sodium chloride and other species that affect corrosion. Therefore it is recommended that further study to be conducted by using the same technique but including other variables such as $O_2$, inhibitor, NaCl, and any other species that promote corrosion at higher $CO_2$ pressure.

Future work on optimization should be started with complex variables. The complex variables can be selected using design experiments to determine the important variables that can be developed further

Different design experiments can be selected for the same case to determine the performance of the experimental design, to investigate the effect of the experimental design to the developed RSM model.

In order to optimize experimental research, it is necessary to choose appropriate experimental design to find an adequate mathematical function. Thus, preliminary study should be conducted in relation to obtaining a predicted model. Preliminary studies can be started by initial identification, examination of collected experimental data and studying history of the data to construct mathematical models.

As an alternative to experimental model, RSM can be combined with the application of neural network. Also, RSM can be applied with mechanistic theory to simplify calculations and to select the most dominant variables involved in corrosion, for screening the appropriate model.

REFERENCES


[1] D. H. Patrick, V. M. Tubes, MR0175 - A History and Development Study," in Proc. Annu. NACE INTERNATIONAL conf. Corrosion, San Antonio, Texas, 1999, p. 418.

[2] M. W. Joosten, K. Justin, W. Hembree, "Organic Acid Corrosion in Oil and Gas Production," in Proc. Annu. NACE INTERNATIONAL conf. Corrosion, Denver, 2002, p.2294.

[3] R. Chengqiang, D.L. Zhenquan, L. Tiehu, "Corrosion Behavior of Oil Tube Steel in Simulant Solution with Hydrogen Sulfide and Carbon Dioxide,"Materials Chemistry and Physics, vol. 93, p. 305 - 309, 2005.

[4] S. Tebbal, H. Schutt, R. Podlecki, C. Sudhakar, "Analysis and Corrosivity Testing of Eight Crude Oils", in Proc. Annu. NACE INTERNATIONAL conf. Corrosion, New Orleans, 2004, p. 04636.

[5] J. A. Dougherty, "Review of The Effect of Organic Acids on $CO_2$ Corrosion," in Proc. Annu. NACE INTERNATIONAL conf. Corrosion, New Orleans, 2004, p. 04376.

[6] S. Nesic, "Key Issues Related to Modelling of Internal Corrosion of Oil and Gas Pipelines – A Review," Corrosion Science, vol. 49: p. 4308 - 4338, 2007.

[7] W. Sun, S. Nesic, "Kinetics of Iron Sulfide and Mixed Iron Sulfide/Carbonate Scale Precitipation in $CO_2/H_2S$, "Ph.D. Dissertation, Department of Chemical Engineering, Russ College of Engineering and Technology, Ohio University, 2006.

[8] C. de Waard, D. E. Milliams, "Carbonic Acid Corrosion of Mild Steel," Corrosion, vol. 31 (5), pp. 131 - 135,1975.

[9] FREECORP V1, Technical Book, Institute for Corrosion and Multiphase Technology, Ohio University, Research Park, Athens, Ohio.

[10] S. Nesic, V. Miran, "A Neural Network Model for $CO_2$ Corrosion of Carbon Steel", JSCE, vol. 1, pp. 6, 1999.

[11] J. O. M. Bockris, M. D. Drazic, A.R. Despic, "The Electrode Kinetics of The Deposition and Dissolution of Iron," Corrosion, vol.4, pp. 325-361, 1961.

[12] K. Videm, "The Effects of Some Enviromental Variabales on The Aqueous $CO_2$ Corrosion of Carbon Steel," The Institute of Material, No. 13, 1994.

[13] S. Nesic, J. L. Crolet, M.D. Drazic, "Electrochemical Properties of Iron Dissolution in the Presence of $CO_2$ - Basics Revisited," in Proc. Annu. NACE INTERNATIONAL conf. Corrosion, New Orleans, 1996, p. 3.

[14] E. Gulbrandsen, K. Biekova, "Solution Chemistry Effects on Corrosion of Carbon Steels in Presence of $CO_2$ and Acetic Acid," in Proc. Annu. NACE INTERNATIONAL conf. Corrosion, San Diego, 2006, p. 6364.

[15] E. Dayalan, F.D. de Moraes, J.R. Shandly, S.A. Shirazi, E.F. Rybicki, "Corrosion Prediction in Pipe Flow under $FeCO_3$ Scale-Forming Conditions," in Proc. Annu. NACE INTERNATIONAL conf. Corrosion, San Diego, 1998, p. 51.

[16] E. W. J. van Hunnik, B. F. M. Pots, E. Hendriksen, "The Formation of Protective $FeCO_3$ Corrosion Product Layers in $CO_2$ Corrosion," in Proc. Annu. NACE INTERNATIONAL conf. Corrosion, New Orleans, 1996, p. 6.

[17] O. A. Nafday, "Film Formation and $CO_2$ Corroson in the Presence of Acetic Acid, Russ College of Engineering and Technology," Master Thesis, Ohio University, 2004.

[18] K. Lee, "A Mechanistic Modeling of $CO_2$ Corrosion of Mild Steel in the Presence of $H_2S$," Department of Chemical Engineering, Russ College of Engineering and Technology, Ph.D. Dissertation, Ohio University, 2004.

[19] M. L Johnson, M. B. Tomson, "Ferrous Carbonate Precipitation Kinetics and its Impact on $CO_2$ Corrosion," in Proc. Annu. NACE INTERNATIONAL conf. Corrosion, Nashville, 1991, p. 268.

[20] W. Sun, S. Nesic, "Kinetics of Iron Sulfide and Mixed Iron Sulfide/Carbonate Scale Precipitation in $CO_2/H_2S$," in Proc. Annu. NACE INTERNATIONAL conf. Corrosion, San Diego, 2006, p. 6644.

[21] S. R. Parakala, "EIS Investigation of Carbon Dioxide and Hydrogen Sulfide Corrosion Under Film Forming Conditions," Master Thesis, Department of Chemical Engineering, Russ College of Engineering and Technology, Ohio University, 2005.

[22] B. Hedges, L.M. Veigh, "The Role of Acetate in $CO_2$ Corrosion: The Double Whammy," in Proc. Annu. NACE INTERNATIONAL conf. Corrosion, San Antonio, Texas, 1999, p. 99.

[23] G. Schmitt, M. Hosstemeier, "Fundamental Aspects of $CO_2$ Metal Loss Corrosion - Part II: Influence of Different Parameters on $CO_2$ Corrosion Mechanisms," in Proc. Annu. NACE INTERNATIONAL conf. Corrosion, San Diego, 2006, p. 6112.

[24] G. Schmitt, M. Mueller, M. Papenfuss, "Understanding Localized $CO_2$ Corrosion of Carbon Steel From Physical Properties of Iron Carbonate Scales Fracture Mechanical Properties of Iron Carbonate Scales," in Proc. Annu. NACE INTERNATIONAL conf. Corrosion, San Antonio, Texas, 1999, p. 38.

[25] U. Masakatsu, H. Takabe, "Effect of Environmental Factor and Microstructure on Morphology of Corrosion Products in $CO_2$ Environments," in Proc. Annu. NACE INTERNATIONAL conf. Corrosion, San Antonio, Texas, 1999, p. 13.

[26] D. A. Lopez, S.N. Simison, S.R. de Sa´nchez, “The Influence of Steel Microstructure on $CO_2$ Corrosion. EIS Studies on The Inhibition Efficiency of Benzimidazole,” Electrochimica Acta, vol. 48, p. 845- 854, 2003.

[27] C. de Waard, "Influence of Liquid Velocity on $CO_2$ Corrosion: a Semi-Emperical Model," in Proc. Annu. NACE INTERNATIONAL conf. Corrosion, Denver, 2002, p. 128.

[28] J.L. Crolet, M.R. Bonis, E. Aquitaine, “Prediction of the Risks of $CO_2$ Corrosion in Oil and Gas Wells,” Society of Petroleum Engineers, v. 6 p. 449-453,1991.

[29] H. Hoffmeister, G. Scheidacker, "Effect of Chloride Contents, pH and Temperature on Crevice Corrosion of Alloy 33 as Determined by Remote Crevice Assembly (RCA)," in Proc. Annu. NACE INTERNATIONAL conf. Corrosion, New Orleans, 2004, p. 4290.

[30] M. Nordsveen, S. Nesic, R. Nyborg, A. Stangeland, “A Mechanistic Model for Carbon Dioxide Corrosion of Mild Steel in the Presence of Protective Iron Carbonate Films—Part 1: Theory and Verification,” Corrosion, Vol. 59, No. 5, 2002

[31] K. D. J. Efird, "The Effect of the Crude Oil on the Corrosion of Steel in Crude Oil/Brine Production," Corrosion, vol. 45, pp. 2, February 1989.

[32] D. C. Silverman, "Simplified Equation for Simulating Velocity-Sensitive Corrosion in the Rotating Cylinder Electrode at Higher Reynolds Numbers," Corrosion, vol. 59(3), pp. 207, 2003.

[33] D. C. Silverman, "Rotating Cylinder Electrode for Velocity Sensitivity Testing," Corrosion, vol. 40(5), pp. 220, 1984.

[34] D. C. Silverman, "Conditions for Similarity of Mass-Transfer Coefficients and Fluid Shear Stresses Between the Rotating Cylinder Electrode and Pipe," Corrosion, vol. 61(6): pp. 515, 2005.

[35] D. C. Silverman, "The Rotating Cylinder Electrode for Examining Velocity-Sensitive Corrosion - A Review," Corrosion, vol. 60(11), pp. 1003, 2004.

[36] D. C. Silverman, "Technical Note: on Estimating Dynamic Conditions in Rotating Cylinder Electrode," Corrosion, vol. 55 (12), pp. 1115, 1999.

[37] D. C. Silverman, "Rotating Cylinder Electrode - An Approach for Predicting Velocity Sensitive Corrosion," in Proc. Annu. NACE INTERNATIONAL conf. Corrosion, Nashville, 1991, p. 20.

[38] D. C. Silverman, "Rotating Cylinder Electrode - Geometry Relationships for Prediction of Velocity Sensitive Corrosion," Corrosion, vol. 44(1), pp. 42, 1988.

[39] J. R. Vera, "Oil Characteristics Water/Oil Wetting and Flow Influence on The Metal Loss, Part 1: Effect of Oil and Flow on $CO_2/H_2S$ Corrosion," in Proc. Annu. NACE INTERNATIONAL conf. Corrosion, San Diego, 2006, p. 6113.

[40] B. Craig, "Predicting the Conductivity of Water-in-Oil Solutions," Corrosion, vol. 8, p.657, 1998.

[41] H. W. Wang, "$CO_2$ Corrosion Mechanistic Modeling in Horizontal Slug Flow," in Department of Chemical Engineering, Russ College of Engineering and Technology, Ph.D. Dissertation, Ohio University, 2002.

[42] F. Wang, "Modeling of Aqueous Carbon Dioxide Corrosion in Turbulent Pipe Flow," Department for Chemical Engineering, Ph.D. Dissertation, University of Saskatchewan, 1999.

[43] C. J.Carew, "$CO_2$ Corrosion of L-80 Steel in Simulated Oil Well Conditions," in Proc. Annu. NACE INTERNATIONAL conf. Corrosion, Denver, 2002, p. 2299.

[44] B. Brown, K. Lee, S. Nesic, "Corrosion in Multiphase Flow Containing Small Amount of $H_2S$," in Proc. Annu. NACE INTERNATIONAL conf. Corrosion, San Diego, 2003, p. 3341.

[45] S.N. Smith, M. W. Joosten, "Corrosion of Carbon Steel by $H_2S$ in $CO_2$ Containing Oilfield Environments," in Proc. Annu. NACE INTERNATIONAL conf. Corrosion, San Diego, 2006, p. 6115.

[46] M. L. Fransson, "Understanding Corrosion Inhibition: A Surface Science Study of Thiophene Derivatives on Iron Surfaces in Gaseous and Liquid Systems," Ph.D. Dissertation, Princeton University, Department of Chemistry, 2005.

[47] Multicorp, Institute for Corrosion and Multiphase Technology, Ohio University.

[48] A. K. Agrawal, C. Durr, and G. H. Koch, "Films and Corrosion Rates of AISI 1018 Carbon Steel in Saline Solutions in The Presence of $H_2S$ and $CO_2$ at Temperatures up to 175°F," in Proc. Annu. NACE INTERNATIONAL conf. Corrosion, New Orleans, 2004, p. 4383.

[49] A. Andrzej, D.Y. Robert, "Simulation of $CO_2/H_2S$ Corrosion Using Thermodynamic and Electrochemical Models," in Proc. Annu. NACE INTERNATIONAL conf. Corrosion, San Antonio, Texas, 1999, p. 31.

[50] J. Kvarekval, R. Nyborg, M. Seiersten" Corrosion Product Films on Carbon Steel in Semi-Sour $CO_2/H_2S$ Environments," in Proc. Annu. NACE INTERNATIONAL conf. Corrosion, Denver, 2002, p. 2296.

[51] B. B. Singer, A. Camacho, S. Nesic, "Combined Effect of $CO_2/H_2S$ and Acetic Acid on Bottom of The Line Corrosion," in Proc. Annu. NACE INTERNATIONAL conf. Corrosion, Nashville, 2007, p. 7661.

[52] L. Zhang, "Effects of Pressure on Wet $H_2S/CO_2$ Corrosion of Pipeline Steel," in Proc. Annu. NACE INTERNATIONAL conf. Corrosion, Atlanta, 2009, p. 9565.

[53] G. Schmitt, M. Papenfuss, "Understanding Localized $CO_2$ Corrosion of Carbon Steel From Physical Properties of Iron Carbonate Scales Fracture Mechanical Properties of Iron Carbonate Scales," in Proc. Annu. NACE INTERNATIONAL conf. Corrosion, San Antonio, Texas, 1999, p. 38.

[54] K. S. George, S. Nesic, "Electrochemical Investigation and Modeling of Carbon Dioxide Corrosion of Carbon Steel in The Presence of Acetic Acid," in Proc. Annu. NACE INTERNATIONAL conf. Corrosion, New Orleans, 2004, p. 4379.

[55] L. Zhang, J. Yang, Jianbo, Sun, Minxu, Lu, "Effect of Pressure on Wet $H_2S/CO_2$ Corrosion of Pipeline Steel," in Proc. Annu. NACE INTERNATIONAL conf. Corrosion, Atlanta, 2009, p. 9565.

[56] B. Kermani, J. Martin, "Materials Design Strategy: Effects of $CO_2/H_2S$ Corrosion on Materials Selection," in Proc. Annu. NACE INTERNATIONAL conf. Corrosion, San Diego, 2006, p. 6121.

[57] R. W. Papavinasam, "Synergistic Effect of Pressure and Flow on Corrosion Rates: Studies Using High-Temperature, High-Pressure Rotating electrode Systems," in Proc. Annu. NACE INTERNATIONAL conf. Corrosion, San Antonio, Texas, 1999, p. 30.

[58] S. P. Makarenko, K. Shatilo, V. A. Gumerskii, Belyaev, "Effect of Oxygen and Hydrogen Sulfide on Carbon Dioxide Corrosion of Welded Structures of Oil and Gas Installations," Chemical and Petroleum Engineering, vol. 36, pp. 2, 2000.

[59] J. Amri, E. Gulbrandsen, Nogueira, "The Effect of Acetic Acid on The Pit Propagation in $CO_2$ Corrosion of Carbon Steel," Electrochemistry Communications, vol. 10, pp. 200–203, 2008.

[60] C. F. Martin, "Prediction $CO_2$ Corrosion with the Presence of Low concentration Acetic Acid in Turbulent Flow Conditions," Master Thesis, UTP, 2009.

[61] M.C. Ismail, "Prediction $CO_2$ corrosion with The Presence of Acetic Acid," Ph.D. Dissertation, UMIST, Manchester, 2005.

[62] K. S. George, S. Nesic, "Investigation of Carbon Dioxide Corrosion of Mild Steel in the Presence of Acetic Acid— Part 1: Basic Mechanisms," in Proc. Annu. NACE INTERNATIONAL conf. Corrosion, Nashville, 2007, p. 181.

[63] G.A. Zhang, Y.F. Cheng, "Corrosion of X65 Steel in $CO_2$-Saturated Oilfield Formation Water in the Absence and Presence of Acetic Acid," Corrosion Science, v.51, issue 8, p. 1589-1595, 2009.

[64] J. L. Crolet, Bonis, "Role of Free Acetic Acid on The $CO_2$ Corrosion of Steels," in Proc. Annu. NACE INTERNATIONAL conf. Corrosion, San Antonio, Texas, 1999, p. 24.

[65] Y. Garsany, D. Pletcher, B. Hedges, "Speciation and Elevtrochemistry of Brines Containing Acetate Ion and $CO_2$," Electroanalytical Chemistry, vol. 538, pp. 285 – 297, 2002.

[66] F. Vanessa, C. Canto, B. Brown, S. Nesic, "Effect of Organic Acids in $CO_2$ Corrosion," in Proc. Annu. NACE INTERNATIONAL conf. Corrosion, Nashville, 2007, p. 7319.

[67] M. Hajeeh, "Estimating Corrosion: A Statistical Approach," Materials and Design, vol. 24, pp. 509–518, 2003.

[68] S.J. Tracey, E. M. Patrick, R. Posey, "Surface Response Design to Study the Effect of Low Oxygen Levels on Carbon Dioxide Corrosion Environments," in Proc. Annu. NACE INTERNATIONAL conf. Corrosion, Atlanta, 2009, p. 9574.

[69] E.C. French, R.L. Martin, J.A. Dougherty, "Corrosion and Its Inhibition in Oil and Gas wells," in Proc. Annu. NACE INTERNATIONAL conf. Corrosion, Houston, 1989, p. 435.

[70] S.N. Smith, "Predicting Corrosion in Slightly Sour Environments," Materials Performance, August, pp 60-64, 2002.

[71] R. Nyborg, "Overview of $CO_2$ Corrosion Models for Wells and Pipelines," in Proc. Annu. NACE INTERNATIONAL conf. Corrosion, Houston, 2002, p. 233.

[72] Norsok standard M-506, "$CO_2$ Corrosion Rate Calculation Model", http:/www.nts.no/ norsok/m/50601.

[73] C. de Waard, "Prediction of $CO_2$ Corrosion of Carbon Steel," in Proc. Annu. NACE INTERNATIONAL conf. Corrosion, Houston, 1993, p. 69.

[74] T. Yuhua, T. Hong, "$CO_2$ Corrosion in Wet Gas Pipelines at Elevated Temperature," in Proc. Annu. NACE INTERNATIONAL conf. Corrosion, Denver, 2002, p. 2281.

[75] ECE - Version 4, "Corrosion Program software," Intetech Ltd. 37, Mount Way, Waverton.

[76] Cassandra, Corrosion Model Software, Webster, Mc Mohan. A., J., BP Report No.1993 - 220, 1993.

[77] M. Eisenberg, C. W. Tobias, C. R. Wilke, "Ionic Mass Transfer and Concentration Polarisation on Rotating Electrodes," Electrochemical Science, vol. 101, pp.306, 1954.

[78] Technical Note, Study of Mass-Transport Limited Corrosion Using Pine Rotating Cylinder Electrodes, Pine, Research Instruments, 2006.

[79] D. R. Wilcox, "Optimizing Engineering Design A Pneumatic Oxygen Valve with Mathematical Modeling and Design Experiments," Master Thesis, Kansas State University, 2007.

[80] N. Bradley, "The Response Surface Methodology," Master Thesis, Department of Mathematical Sciences, Indiana University, 2007.

[81] S. A. Long, "Application of Response Surface Methods to Characterize Missile Performance," Master thesis, Department of Mechanical and Aerospace Engineering, University of Alabama, 2007.

[82] L. Wang, "Recommendations for Design Parameters for Central Composite Designs with Restricted Randomization," Ph.D. Dissertation, Faculty of the Virginia Polytechnic Institute and State University, 2006.

[83] G. Box, N. R. Draper, "Empirical Model Building and Response Surfaces," John Wiley and Sons, New York, 1987.

[84] P. Devore, "The exploration and analysis data," Statistics, fifth edition, Thomson Learning, Belmont, USA, 2005.

[85] V. L. Russell, "Response-Surface Methods in Experiment Using RSM," Journal of Statistical Software, vol. 32, 7, 2009.

[86] K. George, S. Nesic, "Electrochemical Investigation and Modeling of Carbon Dioxide Corrosion of Carbon Steel in The Presence of Acetic Acid," Master Thesis, Ohio University, 2003.

[87] ASTM G 5-94 - "Standard Reference Test Method for Making Potentiostatic and Potentiodynamic Polarization Measurements."

[88] Freecorp V 1.0, Ohio Model, Institute for Corrosion and Multiphase Technology, Ohio University, Ohio.

[89] Minitab Inc. Minitab Statistical Software, State College, Pennsylvania. Minitab®, Minitab Inc., 2006.

[90] F. M. Song, D.W. Kirk, J. W. Graydon, D.E. Cormack, "Prediction for $CO_2$ Corrosion of Active Steel Under A Precipitate," in Proc. Annu. NACE INTERNATIONAL conf. Corrosion, New Orleans, 2004, p. 4382.

[91] J. K. Heuer, "An XPS Characterization of $FeCO_2$ Films from $CO_2$ Corrosion," Corrosion Science, vol. 30, p. 120 - 132, 1998.

[92] Z. D. Cui, S.L. Wu, S.I. Zhu, J. Yang, "Study on corrosion properties of pipelines in simulated produced water saturated with supercritical $CO_2$," Applied Surface Science, vol. 252, p. 2368 - 2374, 2006.

[93] S. Gaute, A. Palencsar, J. Kvarekval, "Investigation of Iron Sulfide Surface Layer Growth in Aqueous $H_2S/CO_2$ Environments," in Proc. Annu. NACE INTERNATIONAL conf. Corrosion, Atlanta , 2009, p. 9359.

[94] R. H. Hausler, "Contribution to the Understanding of $H_2S$ corrosion," in Proc. Annu. NACE INTERNATIONAL conf. Corrosion, New Orleans, 2004, p. 04732.

[95] G. Zhang, "On The Fundamentals of Electrochemical Corrosion of X65 steel in $CO_2$-Containing Formation Water in The Presence of Acetic Acid in Petroleum Production," Corrosion Science, vol.51, pp. 87–94, 2009.

[96] A. Fragiela, S. Sera, R. Perez, "Electrochemical Study of Two Microalloyed Pipelines Steels in $H_2S$ Environments," International Journal Hydrogen Energy, vol. 30, 1303 - 1309, 2005.

[97] Z. Q. Bai, C.F. Chen, M.X. Lu, J.B. Li, "Analyses of EIS Characteristic of $CO_2$ Corrosion of Well Tube Steels with Corrosion Scales," Applied Surface Science, vol. 252, pp. 7578 - 7584, 2006.

# APPENDIX 1

## 1.a Corrosion rate at pH 4

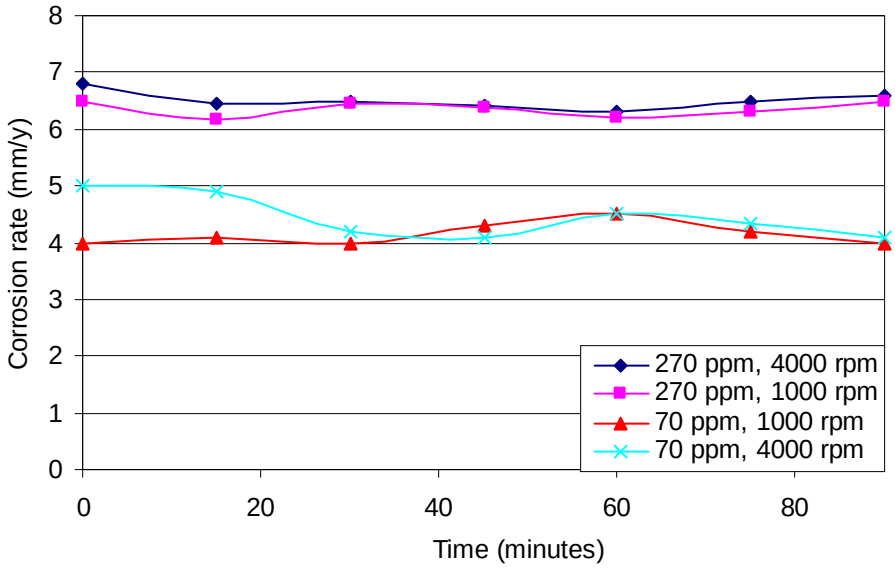


Figure A.1 Average corrosion rate of carbon steel in $CO_2$ saturated NaCl solution: pH 4, 35°C, different HAc concentration and rotation speed.

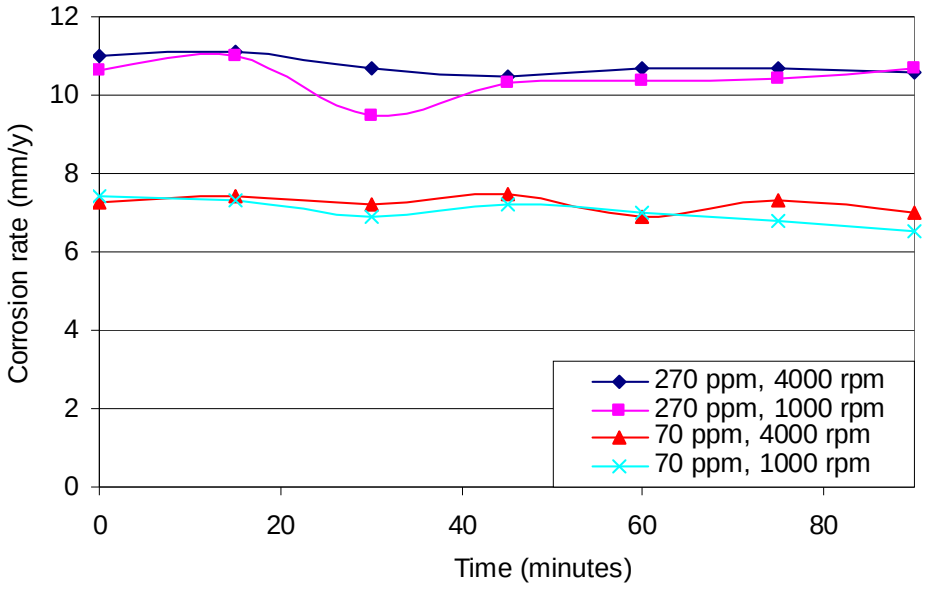

Figure A.2 Average corrosion rate of carbon steel in $CO_2$ saturated NaCl solution: pH 4, 70°C, different HAc concentration and rotation speed.

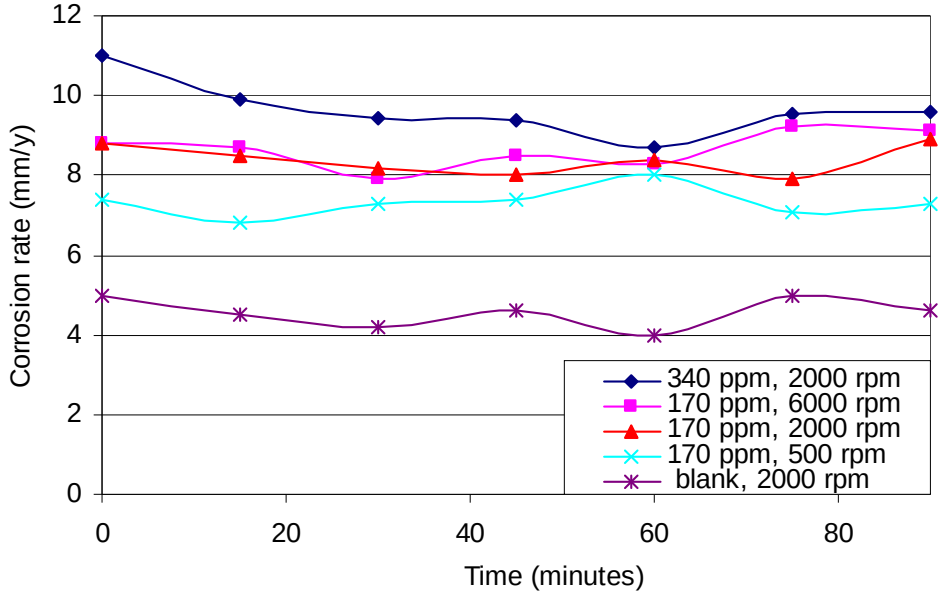


Figure A.3 Average corrosion rate of carbon steel in $CO_2$ saturated NaCl solution: pH 4, 50°C, different HAc concentration and rotation speed.

**1.b Corrosion rate at pH 5.5**

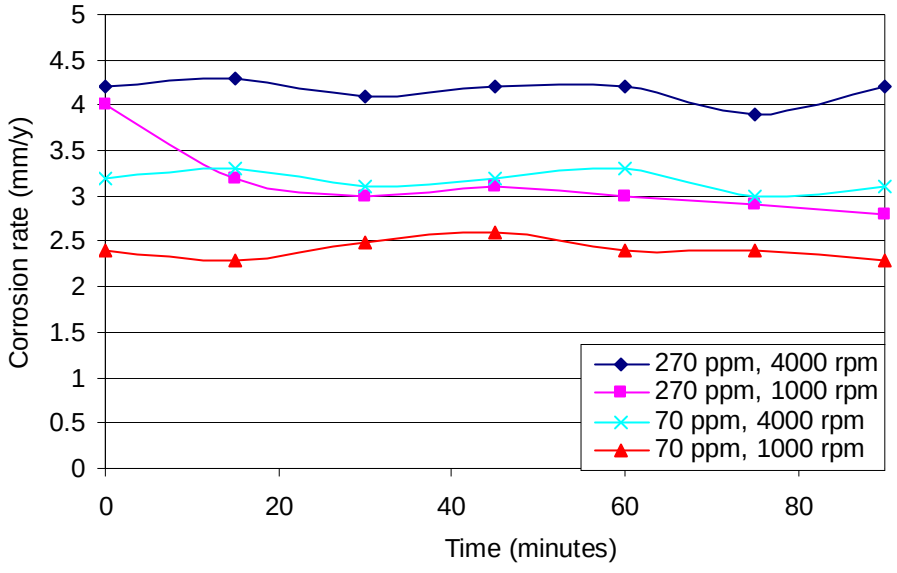

Figure A.4 Average corrosion rate of carbon steel in $CO_2$ saturated NaCl solution: pH 5.5, 35°C, different HAc concentration and rotation speed.

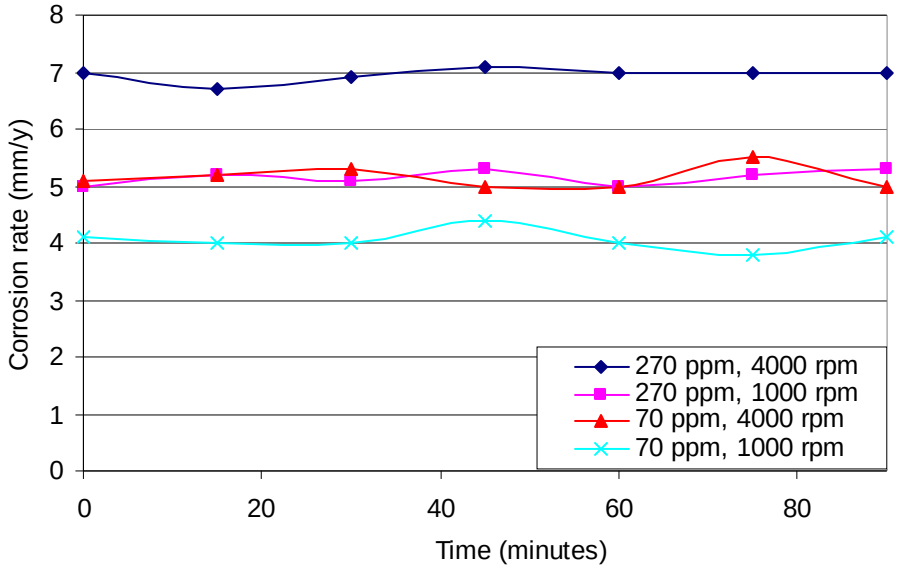


Figure A.5 Average corrosion rate of carbon steel in $CO_2$ saturated NaCl solution: pH 5.5, 70°C, different HAc concentration and rotation speed.

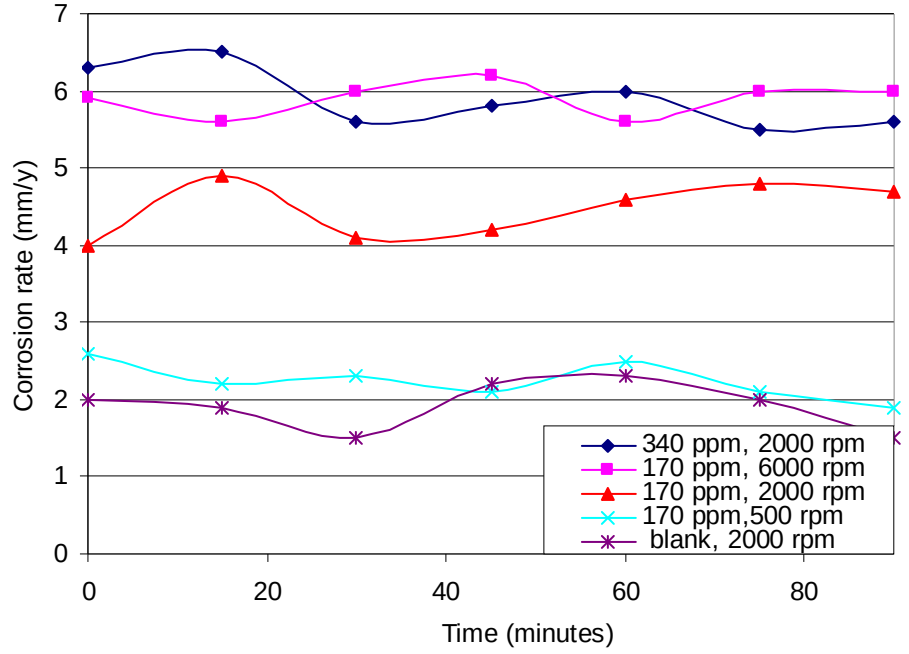


Figure A.6 Average corrosion rate of carbon steel in $CO_2$ saturated NaCl solution: pH 5.5, 50°C, different HAc concentration and rotation speed.

## APPENDIX 2

### 2.a Comparison Between Model Corrosion Rates and Freecorp Corrosion Software at Various Conditions at pH 4.

- **Comparison corrosion rate (mm/y) at blank solutions**

| Temp. (°C) / Rot. (rpm) | 25 | | 30 | | 40 | | 50 | | 60 | | 70 | |
|---|---|---|---|---|---|---|---|---|---|---|---|---|
| | Frc | Model | Frc | Model | Frc | Model | Frc | Model | Frc | Model | Frc | Model |
| 100 | 1.6 | 0.4 | 1.8 | 1.3 | 2.5 | 2.8 | 3.4 | 3.8 | 4.8 | 4.6 | 5.6 | 4.5 |
| 1000 | 2.7 | 0.8 | 3 | 2 | 4 | 3.3 | 5 | 4.3 | 7 | 5.1 | 7 | 5 |
| 2000 | 3.0 | 1.4 | 3.4 | 2.5 | 4.5 | 4 | 5.8 | 5 | 7.6 | 5.6 | 8.5 | 5.6 |
| 3000 | 3.2 | 1.9 | 3.6 | 3 | 4.7 | 4.3 | 6 | 5.5 | 7.9 | 6.1 | 8.8 | 6 |
| 4000 | 3.3 | 2.4 | 3.7 | 3.3 | 4.8 | 4.8 | 6.2 | 6 | 8 | 6.6 | 9 | 7 |
| 5000 | 3.3 | 2.9 | 3.8 | 4 | 5 | 5.6 | 6.3 | 6.4 | 8 | 7.1 | 9.2 | 7 |
| RSQ : | | 0.7 | | 0.8 | | 0.8 | | 0.8 | | 0.99 | | 0.8 |
| Correlation : | | 0.8 | | 0.9 | | 0.9 | | 0.9 | | 0.99 | | 0.9 |
| St. error : | | 0.5 | | 0.2 | | 0.1 | | 0.1 | | 0.02 | | 0.2 |

- **Comparison corrosion rate (mm/y) at 5 ppm HAc**

| Temp. (°C) / Rot. (rpm) | 25 | | 30 | | 40 | | 50 | | 60 | | 70 | |
|---|---|---|---|---|---|---|---|---|---|---|---|---|
| | Frc | Model | Frc | Model | Frc | Model | Frc | Model | Frc | Model | Frc | Model |
| 100 | 1.7 | 0.48 | 2 | 1.4 | 2.8 | 2.9 | 3.7 | 4 | 4.9 | 4.6 | 5.7 | 4.7 |
| 1000 | 3.1 | 0.9 | 3.6 | 1.9 | 4.7 | 3.4 | 6.1 | 4.5 | 7.7 | 5 | 9 | 5.2 |
| 2000 | 3.6 | 1.5 | 4 | 2.4 | 5.4 | 4 | 6.9 | 5 | 8.6 | 5.6 | 10 | 5.7 |
| 3000 | 3.9 | 2 | 4.5 | 2.9 | 5.8 | 4.5 | 7.4 | 5.5 | 9.2 | 6.1 | 11 | 6.2 |
| 4000 | 4.1 | 2.5 | 4.7 | 3.4 | 6.1 | 5 | 7.8 | 6 | 9.7 | 6.6 | 11.5 | 6.8 |
| 5000 | 4.2 | 3 | 4.9 | 4 | 6.4 | 5.5 | 8.1 | 6.5 | 10 | 7.1 | 12 | 7.3 |
| RSQ : | | 0.8 | | 0.8 | | 0.9 | | 0.8 | | 0.8 | | 0.8 |
| Correlation : | | 0.9 | | 0.9 | | 0.9 | | 0.9 | | 0.9 | | 0.9 |
| St. error : | | 0.5 | | 0.3 | | 0.1 | | 0.2 | | 0.2 | | 0.3 |

- **Comparison corrosion rate (mm/y) at 20 ppm HAc**

| Temp. (°C) / Rot. (rpm) | 25 | | 30 | | 40 | | 50 | | 60 | | 70 | |
|---|---|---|---|---|---|---|---|---|---|---|---|---|
| | Frc | Model | Frc | Model | Frc | Model | Frc | Model | Frc | Model | Frc | Model |
| 100 | 1.9 | 0.9 | 2.3 | 1.8 | 3.1 | 3.3 | 4.1 | 4.4 | 5.2 | 5 | 6 | 5.2 |
| 1000 | 4.1 | 1.4 | 4.7 | 2.3 | 6.1 | 3.8 | 7.9 | 4.9 | 9 | 5.5 | 11 | 5.7 |
| 2000 | 4.9 | 1.9 | 5.7 | 2.8 | 7.5 | 4.3 | 9.6 | 5.4 | 11 | 6 | 14 | 6.2 |
| 3000 | 5.4 | 2.4 | 6.3 | 3.3 | 8.3 | 4.8 | 10.8 | 5.9 | 13 | 6.6 | 16 | 6.7 |
| 4000 | 5.7 | 2.9 | 6.7 | 3.9 | 9 | 5.4 | 11 | 6.5 | 14 | 7.1 | 17 | 7.2 |
| 5000 | 6 | 3.4 | 7 | 4.4 | 9.5 | 5.9 | 12 | 7 | 16 | 7.6 | 19 | 7.8 |
| RSQ : | | 0.8 | | 0.8 | | 0.9 | | 0.8 | | 0.95 | | 0.9 |
| Correlation : | | 0.9 | | 0.9 | | 0.9 | | 0.9 | | 0.99 | | 0.96 |
| St. error : | | 0.5 | | 0.4 | | 0.3 | | 0.3 | | 0.4 | | 0.5 |

## 2.b Comparison Between Model Corrosion Rates and Freecorp Corrosion Software at Various Conditions at pH 5.5

- **Comparison corrosion rate (mm/y) at blank solutions**

| Temp. (°C) / Rot. (rpm) | 25 | | 30 | | 40 | | 50 | | 60 | | 70 | |
|---|---|---|---|---|---|---|---|---|---|---|---|---|
| | Frc | Model | Frc | Model | Frc | Model | Frc | Model | Frc | Model | Frc | Model |
| 100 | 0.9 | 0.6 | 1 | 0.9 | 1.9 | 0.8 | 2.5 | 1.9 | 3.2 | 2.2 | 4 | 2.3 |
| 1000 | 1 | 1.1 | 1.2 | 1.5 | 1.9 | 1.4 | 2.5 | 2.6 | 3.3 | 2.9 | 4.1 | 3.1 |
| 2000 | 1 | 1.7 | 1.2 | 2.0 | 2 | 2 | 2.6 | 3.2 | 3.3 | 3.6 | 4.1 | 3.9 |
| 3000 | 1 | 2.0 | 1.2 | 2.4 | 2 | 2.5 | 2.6 | 3.7 | 3.3 | 4.2 | 4.1 | 4.5 |
| 4000 | 1 | 2.2 | 1.2 | 2.7 | 2 | 2.7 | 2.6 | 4.1 | 3.3 | 4.6 | 4.1 | 4.9 |
| 5000 | 1 | 2.3 | 1.2 | 2.8 | 2 | 2.9 | 2.6 | 4.3 | 3.3 | 4.8 | 4.1 | 5.2 |
| RSQ : | | 0.6 | | 0.6 | | 0.8 | | 0.8 | | 0.6 | | 0.5 |
| Correlation : | | 0.8 | | 0.8 | | 0.9 | | 0.9 | | 0.8 | | 0.7 |
| St. error : | | 0.4 | | 0.2 | | 0.2 | | 0.2 | | 0.2 | | 0.2 |

- **Comparison corrosion rate (mm/y) at 5 ppm HAc**

| Temp. (°C) / Rot. (rpm) | 25 | | 30 | | 40 | | 50 | | 60 | | 70 | |
|---|---|---|---|---|---|---|---|---|---|---|---|---|
| | Frc | Model | Frc | Model | Frc | Model | Frc | Model | Frc | Model | Frc | Model |
| 100 | 1 | 0.6 | 1.1 | 0.9 | 1.8 | 1.5 | 2.5 | 2.0 | 3.3 | 2.2 | 4 | 2.4 |
| 1000 | 1.1 | 1.2 | 1.3 | 1.6 | 1.9 | 2.2 | 2.7 | 2.7 | 3.5 | 3.0 | 4.3 | 3.2 |
| 2000 | 1.1 | 1.7 | 1.3 | 2.1 | 2 | 2.8 | 2.8 | 3.3 | 3.6 | 3.7 | 4 | 3.9 |
| 3000 | 1.1 | 2.1 | 1.4 | 2.5 | 2 | 3.2 | 2.9 | 3.8 | 3.7 | 4.2 | 4.5 | 4.5 |
| 4000 | 1.2 | 2.3 | 1.4 | 2.7 | 2.1 | 3.5 | 2.9 | 4.1 | 3.8 | 4.6 | 4.6 | 5.0 |
| 5000 | 1.2 | 2.4 | 1.4 | 2.8 | 2.1 | 3.7 | 3 | 4.3 | 3.8 | 4.9 | 4.7 | 5.3 |
| RSQ : | | 0.8 | | 0.9 | | 0.96 | | 0.97 | | 0.98 | | 0.7 |
| Correlation : | | 0.9 | | 0.9 | | 0.98 | | 0.98 | | 0.99 | | 0.8 |
| St. error : | | 0.3 | | 0.3 | | 0.2 | | 0.17 | | 0.14 | | 0.3 |

- **Comparison corrosion rate (mm/y) at 20 ppm HAc**

| Temp. (°C) / Rot. (rpm) | 25 | | 30 | | 40 | | 50 | | 60 | | 70 | |
|---|---|---|---|---|---|---|---|---|---|---|---|---|
| | Frc | Model | Frc | Model | Frc | Model | Frc | Model | Frc | Model | Frc | Model |
| 100 | 1 | 0.8 | 1.2 | 1.1 | 1.8 | 1.7 | 2.6 | 2.1 | 3.4 | 2.4 | 4.1 | 2.6 |
| 1000 | 1.2 | 1.4 | 1.5 | 1.7 | 2.2 | 2.4 | 3.1 | 2.8 | 3.9 | 3.2 | 4.8 | 3.4 |
| 2000 | 1.3 | 1.9 | 1.6 | 2.3 | 2.4 | 3.0 | 3.3 | 3.5 | 4.3 | 3.9 | 5.3 | 4.1 |
| 3000 | 1.4 | 2.2 | 1.7 | 2.7 | 2.5 | 3.4 | 3.5 | 4.0 | 4.5 | 4.4 | 5.6 | 4.7 |
| 4000 | 1.5 | 2.5 | 1.8 | 2.9 | 2.6 | 3.7 | 3.5 | 4.3 | 4.7 | 4.8 | 5.8 | 5.2 |
| 5000 | 1.6 | 2.5 | 1.8 | 3.0 | 2.6 | 3.8 | 3.6 | 4.5 | 4.8 | 5.1 | 6 | 5.5 |
| RSQ : | | 0.97 | | 0.97 | | 0.95 | | 0.9 | | 0.98 | | 0.98 |
| Correlation : | | 0.98 | | 0.98 | | 0.97 | | 0.97 | | 0.99 | | 0.99 |
| St. error : | | 0.4 | | 0.43 | | 0.2 | | 0.16 | | 0.10 | | 0.19 |

## 2.c Comparison Between RSM Model Corrosion Rates and Experimental Data [60] at Various Conditions at pH 6

- **Comparison corrosion rate (mm/y) at temperature 25°C**

| N(rpm) | 0 | | 10 | | 20 | | 40 | | 60 | |
|---|---|---|---|---|---|---|---|---|---|---|
| | Model | Freecorp | Model | Freecorp | Model | Freecorp | Model | Freecorp | Model | Freecorp |
| 0 | 0.36 | 0.7 | 0.33 | 1.1 | 0.29 | 1.2 | 0.21 | 1.2 | -0.11 | 1.5 |
| 1000 | 0.54 | 0.9 | 0.57 | 1.2 | 0.60 | 1.3 | 0.67 | 1.4 | 0.76 | 1.6 |
| 2000 | 1.30 | 1.2 | 1.32 | 1.4 | 1.34 | 1.4 | 1.41 | 1.5 | 1.48 | 1.8 |
| 4000 | 2.35 | 1.3 | 2.36 | 1.4 | 2.38 | 1.5 | 2.41 | 1.5 | 2.47 | 1.9 |
| 6000 | 2.7 | 1.5 | 2.79 | 1.5 | 2.79 | 1.6 | 2.81 | 1.7 | 2.84 | 2 |
| RSQ | 0.92 | | 0.80 | | 0.97 | | 0.72 | | 0.95 | |
| Correlation | 0.96 | | 0.89 | | 0.98 | | 0.85 | | 0.97 | |
| St. error | 0.39 | | 0.52 | | 0.53 | | 0.51 | | 0.52 | |

- **Comparison corrosion rate (mm/y) at temperature 40°C**

| N(rpm) | 0 | | 10 | | 20 | | 40 | | 60 | |
|---|---|---|---|---|---|---|---|---|---|---|
| | Model | Freecorp | Model | Freecorp | Model | Freecorp | Model | Freecorp | Model | Freecorp |
| 0 | 1.32 | 0.9 | 1.39 | 1.3 | 1.47 | 1.7 | 1.64 | 2 | 1.83 | 2.2 |
| 1000 | 2.21 | 1.1 | 2.28 | 1.9 | 2.35 | 2 | 2.51 | 2.1 | 2.69 | 2.5 |
| 2000 | 2.95 | 1.9 | 3.02 | 2.1 | 3.08 | 2.2 | 3.23 | 2.5 | 3.39 | 2.8 |
| 4000 | 3.97 | 2 | 4.03 | 2.2 | 4.08 | 2.8 | 4.21 | 2.9 | 4.35 | 3 |
| 6000 | 4.38 | 2.1 | 4.42 | 2.8 | 4.46 | 2.9 | 4.57 | 3 | 4.68 | 3.1 |
| RSQ : | 0.78 | | 0.75 | | 0.97 | | 0.98 | | 0.97 | |
| Correlation: | 0.88 | | 0.86 | | 0.98 | | 0.99 | | 0.98 | |
| St. error : | 0.50 | | 0.16 | | 0.15 | | 0.16 | | 0.07 | |

- **Comparison corrosion rate (mm/y) at temperature 60°C**

| N(rpm) | 0 | | 10 | | 20 | | 40 | | 60 | |
|---|---|---|---|---|---|---|---|---|---|---|
| | Model | Freecorp | Model | Freecorp | Model | Freecorp | Model | Freecorp | Model | Freecorp |
| 0 | 1.35 | 1.6 | 1.48 | 1.8 | 1.62 | 2.1 | 1.90 | 2.1 | 2.21 | 2.4 |
| 1000 | 2.23 | 1.9 | 2.35 | 2 | 2.48 | 2.5 | 2.75 | 2.5 | 3.05 | 2.7 |
| 2000 | 2.95 | 2.2 | 3.07 | 3.5 | 3.19 | 3.5 | 3.45 | 3.6 | 3.73 | 3.9 |
| 4000 | 3.92 | 3.4 | 4.03 | 3.5 | 4.14 | 3.7 | 4.38 | 3.9 | 4.64 | 4.2 |
| 6000 | 4.28 | 3.6 | 4.38 | 4.1 | 4.48 | 4.1 | 4.70 | 4.2 | 4.93 | 4.5 |
| RSQ : | 0.96 | | 0.79 | | 0.88 | | 0.89 | | 0.89 | |
| Correlation: | 0.98 | | 0.89 | | 0.94 | | 0.94 | | 0.94 | |
| St. error : | 0.14 | | 0.15 | | 0.005 | | 0.09 | | 0.11 | |

## 2.d Comparison Between Model Corrosion Rates and Experimental Data [60] at Various Conditions in pH 5

- **Comparison corrosion rate (mm/y) at temperature 25°C**

| N(rpm) | Blank Solution | | 10 ppm | | 20 ppm | | 40 ppm | | 60 ppm | |
|---|---|---|---|---|---|---|---|---|---|---|
| | Model | Exp. | Model | Exp. | Model | Exp. | Model | Exp. | Model | Exp. |
| 0 | 0.53 | 1.32 | 0.63 | 1.62 | 0.73 | 1.8 | 0.95 | 1.88 | 1.19 | 1.92 |
| 1000 | 1.28 | 1.35 | 1.38 | 1.7 | 1.48 | 1.91 | 1.68 | 1.95 | 1.91 | 2.17 |
| 2000 | 1.88 | 1.76 | 1.97 | 1.78 | 2.06 | 1.97 | 2.26 | 2.12 | 2.47 | 2.22 |
| 4000 | 2.62 | 1.93 | 2.70 | 2.08 | 2.78 | 2.24 | 2.95 | 2.76 | 3.14 | 2.29 |
| RSQ | 0.88 | | 0.88 | | 0.91 | | 0.81 | | 0.88 | |
| Correlation | 0.94 | | 0.94 | | 0.95 | | 0.90 | | 0.94 | |
| St. error | 0.59 | | 0.60 | | 0.58 | | 0.49 | | 0.37 | |

- **Comparison corrosion rate (mm/y) at temperature 40°C**

| N(rpm) | Blank | | 10 ppm | | 20 ppm | | 40 ppm | | 60 ppm | |
|---|---|---|---|---|---|---|---|---|---|---|
| | Model | Exp. | Model | Exp. | Model | Exp. | Model | Exp. | Model | Exp. |
| 0 | 2.57 | 2.13 | 2.71 | 2.18 | 2.86 | 2.2 | 3.16 | 2.63 | 3.48 | 2.93 |
| 1000 | 3.31 | 2.26 | 3.44 | 2.3 | 3.58 | 2.4 | 3.88 | 2.78 | 4.19 | 3.23 |
| 2000 | 3.89 | 2.3 | 4.02 | 2.34 | 4.15 | 2.45 | 4.44 | 2.85 | 4.73 | 3.51 |
| 4000 | 4.59 | 2.33 | 4.714 | 2.44 | 4.83 | 2.49 | 5.09 | 3.52 | 5.37 | 3.92 |
| RSQ | 0.89 | | 0.98 | | 0.87 | | 0.80 | | 0.99 | |
| Correlation | 0.95 | | 0.99 | | 0.93 | | 0.89 | | 0.99 | |
| St. error | 0.17 | | 0.19 | | 0.23 | | 0.16 | | 0.16 | |

- **Comparison corrosion rate (mm/y) at temperature 60°C**

| | Blank | | 10 ppm | | 20 ppm | | 40 ppm | | 60 ppm | |
|---|---|---|---|---|---|---|---|---|---|---|
| N(rpm) | Model | Exp. | Model | Exp. | Model | Exp. | Model | Exp. | Model | Exp. |
| 0 | 3.08 | 2.93 | 3.27 | 2.97 | 3.48 | 3.31 | 3.90 | 4.19 | 4.33 | 3.79 |
| 1000 | 3.79 | 3.15 | 3.98 | 3.47 | 4.18 | 4.06 | 4.59 | 5.16 | 5.01 | 4.76 |
| 2000 | 4.35 | 3.77 | 4.54 | 4.09 | 4.73 | 4.57 | 5.13 | 5.27 | 5.54 | 4.77 |
| 4000 | 5.01 | 3.86 | 5.19 | 4.11 | 5.37 | 4.77 | 5.74 | 5.69 | 6.13 | 4.83 |
| RSQ | 0.91 | | 0.90 | | 0.95 | | 0.90 | | 0.7 | |
| Correlation | 0.95 | | 0.95 | | 0.98 | | 0.95 | | 0.83 | |
| St. error | 0.04 | | 0.09 | | 0.04 | | -0.07 | | 0.12 | |

## 2.e Comparison Between Model Corrosion Rates and Freecorp Corrosion Software at Various Conditions at pH 4 and $CO_2/H_2S$ System.

- **Comparison corrosion rate (mm/y) at blank solutions**

| Temp. (°C) / Rot. (rpm) | 25 | | 30 | | 40 | | 50 | | 60 | | 70 | |
|---|---|---|---|---|---|---|---|---|---|---|---|---|
| | Frc | Model | Frc | Model | Frc | Model | Frc | Model | Frc | Model | Frc | Model |
| 100 | 1.1 | 1.5 | 1.3 | 1.6 | 1.6 | 1.7 | 1.9 | 1.9 | 2.4 | 2.2 | 2.9 | 2.6 |
| 1000 | 1.5 | 1.6 | 1.6 | 1.7 | 2.1 | 1.8 | 2.5 | 2.0 | 3.3 | 2.3 | 4 | 2.7 |
| 2000 | 1.5 | 1.7 | 1.7 | 1.8 | 2.1 | 2.0 | 2.6 | 2.2 | 3.4 | 2.4 | 4.1 | 2.8 |
| 3000 | 1.5 | 1.8 | 1.7 | 1.9 | 2.1 | 2.0 | 2.6 | 2.2 | 3.4 | 2.5 | 4.2 | 2.8 |
| 4000 | 1.5 | 1.9 | 1.7 | 1.9 | 2.1 | 2.0 | 2.6 | 2.3 | 3.4 | 2.6 | 4.2 | 2.9 |
| 5000 | 1.5 | 1.9 | 1.7 | 2.0 | 2.2 | 2.1 | 2.6 | 2.3 | 3.4 | 2.6 | 4.2 | 2.9 |
| RSQ : | | 0.5 | | 0.7 | | 0.7 | | 0.7 | | 0.6 | | 0.7 |
| Correlation : | | 0.7 | | 0.8 | | 0.8 | | 0.8 | | 0.8 | | 0.9 |
| St. error : | | 0.1 | | 0.1 | | 0.1 | | 0.3 | | 0.3 | | 0.1 |

- **Comparison corrosion rate (mm/y) at 5 ppm HAc**

| Temp. (°C) / Rot. (rpm) | 25 | | 30 | | 40 | | 50 | | 60 | | 70 | |
|---|---|---|---|---|---|---|---|---|---|---|---|---|
| | Frc | Model | Frc | Model | Frc | Model | Frc | Model | Frc | Model | Frc | Model |
| 100 | 1.2 | 1.6 | 1.3 | 1.6 | 1.7 | 1.7 | 2 | 1.9 | 2.5 | 2.2 | 3 | 2.6 |
| 1000 | 1.5 | 1.7 | 1.7 | 1.7 | 2.1 | 1.8 | 2.6 | 2.0 | 3.4 | 2.3 | 4 | 2.7 |
| 2000 | 1.5 | 1.8 | 1.8 | 1.8 | 2.2 | 1.9 | 2.7 | 2.1 | 3.5 | 2.4 | 4.3 | 2.8 |
| 3000 | 1.6 | 1.9 | 1.8 | 1.9 | 2.2 | 2.0 | 2.7 | 2.2 | 3.5 | 2.5 | 4.3 | 2.8 |
| 4000 | 1.6 | 1.9 | 1.8 | 1.9 | 2.2 | 2.1 | 2.7 | 2.3 | 3.5 | 2.6 | 4.4 | 2.9 |
| 5000 | 1.6 | 1.9 | 1.8 | 2.0 | 2.2 | 2.1 | 2.7 | 2.3 | 3.6 | 2.6 | 4.4 | 2.9 |
| RSQ : | | 0.8 | | 0.7 | | 0.6 | | 0.6 | | 0.6 | | 0.8 |
| Correlation : | | 0.9 | | 0.8 | | 0.8 | | 0.8 | | 0.8 | | 0.9 |
| St. error : | | 0.2 | | 0.1 | | 0.1 | | 0.2 | | 0.2 | | 0.3 |

- **Comparison corrosion rate (mm/y) at 20 ppm HAc**

| Temp. (°C) / Rot. (rpm) | 25 | | 30 | | 40 | | 50 | | 60 | | 70 | |
|---|---|---|---|---|---|---|---|---|---|---|---|---|
| | Frc | Model | Frc | Model | Frc | Model | Frc | Model | Frc | Model | Frc | Model |
| 100 | 1.3 | 1.6 | 1.5 | 1.7 | 1.9 | 1.8 | 2.3 | 2.0 | 2.9 | 2.3 | 3.5 | 2.6 |
| 1000 | 1.7 | 1.7 | 1.9 | 1.8 | 2.4 | 1.9 | 2.5 | 2.1 | 3.7 | 2.4 | 4.6 | 2.7 |
| 2000 | 1.7 | 1.8 | 1.9 | 1.9 | 2.4 | 2.0 | 2.9 | 2.2 | 3.8 | 2.5 | 4.7 | 2.8 |
| 3000 | 1.7 | 1.9 | 1.9 | 1.9 | 2.4 | 2.1 | 3 | 2.3 | 3.9 | 2.5 | 4.8 | 2.9 |
| 4000 | 1.7 | 2.0 | 2 | 2.0 | 2.5 | 2.2 | 3 | 2.3 | 3.9 | 2.6 | 4.8 | 2.9 |
| 5000 | 1.7 | 2.0 | 2 | 2.1 | 2.5 | 2.2 | 3 | 2.4 | 3.9 | 2.6 | 4.8 | 3.0 |
| RSQ : | | 0.5 | | 0.7 | | 0.7 | | 0.9 | | 0.8 | | 0.7 |
| Correlation : | | 0.7 | | 0.8 | | 0.8 | | 0.9 | | 0.9 | | 0.8 |
| St. error : | | 0.1 | | 0.03 | | 0.1 | | 0.2 | | 0.3 | | 0.3 |

## LIST OF PUBLICATIONS

**Journals**

1. A Statistics Approach for the Prediction of CO2 Corrosion in Mixed Acid Gases, Corrosion and materials, Australasian Corrosion Association, 2009.
2. Application of response surface methodology for Prediction CO2 Corrosion Models at pH 4, International Journal of Corrosion, Hindawi, 2009 (minor correction).
3. Optimization Design and Analytical Modeling in of CO2 corrosion Experiments, International Journal of Corrosion , Hindawi, 2010 (in press).
4. Application of response surface methodology for Prediction CO2 Corrosion Models at pH 5.5 (submitted to Engineering Journal, Taylor University, 2010)

**Conferences**

5. Mechanistic Prediction Model of CO2 Corrosion, International Graduated Conference, UTM, Malaysia, 2008.
6. Study Corrosion Prediction Models in CO2 Environment, International Conference, UTP, Malaysia, 2008
7. Modeling Simultaneous Effects of Pressure, Temperature and pH on CO2 Corrosion, Submitted to National Conference, UTP, Malaysia, 2009
8. Application of Response Surface Design to Characterize CO2 Corrosion Mechanistically, Asia Pacific Nace Conference, 2009. *(selected to published in magazine of petromin/pipeline)*
9. Study Combinations Effects of HAc in H2S/CO2 Corrosion, submit to ICPER, UTP, 2010 *(selected to publish in applied science journal)*
10. Study on the Effect of Surface Finish on Corrosion of Carbon Steel in CO2 Environment, ICPER, 2010. *(selected to publish in applied science journal)*